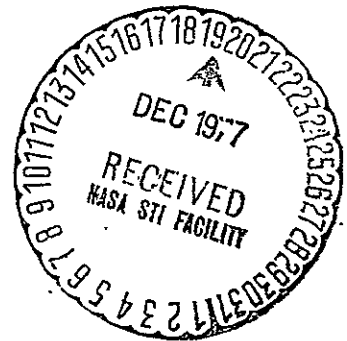(NASA-CR-155334) STRUCTURAL ANALYSIS OF
ULTRA-HIGH SPEED AIRCRAFT STRUCTURAL
COMPONENTS Final Report (Kansas Univ.)
148 p HC A07/MF A01   CSCL 20K

N78-13476

Unclas
G3/39   53635

THE UNIVERSITY OF KANSAS CENTER FOR RESEARCH, INC.

2291 Irving Hill Drive—Campus West
Lawrence, Kansas 66045

FINAL REPORT

for

STRUCTURAL ANALYSIS OF ULTRA-HIGH
SPEED AIRCRAFT STRUCTURAL COMPONENTS

December 1977

Kenneth H. Lenzen
Principal Investigator

William H. Siegel
Graduate Research Assistant

THE UNIVERSITY OF KANSAS CENTER FOR RESEARCH, INC.

2291 Irving Hill Drive—Campus West
Lawrence, Kansas 66045

CONTENTS

CONTENTS (continued)

FIGURES

iv

APPENDIX FIGURES

TABLES

APPENDICES TABLES

ABSTRACT

The concept of a hypersonic research airplane is one which has been studied for several years. The project reported on in this paper involved the testing of a hypersonic beaded skin panel to failure. The primary interest was focused upon the buckling characteristics of the panel under pure compression with boundary conditions similar to those found in a wing mounted condition. Three primary phases of analysis are included in this report. These phases include: Experimental testing of the panel to failure; Finite element structural analysis of the beaded panel with the computer program Nastran; A summary of the semiclassical buckling equations for the beaded panel under purely compressive loads. A comparison of each of the analysis methods is also included.

NOMENCLATURE

a	Half pitch dimension, inches (cm)
A_a	Cross sectional area of section defined by half pitch dimension, a, (see fig. 28) at the center cross section of the panel, inches^2 (cm^2)
b	Width of the flat, inches (cm)
C	Bead depth, inches (cm)
D	Bending or twisting rigidity, LBf·in (N·m)
E	Modulus of elasticity, tension, psi (N/m^2)
E_c	Modulus of elasticity, compression, psi (N/m^2)
F_{Cb}	Critical axial compressive stress for bead instability, psi (N/m^2)
F_{Bb}	Critical bending stress for bead instability, psi (N/m^2)
F_{CF}	Critical axial buckling load for flat instability, LBf (N)
I	Moment of inertia per unit length, XY plane
$\hat{I}$	Moment of inertia per unit length, ξY plane
L	Panel length, inches (cm)
N_{Cr}	Critical axial buckling load, LBf (N)
N_{YCr}	Critical axial buckling load for general instability, LBf (N)
N_{YDCr}	Critical axial buckling load for diagonal instability, LBf (N)
R	Bead radius, inches (cm)
Rx,Ry,Rz	Restricted degrees of freedom, rotation
s_a, s_δ	Developed length, inches (cm)

NOMENCLATURE (continued)

S_1, S_2	Distance, inches (cm)
t	Bead thickness, inches (cm)
t_F	Flat thickness, inches (cm)
X, Y, Z	Coordinate axes
x, y, z	Restricted degrees of freedom, translation
α	Magnitude of eccentricity
δ	Distance or dimension
ε	Strain, μinches/inch (μcm/cm)
γ	Shear, strain μinches/inch (μcm/cm)
θ	Angle, degrees or radians
ν	Poisson's ratio

SUBSCRIPTS

Cr	Critical
XX	Axis
XZ	Axis
ZZ	Axis
ξ	Refers to ξ direction
$\xi\xi$	Diagonal axis
ξY	Diagonal plane

Abbreviations

DT	Displacement transducer
HRA	Hypersonic Research Airplane
HWTS	Hypersonic Wing Test Structure
SG	Strain gage

SUMMARY

The concept of a hypersonic research airplane is one which has been studied for several years. Early studies included research into new structural concepts with emphasis placed upon developing the best cost/weight efficiency, performance and reliability obtainable.

As a part of NASA's continuing research into hypersonics, Dryden Flight Research Center has been laboratory testing an 85 square foot $(7.9m^2)$ hypersonic wing test section of a proposed hypersonic research airplane. In tests performed to date on the wing test section, the structure has exceeded all expectations of strength and durability

The project reported on in this paper has carried the hypersonic wing test structure project one step further by testing a single beaded panel to failure. The primary interest was focused upon the buckling characteristics of the panel under pure compression with boundary conditions similar to those found in a wing mounted condition. Three primary phases of analysis are included in the report. These phases include: Experimental testing of the beaded panel to failure; finite element structural analysis of the beaded panel with the computer program Nastran; a summary of the semiclassical buckling equations for the beaded panel under purely compressive loads. Comparisons between each of the analysis methods is also included.

INTRODUCTION

The Hypersonic Research Airplane

The concept of a hypersonic research airplane (HRA) is one which has been studied for several years (ref. 1-10). Early studies included not only basic conceptual design, but also research into new structural concepts. This research has provided a portion of the technological base necessary for future hypersonic developments.

Much of the research done has been devoted to theoretical analysis of various structural concepts which meet the requirements of a hypersonic airplane. Emphasis has been placed upon developing the best cost/weight efficiency, performance and reliability obtainable. Weight efficiency in high performance aircraft is a critical factor explaining the need for a weight efficient structure.

One HRA concept studied by NASA is shown in figure 1. This proposed vehicle would cruise at Mach 8 for five minutes. It is a single place design with a wing span of 38 feet (11.58m), a length of 101 feet (30.78m) and an estimated weight of 75,600 pounds (3.36×10^5N). The wings and tail are hot radiating structures fabricated from super alloys.
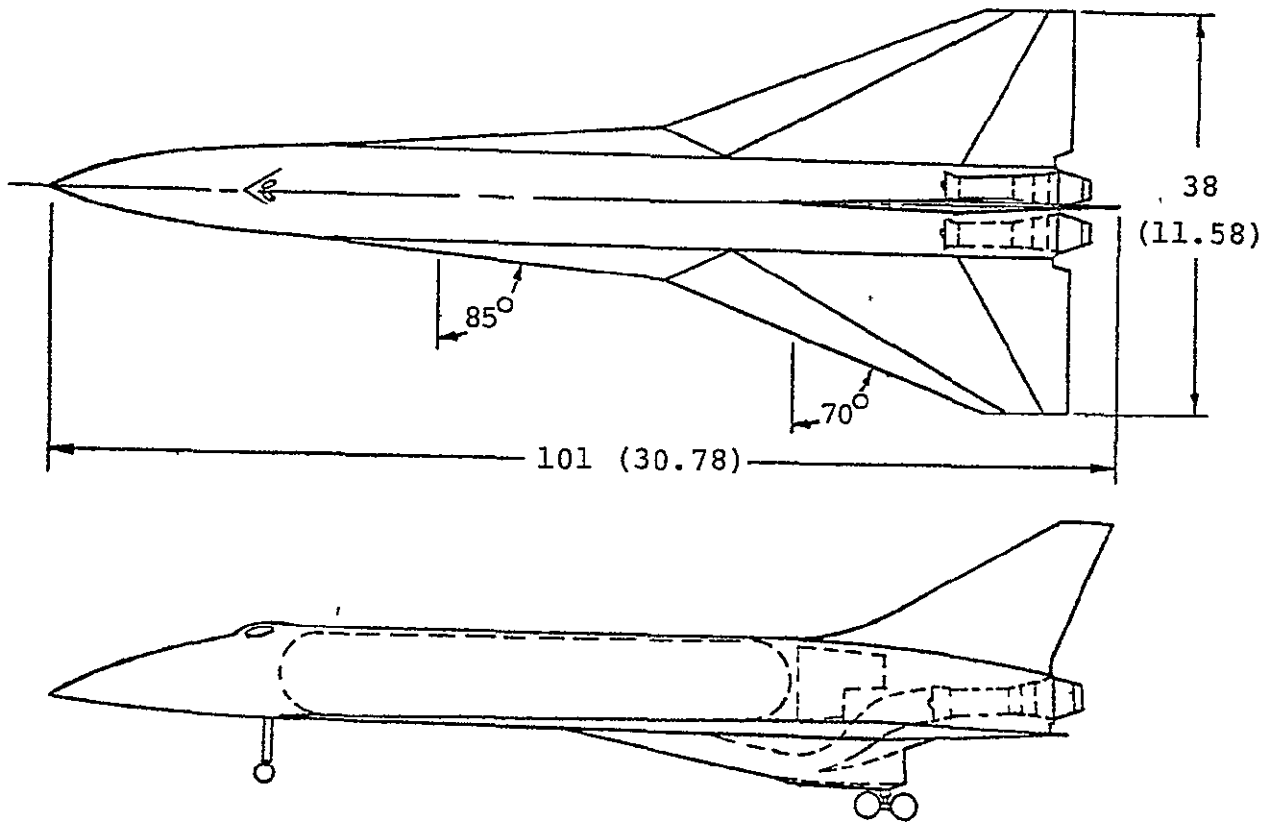
Figure 1. Hypersonic research airplane configuration concept.
Note· Dimensions are in feet and (meters).

The Hypersonic Wing Test Structure

As part of NASA's continuing research into hypersonics, Dryden Flight Research Center has been laboratory testing an 85 square foot $(7.9m^2)$ hypersonic wing test section, shown in figure 2, of the proposed HRA vehicle. The objectives of this program are to verify analytical predictions, construction techniques, assembly techniques and in general to improve flight loads measurement technology.

The hypersonic wing test structure (HWTS), shown in figure 3, is made from René 41 (with the exception of the lower leading edge heat shield panels which are TD Ni Cr) and is capable of operating with surface temperatures in excess of 1800° F (1250°K). The HWTS employs corrugated spar and rib webs and beaded skin panels. Aerodynamic smoothness is accomplished by attaching heat shields over the beaded panels.

The HWTS carries loads somewhat differently than do conventional aircraft. Bending loads normally carried by spars in conventional wing structures are instead carried by the beaded skin panels in the HWTS. Shear and torque are carried in much the same manner as in conventional wings.

4
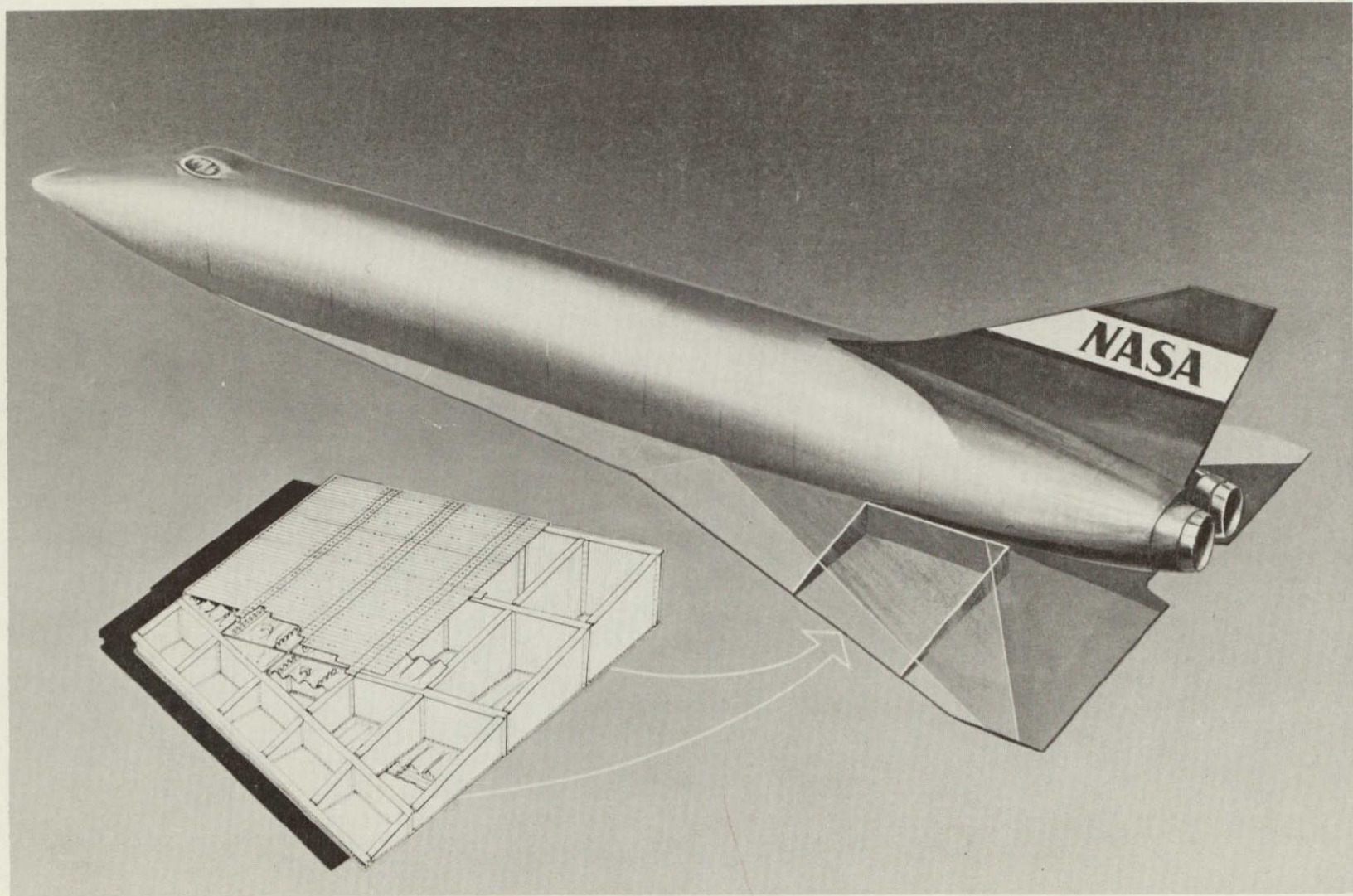
Figure 2. Hypersonic wing test section of the proposed hypersonic research airplane.
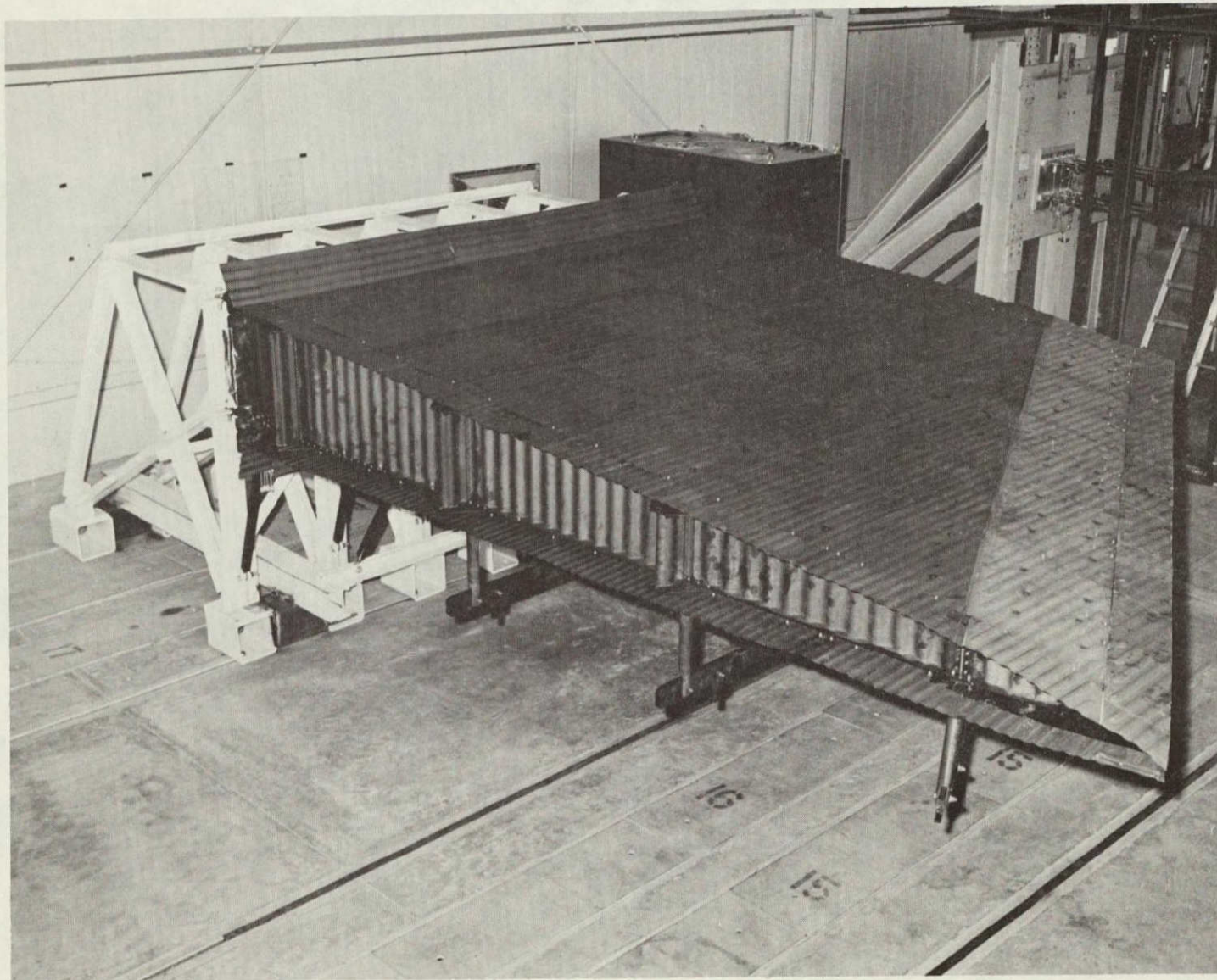
Figure 3. The hypersonic wing test structure (HWTS).

transducers (DT's). The second technique used was the Moiré fringe
(or grid shadow) technique (ref 12). The Moiré fringe technique pro-
vided deflection data for the entire panel versus the descrete measure-
ment of the DT. The DT data also provided a check of the Moiré data.
A brief description of the Moiré fringe technique is included in appen-
dix C.

The second phase of the project was the finite element structural
analysis of the panel. The stresses, deflections, and buckling char-
acteristics were calculated with Nastran (ref 13) a finite element
structural analysis computer program.

The third phase of the project included a summary of the semi-
classical analysis previously done for the beaded panels. Semiclassi-
cal equations of buckling strength were developed for beaded panels of
the type used for this test in references 2, 3, and 4.

THE BEADED PANEL TEST SPECIMEN

Beaded Panel Description

The beaded panel concept meets the requirements of high strength and weight efficiency required for a hypersonic airplane. The panel, as shown in figure 4, is 42.9 inches (109 cm) long and 19.1 inches (48.5 cm) wide. It has seven alternating up and down semicircular beads separated by about 0.4 inches (1 cm) wide flats. The perimeter of the panel is flat to permit mounting to the spar caps and rib caps of a wing.

Doublers made from René 41 sheet stock were spot welded to the ends of the panel on both sides, tripling the nominal thickness of the ends. These doublers extend about 10.7 inches (27.2 cm) towards the center of the panel, gradually reducing in thickness as they progress down the flats. The doublers reduce the possibility of local end failures and help to distribute the load more uniformly into the panel.

Provisions were made to attach heat shields to the panels at eight locations two of which are pointed out in figure 4. The remaining six attachment points are symmetric to those shown.

The beaded panel dimensions were derived using a computerized optimization program (ref. 2). The optimization program varied such parameters as panel length, width, number of beads and thickness to derive a least weight configuration capable of carrying prescribed mechanical and thermal loads (based upon semiclassical analysis). Strength interaction curves such as that shown in figure 5, were then made for each panel configuration. The various combinations of
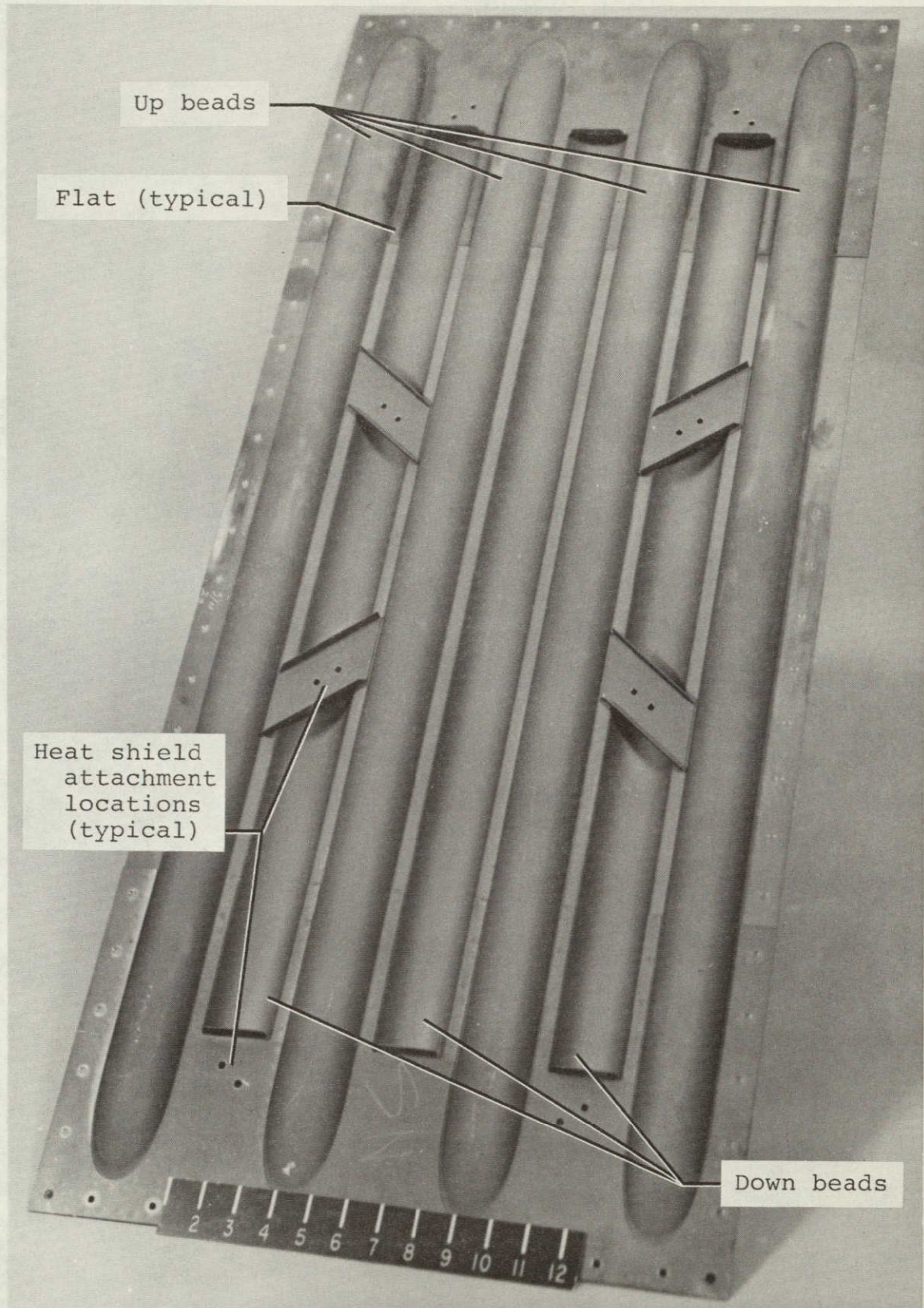
Figure 4.   The hypersonic beaded skin panel used for this project.

10

Rene 41 Material and Formability Properties

Tensile specimens, shown in figure 6, were supplied with the beaded panels. These specimens and the panels were cut from the same sheet stock. A number of them were cut in the direction of rolling; an equal number were cut perpendicular to that direction. Six specimens, three of each type, were tested in a universal testing machine to experimentally determine the modulus of elasticity and the 0.2% offset yield strength of the Rene 41. Figure 7 is a typical stress-strain plot using test data. The average modulus of elasticity was found to be 30.422×10^6 psi $(2.10 \times 10^{11} N/m^2)$ compared to 31.6×10^6 psi $(2.18 \times 10^{11} N/m^2)$
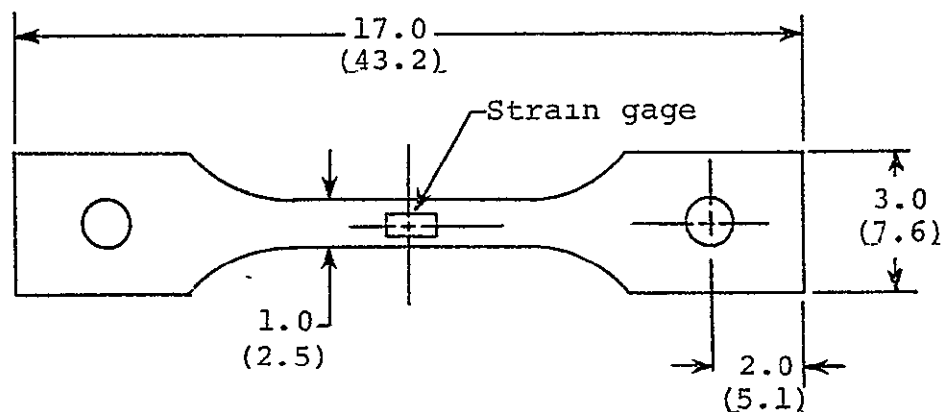
Figure 6. *Rene 41 tensile specimen dimensions 0.037 inches (0.094 cm) thick. Dimensions in inches and (cm).*

as reported in reference 14. Table 1 summarizes the results of the

six tensile specimen tests   In table 2, a number of material properties

are summarized as reported in reference 14.

The beaded panels were formed in a 5 million pound $(2.22 \times 10^7 N)$

hydraulic press. At least two and sometimes four anneals were required

before fully developing the bead (ref. 15). The stretch forming process

reduced the thickness of the bead from an original thickness of 0.037

inches (0.094 cm) to about 0.028 inches (0.071 cm).

Due to the extreme hardness of René 41, standard high speed steel

drills could not be used. Strict drilling procedures in addition to

cobalt drills had to be used to prevent work hardening the René 41 and

to obtain maximum life from the drill bits (ref. 15).
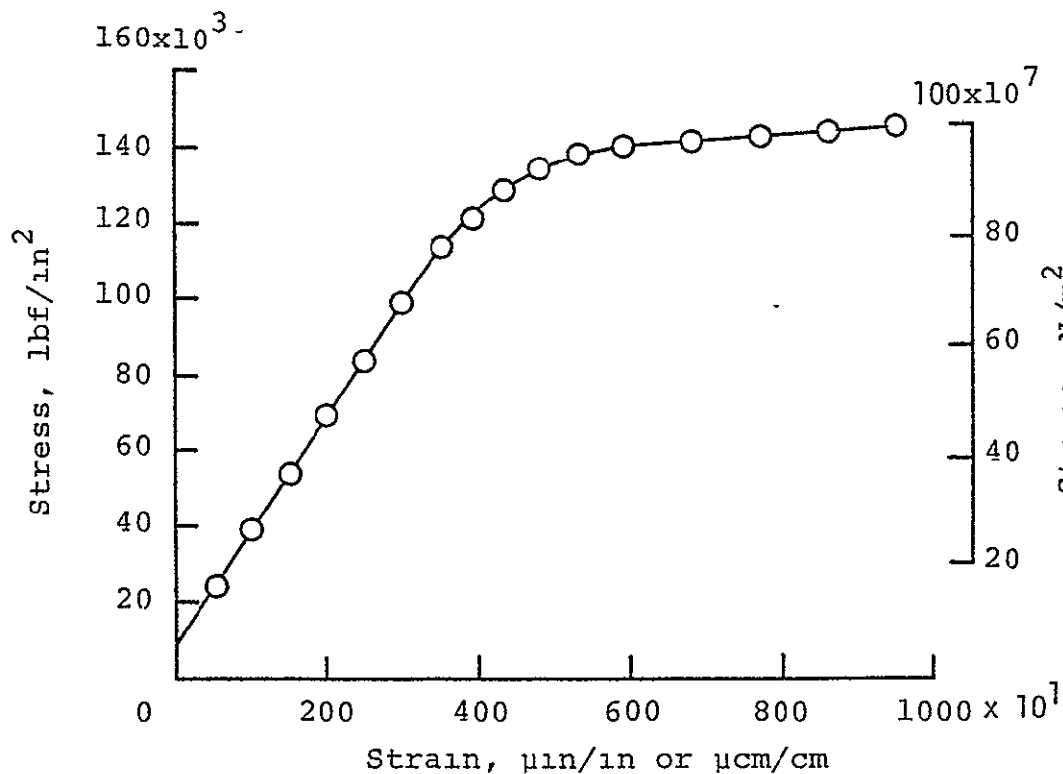
Figure 7. *Typical stress-strain curve for*
René 41 tensile specimen test.

13

Table 1. Experimentally determined modulus and 0.2% offset yield strain of René 41.

Specimen ID	Modulus of Elasticity lbf/in^2 (N/cm^2)	0.2% offset Yield strain μin/in (μcm/cm)
003-L-8*	30.205x10^6 (20.826x10^6)	6,350
003-L-9	30.358x10^6 (20.931x10^6)	6,450
003-L-10	30.091x10^6 (20.747x10^6)	6,200
003-T-8**	30.668x10^6 (21.145x10^6)	6,250
003-T-9	30.126x10^6 (20.771x10^6)	6,600
003-T-10	31.082x10^6 (21.430x10^6)	6,400
Average	30.422x10^6 (20.975x10^6)	6,380

*L-Longitudinal specimens   **T-Transverse specimens

Table 2. Material properties of René 41 as reported in reference 14.

Property	Value
Modulus of elasticity (Tension), E	31.6×10^6 lbf/in^2 (21.8×10^6 N/cm^2)
Modulus of elasticity (Compression), E_c	31.6×10^6 lbf/in^2 (21.8×10^6 N/cm^2)
Shear modulus, G	12.1×10^6 lbf/in^2 (8.3×10^6 N/cm^2)
Density, ρ	.298 lbm/in^3 (.008 kg/cm^3)
Tensile ultimate strength	185,000 lbf/in^2 (127,550 N/cm^2)
Tensile yield strength	132,000 lbf/in^2 (91,000 N/cm^2)
Compressive yield strength	141,000 lbf/in^2 (97,200 N/cm^2)
Poisson's ratio, ν	.31

PRETEST PREPARATION

Beaded Panel Measurements

Detailed drawings accompanying the beaded panels to NASA specified
the various dimensions of the panel which are summarized in table 3.
Also included in table 3 are the values obtained from direct measure-
ment which vary somewhat from the specifications. The measured values
were used in all analyses of this project.

The buckling characteristics of any structure are affected by
eccentricities. Therefore, measurements were made at over 100 loca-
tions on the beaded panel to determine the magnitude of the manufactur-
ing eccentricities present in the panel. The edge stiffeners (which
will be discussed in a later section) were attached to the panel during
these measurements. The maximum out-of-plane eccentricity of the panel
was found to be only 0.019 inches (0.048 m).

Table 3. Specified and measured thicknesses of the beaded panel.

Location	Specified thickness in (cm)	Measured thickness in (cm)	% difference
1	.034 (.086)	.0347 (.0881)	2.06
2	.026 (.066)	.0285 (.0724)	9.62
3	.036 (.091)	.0345 (.0876)	4.17
4	.076 (.193)	.0751 (.1908)	1.18
5	.110 (.279)	.1091 (.2771)	0.82
6	.068 (.173)	.0725 (.1842)	6.62
7	.082 (.208)	.0838 (.2129)	2.20
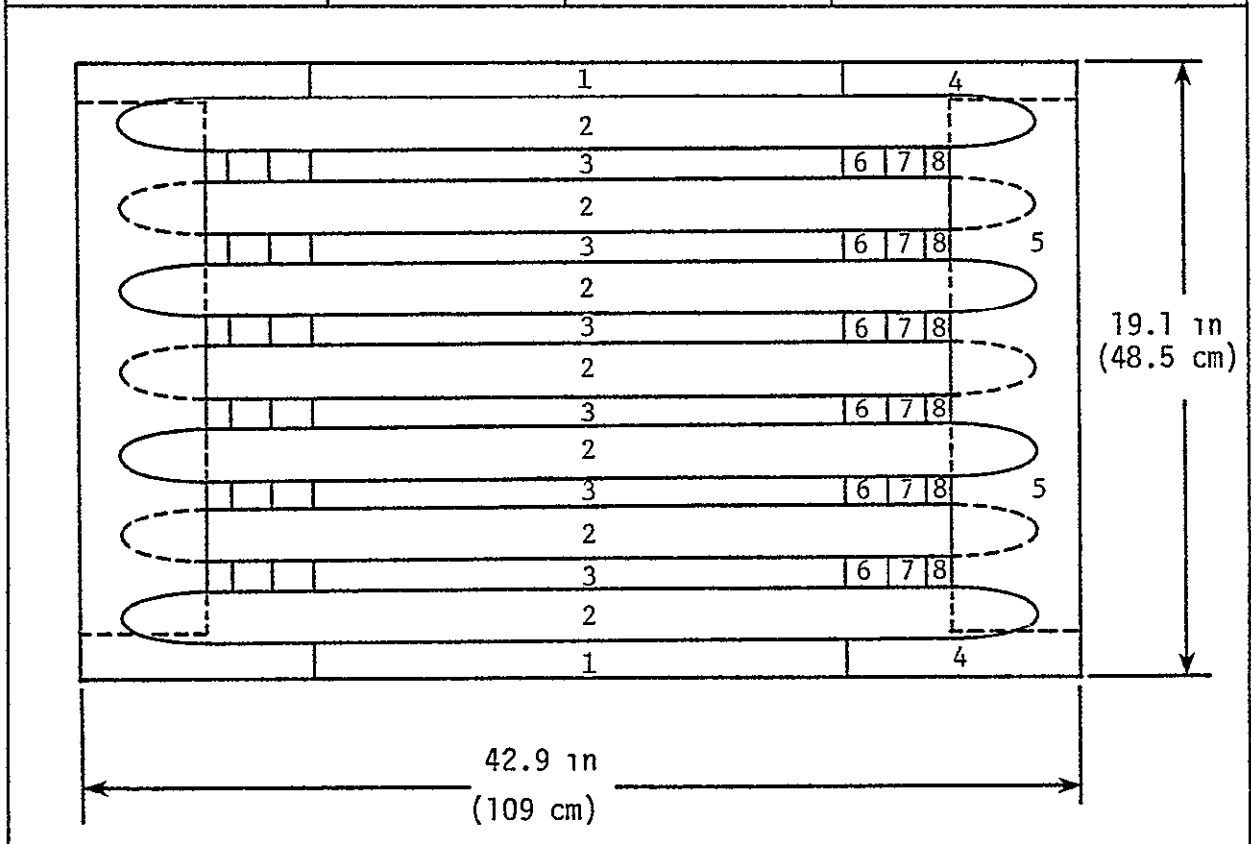
Edge Stiffeners

An attempt was made in this project to stiffen the edges of the panel in a manner which would closely approximate the stiffness conditions of a wing mounted condition. Therefore, the edge stiffeners which run parallel to the bead as shown in figure 8 were sized with the intention of not only preventing local edge failures but also simulating the stiffness of adjacent spars, and panels in the HWTS. These stiffeners were made in the shape of Z-sections from annealed stainless steel and mounted on the heat shield side of the panel as shown in figure 9.

The Z-sections were designed with the aid of Nastran, a finite element structural analysis program. Nastran was used in an iterative manner utilizing two finite element models entitled EDGE1 and EDGE2.

Model EDGE1, shown in figure 10, consisted of a quarter panel,
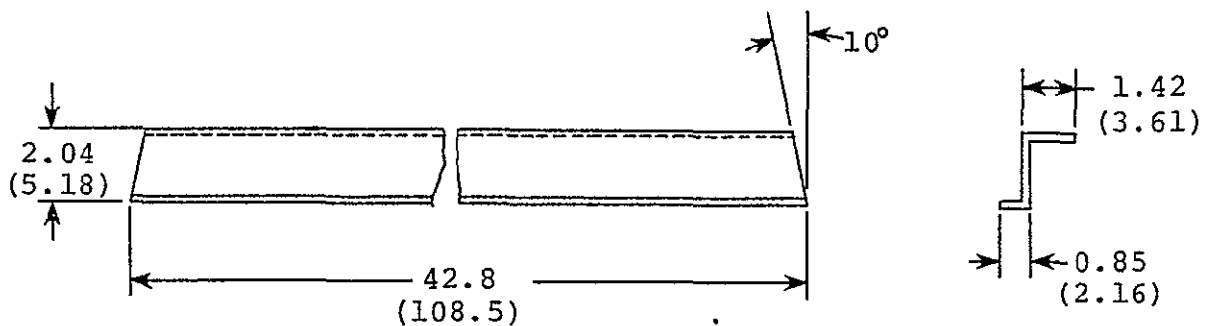
Figure 8. *Dimensions of the Z-section edge stiffeners made from annealed stainless steel. Dimensions in inches and (cm).*
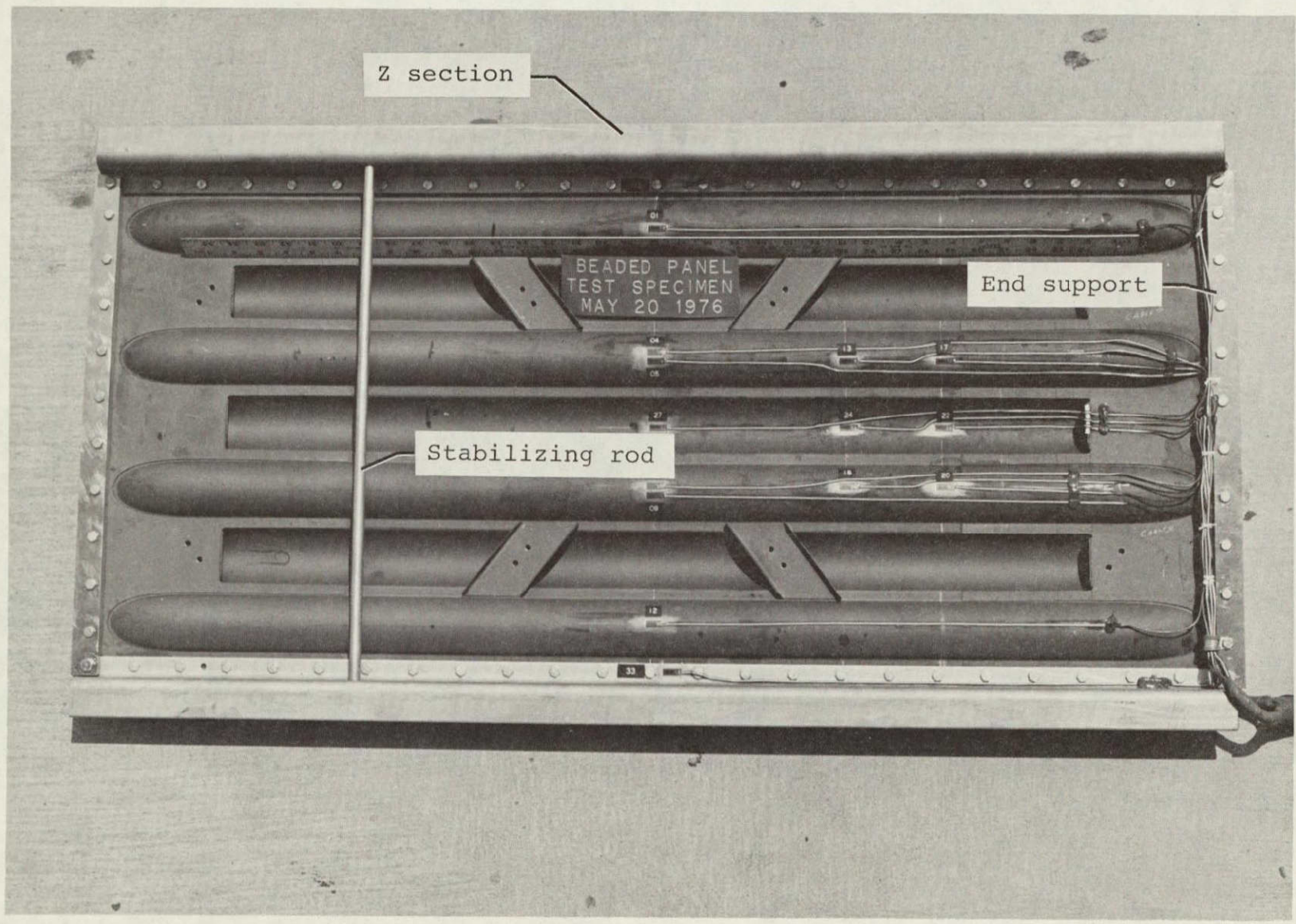
Figure 9. *Side stiffeners, end supports and stabilizing rod mounted to the beaded panel.*

spar cap, spar web and an adjacent panel assembly. This model was intended to be a representative section of an actual hypersonic wing.

Model EDGE2, as shown in figure 11, consisted of the same quarter panel as used in EDGE1 but bar elements replaced the spar cap, spar web and adjacent half panel assembly. The design procedure employed was to apply identical compressive loads (parallel to the beads) to both models, then adjust the sizes of the bar elements until the out-of-plane displacements of model EDGE2 were comparable to model EDGE1. This procedure provided the dimensions of bar elements which approached the bending stiffness of the spar cap, spar web and adjacent half panel assembly.

The results of this iterative procedure are shown in figure 12. The curves, shown in figure 12, represent about twenty iterations and are the best possible correlations obtainable. The Z-sections were dimensioned on the basis of the computer run of model EDGE2 corresponding to the curve shown in figure 12.
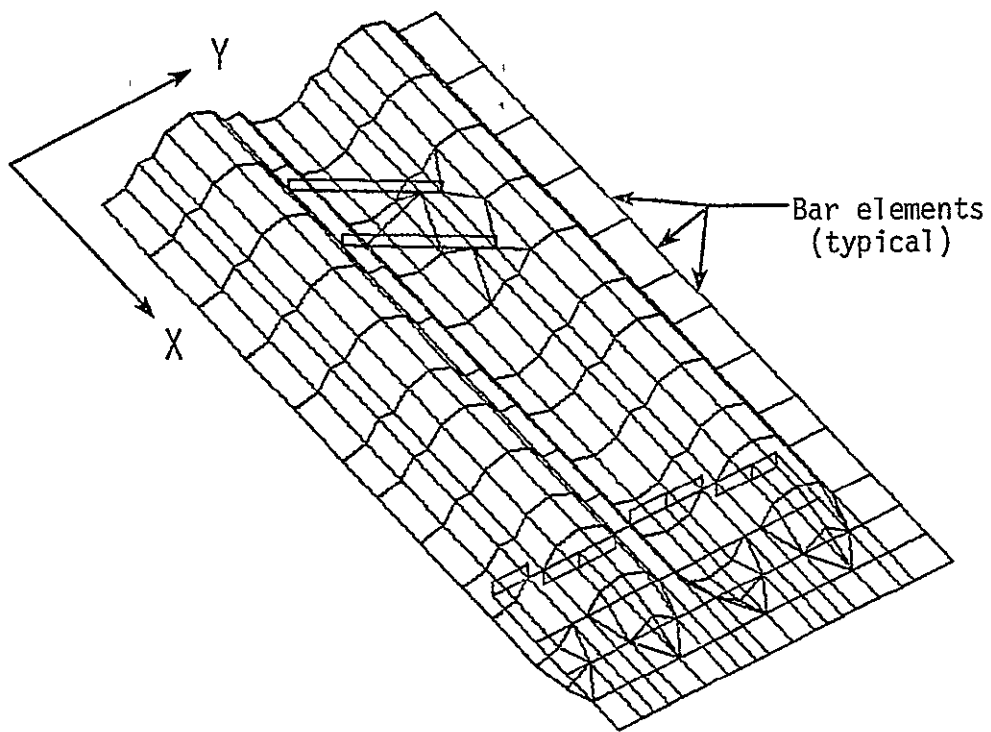
Figure 11.   Nastran model EDGE2.
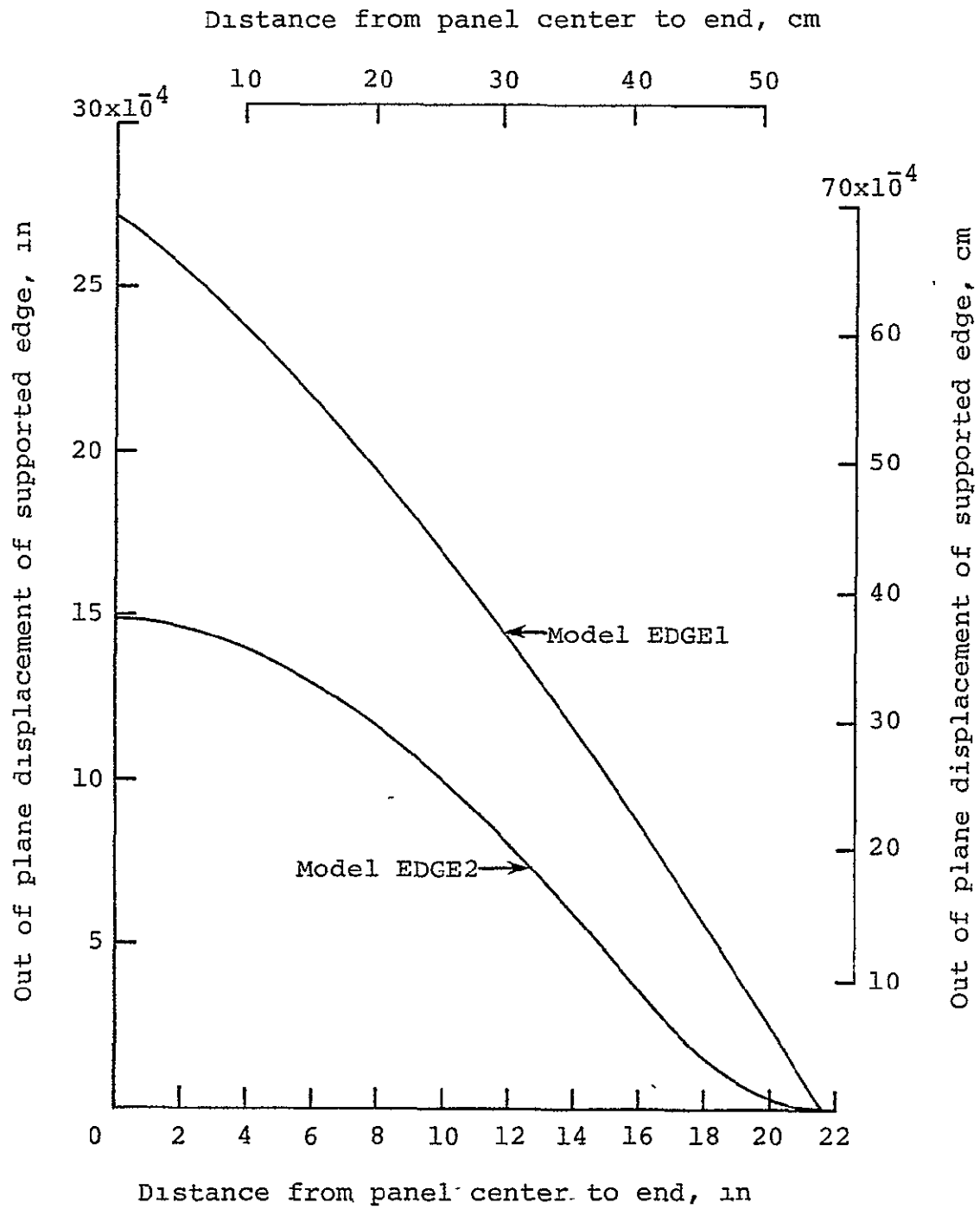
Figure 12. Displacements of the edges of the Nastran models EDGE1 and EDGE2.

End Supports

The end supports shown mounted on the panel (previously shown in figure 9) were made from machined flat tool steel bars. The bars had a rectangular cross section of 1 inch by 0.5 inch (2.54x1.27 cm) and were flat to within 0.001 inches/inch. When mounted on the panel the end stiffeners served two functions. They provided a surface approximately 1.10 inches (2.79 cm) wide (including stiffeners and panel thickness) through which the load was transferred into the panel and eliminated warping of the end of the panel.

After the side and end stiffeners were mounted on the panel, the entire assembly was mounted in a milling machine square with the cutting tool. The end stiffeners were then milled off parallel with one another and perpendicular to the beads. This process was necessary to ensure that bending loads would not be introduced into the panel due to misaligned ends. The side and end stiffeners were not removed after this process had been completed.

Strain Gage Instrumentation

Figures 13 (a) and (b) show the location of the 39 strain gages mounted on either side of the panel to measure strains. The gages are mounted on cross sectional lines corresponding to 1/4, 1/3, and 1/2 the panel length. Of the 39 gages, 33 were standard axial gages. The remaining six gages were grouped into threes and used as equiangular rosettes [labeled 34 and 37 in figure 13(b)]. All of the gages were attached using standard strain gage adhesives.

Positioning of Strain Gages on Beads

As discussed in the Semiclassical Buckling Analysis section (later in this paper), a diagonal mode of local instability which occurs between two adjacent beads has been suggested as a possible failure mode (ref. 2, 3, 4). For the beaded panels, the buckling load for this mode was determined for a value of θ_2 equal to 12.875° (see fig. 14). Thus the majority of gages mounted on the beads were mounted at about 12.8° off of the bead peaks as shown in figure 14. This placed the gages at locations that would optimize their sensitivity to both the proposed diagonal and general instability modes.

The strain gages were mounted at three cross sections of the panel corresponding to 1/2, 1/3, and 1/4 panel lengths. The majority of the gages were mounted on the 1/2 panel cross section, in anticipation of maximum panel deflection at that location. At the 1/3 and 1/4 panel cross sections the gages were clustered around the center three beads [see fig. 13(a) and (b)].
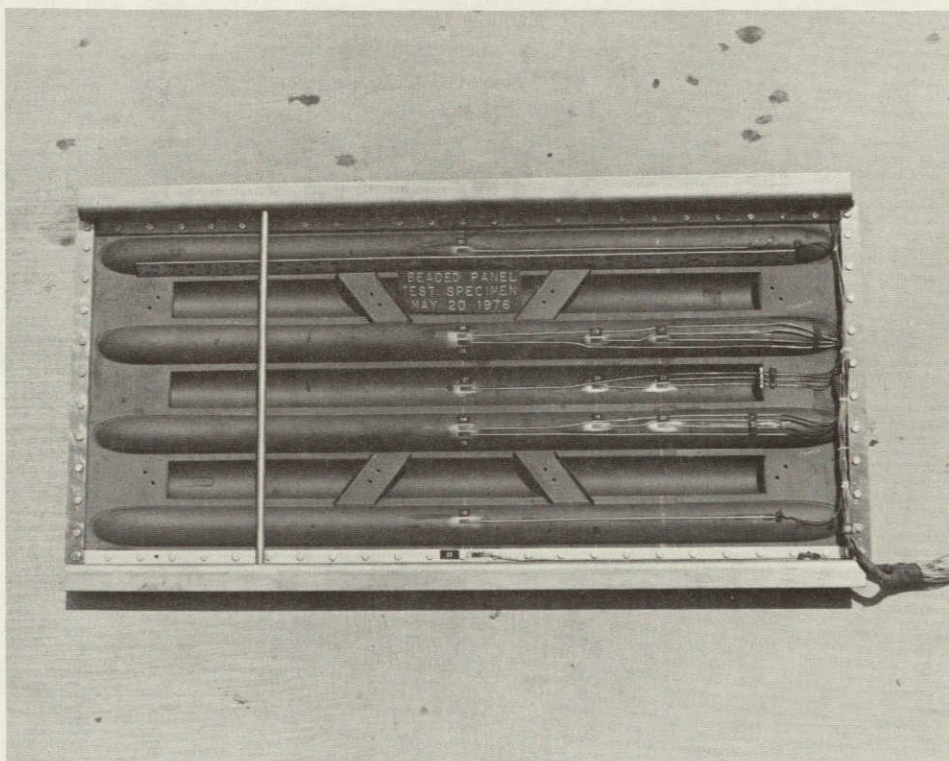
(a) Side 1.
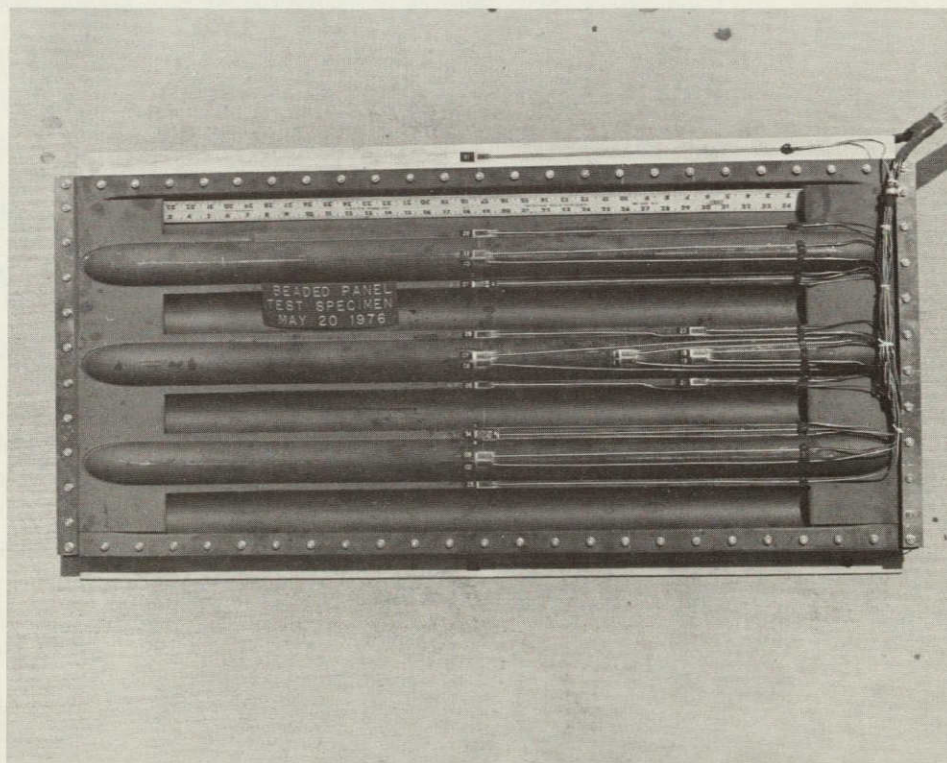
(b) Side 2.

Figure 13.   Strain gage instrumentation locations.   Note: Strain
gage identification numbers should be preceeded by the
number 4 to correspond to the remainder of the report.
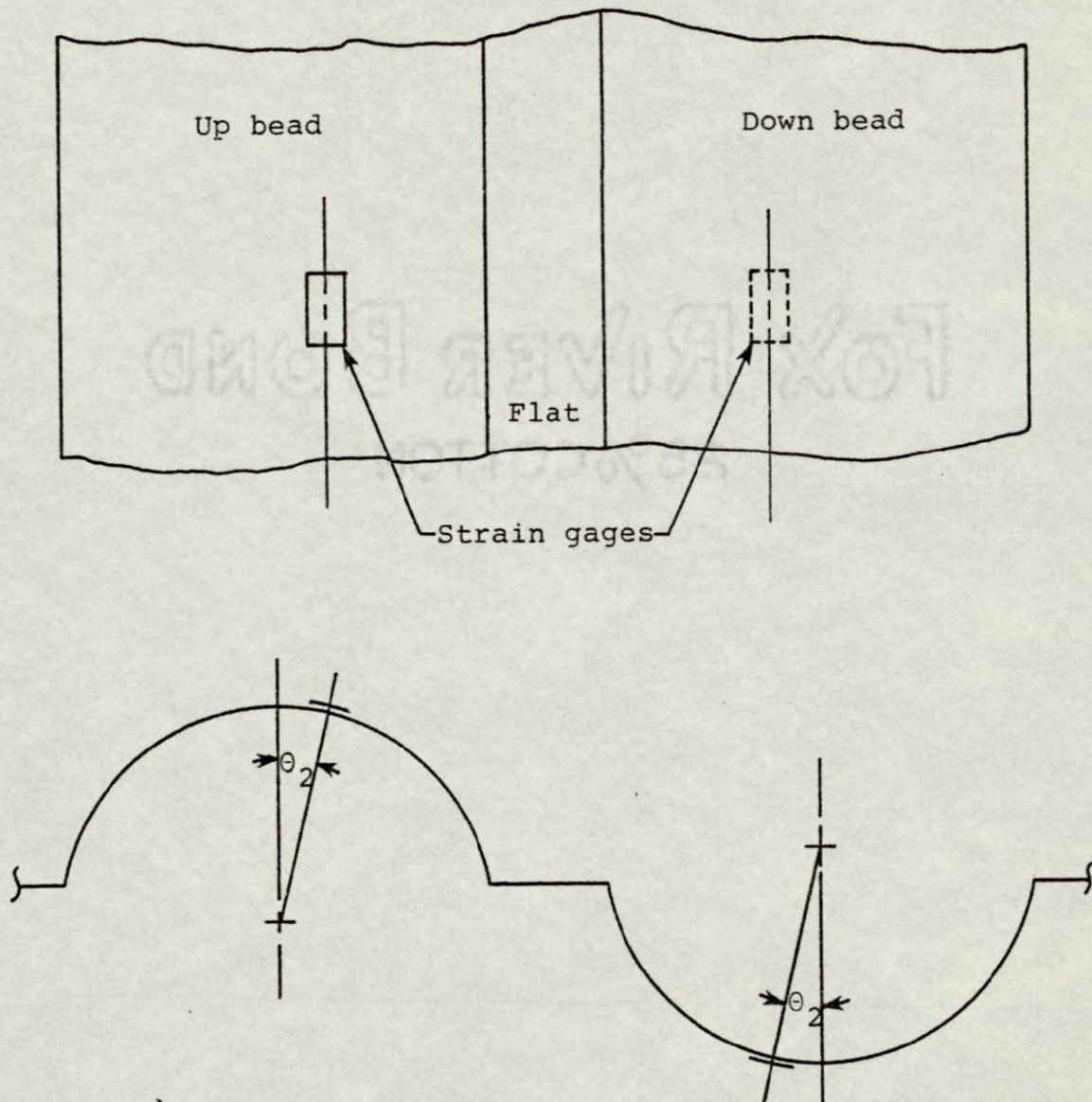
Figure 14. *Location of strain gages mounted on the beads for maximum sensivity to the diagonal mode of instability proposed in the semiclassical analysis.   Note:* $\theta_2 \cong 12.8°$.

Displacement Transducer Instrumentation

Displacement transducers (DT's) were located on panel cross sections at 1/4, 1/3 and 1/2 panel lengths as were the strain gages. As shown in figure 15, five DT's were attached at the 1/2 panel cross section in anticipation of maximum out of plane displacement at that location. Three additional DT's were placed at the 1/4 panel cross section and one DT was located at the 1/3 panel cross section. All nine of these DT's were positioned to measure displacements perpendicular to the plane of the beaded panel. A tenth DT was used to measure longitudinal compression of the panel.

Moiré Fringe Technique Preparations

The photographic material to which the Moiré fringe grid lines were applied was only 0.007 inches (.018 cm) thick (see appendix C). The plastic was attached to a 0.25x20x42 inch (.62x50.8x106.7 cm) sheet of plate glass to enable mounting the grid plane in front of the panel. Mineral oil was used as an adhesive between the glass and the plastic. Excess oil was squeezed from between the glass and the plastic creating a thin uniform adhesive bond.

The Moiré fringe glass was supported by aluminum bars which ran the length of the glass. A 0.25 inch (0.64 cm) groove was cut into each of the aluminum bars and the glass fitted and glued with silicone rubber cement into the grooves. The aluminum bars were then attached to the panel by aluminum brackets such that the grid was maintained parallel and at a fixed distance from the ends of the panel. The bottom
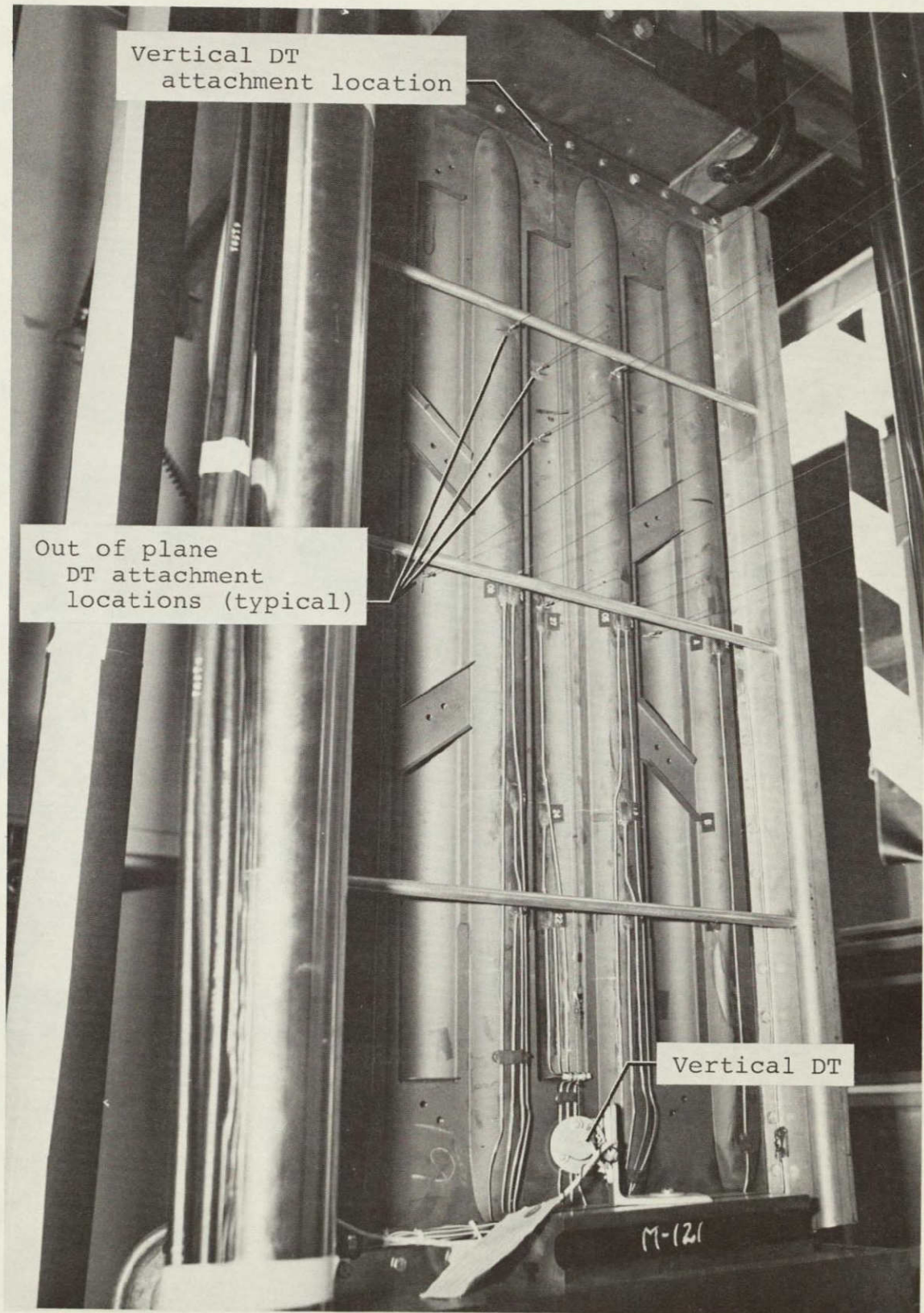
Figure 15.   Displacement transducer (DT) locations.

brackets were rigidly attached to the panel and the top ones were free to slide, thus preventing the glass from taking any load and possibly breaking, or from deflecting and causing errors in the measurements. The distance from the top of a bead to the surface of the glass was approximately 0.25 inches (0.64 cm) in the unloaded condition. Prior to mounting the glass to the panel, the panel was painted white to create a greater contrast between the dark and light fringes.

The camera film plane was located about 60 inches (152.4 cm) from the surface of the glass (S_1 in fig. Cl in appendix C). The distance between the camera and the light source, was 60 inches (152.4 cm) (S_2 in fig. C2 in appendix C).

According to reference 12, it is necessary to use a point source of light when the field of interest is large. Therefore, a photographic flash with a 1 inch by 0.2 inch (2.54x.51 cm) iris was used as a light source for this project. The iris effectively created the necessary point source of light. Figure 16 is a photograph of the entire photographic system in place.

Test Equipment

The panel was tested in a universal compression-tension testing machine. Figure 17 shows the panel mounted in the machine. The platens which come into direct contact with the panel were specially made and machined flat to within 0.001 inches/in. The platens helped to insure that the load introduced into the panel was purely axial in nature and that bending loads due to misaligned heads would be eliminated. The bottom platen rested on a spherical seat which insured
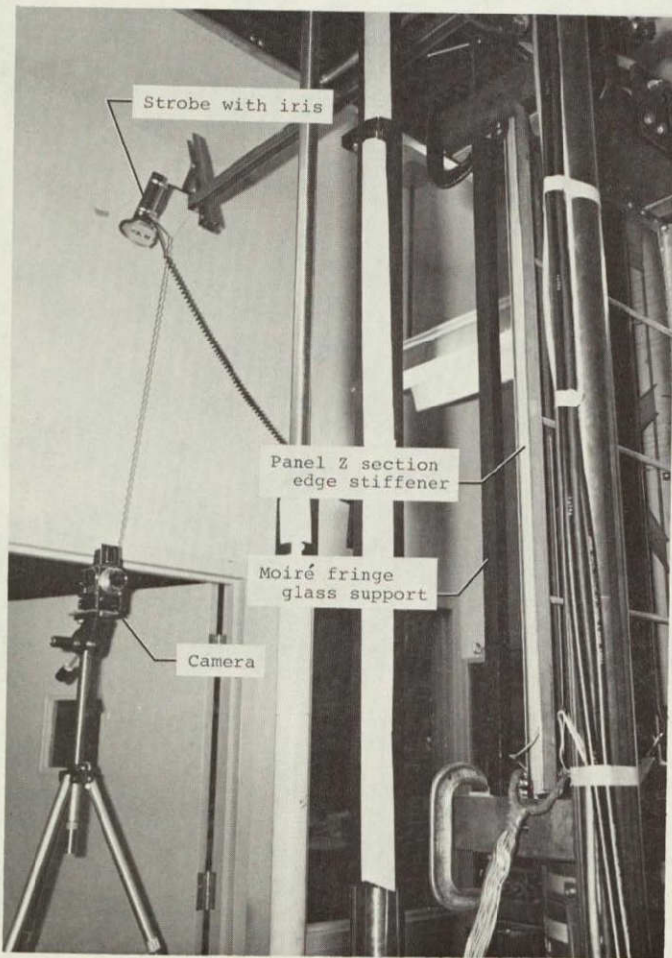
Figure 16. *Moiré fringe photographic equipment positions.*

Labels: Strobe with iris; Panel Z section edge stiffener; Moiré fringe glass support; Camera
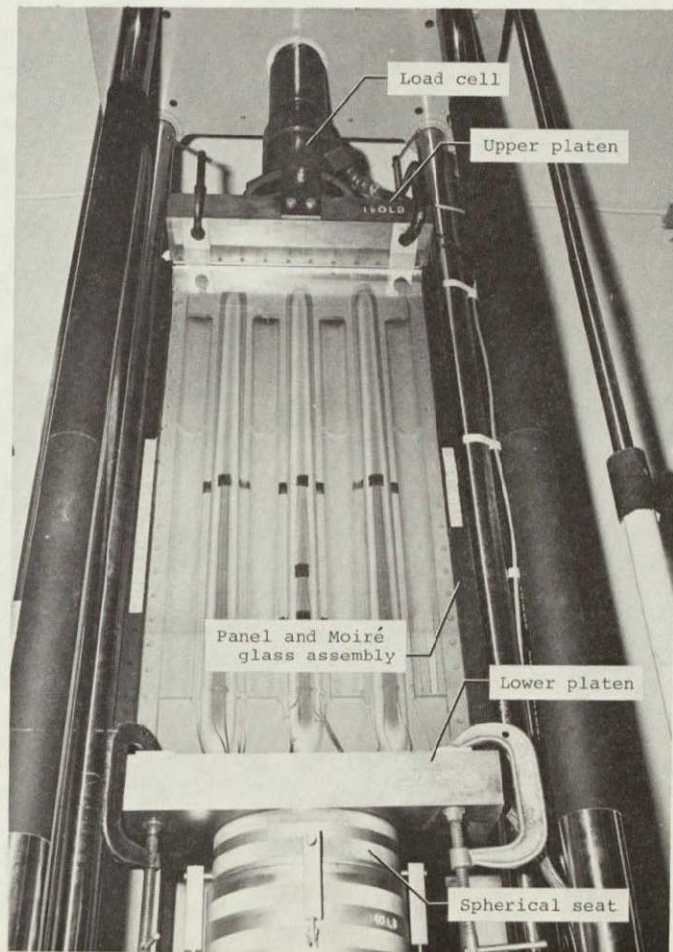
Figure 17. *Beaded panel test assembly installed in the testing machine.*

Labels: Load cell; Upper platen; Panel and Moiré glass assembly; Lower platen; Spherical seat

Test Procedure

A total of 19 tests were performed on the panel up to the failure test of 48,600 pounds (216,184 N). The first two tests were system checkout tests of 2,000 and 10,000 pounds (8,900 and 44,480 N) respectively. The remaining 17 tests were buildup tests to failure.

A typical test would begin by warming up the testing machine for 30 minutes. Before loads were applied to the panel, Moiré fringe calibration photographs were taken. In addition, strain gage and displacement transducer zeros were recorded by the data acquisition system. After data sampling was started at prescribed rates, loads were applied to the panel. At predetermined load points, the load was held constant and Moiré fringe photographs were taken. This process was repeated until the maximum load was reached.

DISCUSSION OF EXPERIMENTAL RESULTS

Moiré Fringe and Displacement Transducer Results

The Moiré fringe photographs proved to be extremely useful for identifying the elastic buckling load and the mode shape. The Moiré fringe photographs show subtle changes in panel curvature which might not have been otherwise detected. Experimental data, including Moiré fringe data, is included in appendix A.

Figure A1(a) is a calibration photo taken while no load was being applied to the panel. Calibration bars (with different slopes) are shown in the upper and lower right corners of the panel between the glass and the panel. The bars were used to verify uniform calibration from end to end. Note that the beads and flats are all straight in figure A1(a) as indicated by constant fringe patterns on bead peaks and flats.

Figure A1(b) shows the panel under an applied load of 24,000 pounds (106,760 N). A very slight curvature of the center two flats is visible, compressing the sides of the center bead. This inward deflection is even more apparent at 36,000 pounds (160,140N), as shown in figure A1(c). The sides of the other beads are similarly compressed inward or spread outward but to a lessor extent than the center bead. This deflection represents lateral distortion of the panel across section due to out-of plane bending.

The first visible indication of elastic buckling of the panel occurred at 40,000 pounds (177,930 N), as shown in figure A1(d). The flat immediately to the left of the center bead has changed its direction of lateral deflection and is now moving outward, away from the center bead, instead of its original inward direction. At 42,000 pounds

(186,825 N), shown in figure A1(e), this change in curvature is distinct, while at 44,000 pounds (195,520 N), shown in figure A1(f), it is quite pronounced   This mode of buckling is similar to the diagonal mode of instability discussed later in the semiclassical analysis section

In figure A1(g) the panel is under an applied load of 48,500 pounds (215,740 N). Severe curvature of the center bead and the inner most flats is clearly visible. Unlike figure A1(f) which shows the panel under an applied load of 44,000 pounds (195,720 N), the beads immediately adjacent to the center bead are beginning to exhibit curvature similar to that of the center bead. The remaining beads, however, remain relatively straight. This curvature of the panel center portion suggests that the center portion of the panel is carrying less of the applied load, having transferred some of the load to the outer portions of the panel. This load transfer was further substantiated by the strain gage results which will be discussed in the next section.

Ultimate panel failure occurred at a load of 48,600 pounds (216,184 N). Figure A1(h) is a Moiré fringe photo taken after failure. Figures A1(i) and (j) are photos of the panel after failure. Permanent deformation is visible in these photos. These figures show that the panel suffered catastrophic local failure at the center of the panel. Local failures are also visible between the fasteners on the panel edges.

Out-of-plane displacement measurements using the Moiré fringe tech- nique were made at 49 locations as shown in figure A2(a). All of the measurement points were located on the peaks of the seven beads. Note that the panel deflected away from the Moiré fringe glass. In figure A2(b) through (h), plots of out-of-plane displacements are shown for each individual bead. Where possible, displacement transducer data is

also plotted. The curvature of these plots indicate that the panel was loaded eccentrically which caused out-of-plane bending of the panel even at small loads. The eccentric behavior was the result of loading the panel through the flat end of the panel, rather than the neutral axis of the panel/side stiffener assembly. The maximum out-of-plane displacement at a load of 48,500 pounds (215,740 N) was 0.432 inches (1.097 cm) as shown in figure A2(e). This displacement occurred on the center bead at point 25 in figure A2(a).

Strain Gage Results

Initial interest in the strain gage results was focused upon the degree to which uniform loading had been accomplished. Uniform loading, in this case, refers to a uniform load across the entire width of the panel. The two rosettes (gages 434 and 437) mounted on the panel flats provided part of this information by making it possible to resolve the axial strains into principle strains and principle directions. At all load levels the difference between the measured longitudinal strain and the calculated principle strain was negligible. In addition, the direction of the principle strains varied by a maximum of only 5° from an axis parallel to a bead. This small variation indicated that the load was introduced into the panel in a uniform manner and that there was virtually no shear. Sample data is shown in table 4 for a load of 20,000 pounds (88,960 N).

Another indication of the uniformity of the load is illustrated by the data shown in figure 18. This figure shows the strains from all strain gages recorded at a load of 2,000 pounds (8,900 N). At this

low load very little bending is present, thus the indicated strain is due primarily to axial compression. Similar comparisons of strains on beads at higher loads cannot be made due to the increased effects of bending. However, strain comparisons can be made of the responses of gages mounted on flats at higher loads. Figure 19 shows the strain measurements made at four load levels on the flats at the center cross section. The maximum difference between any two gages at a particular load is 150 microinches/inch. The data in this figure shows that (1) the strains are increasing in nearly equal increments with each load level and (2) that the compressive load is uniform across the beaded panel cross section up to the onset of elastic buckling (about 40,000 pounds or 177,930 N).

Table 4. Principle strains and their directions at a load of 20,000 pounds (88,960 N). Strains in µinches/inch.

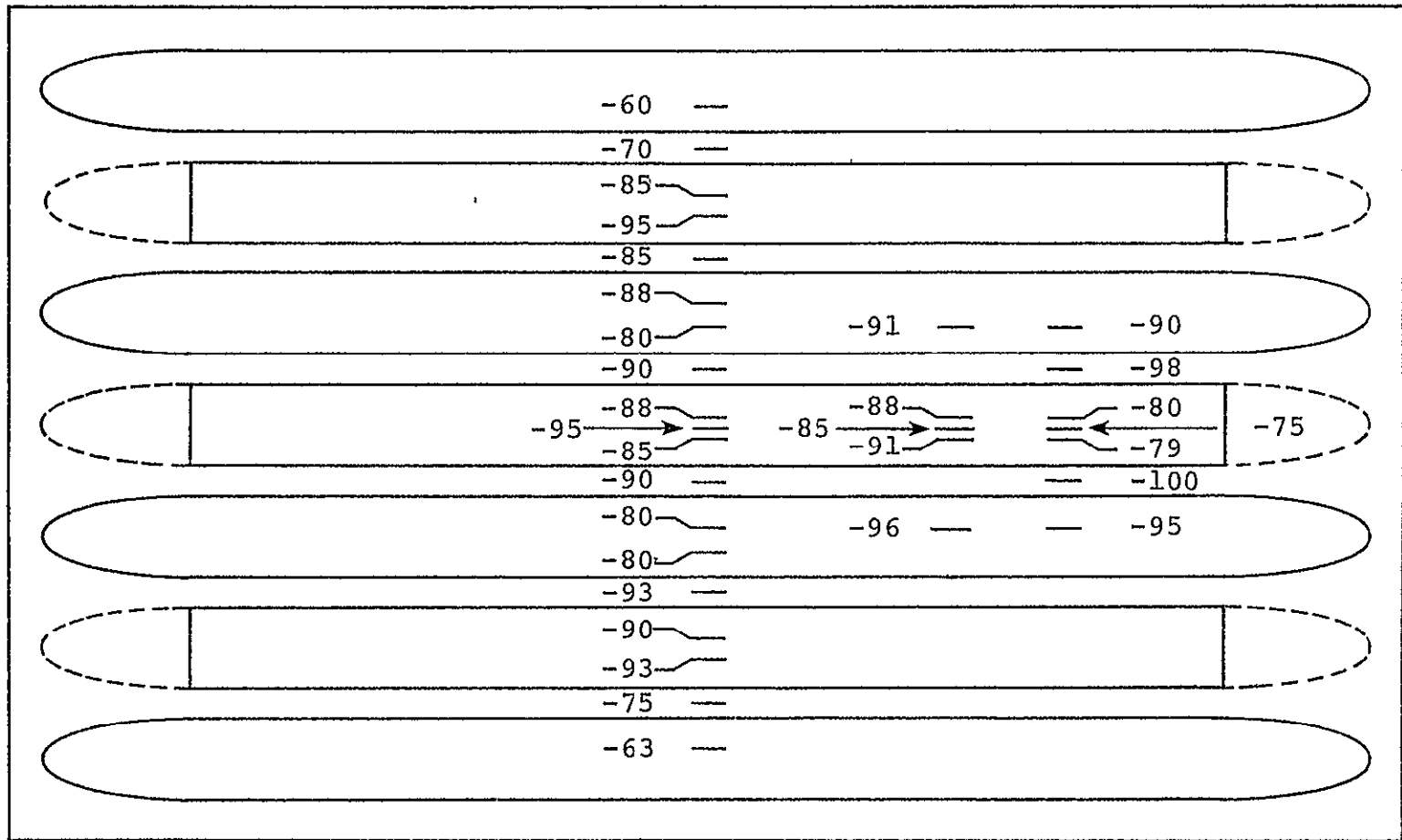| Rosette 34		Rosette 37	
measured	calculated	measured	calculated
Leg A -876	ε_1 -876	Leg A -864	ε_1 -868
Leg B - 25	ε_2 -252	Leg B - 78	ε_2 -272
Leg C - 35	γ - 12	Leg C + 48	γ 145
principle angle 89.7°		principle angle 86°	

Figure 18. Strains recorded by axial gages at an applied load of 2,000 pounds (8,900 N) in μinches/inch.
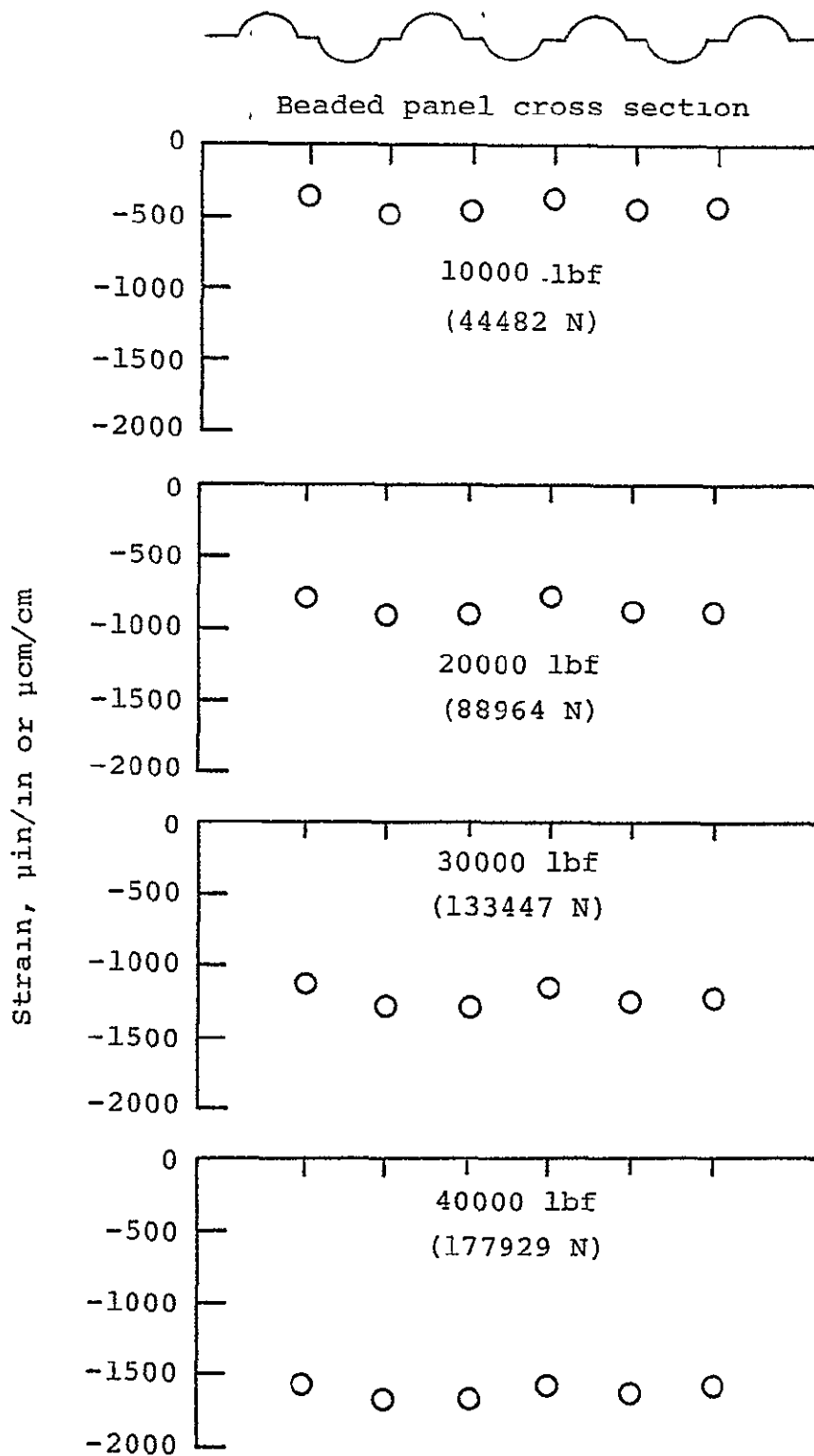
Figure 19. Strain measurements recorded by gages mounted on the center section of the beaded panel.

Individual strain gage plots are shown in figures A3(a) through (w). Most of these plots are nonlinear. These nonlinearities are due to out-of-plane bending which is the direct result of eccentric loading of the panel.

This nonlinear load deflection response is typical for most column structures under compressive load (ref. 17) and is the reason for the difficulty associated with pinpointing elastic buckling loads from strain gage plots alone. A column with no eccentricities and concentric loading would have a load-bending deflection response similar to that shown in figure 20(a). This figure represents a perfect column under compressive load, where the column simply compresses until the buckling load is reached. For a column with eccentricities (or eccentric loading) the load-bending deflection response is represented by figure 20(b) where α_1 is a measure of the eccentricity and $\alpha_1 < \alpha_2 < \alpha_3$ etc. Since the beaded panel was eccentrically loaded, the strain gage plots are similar to figure 20(b). In those cases where the strain gage measured axial compression plus compressive bending, the resulting plot is similar to that shown in figure A3(b). For the case where the gage measured axial

Figure 20. *Load bending-deflection responses for structures with (a) no eccentricities and (b) with eccentricities of magnitude α_i.*

compression plus tensile bending, the plots are similar to that shown
in figure A3(h), (note the reverse curvature). A precise determination
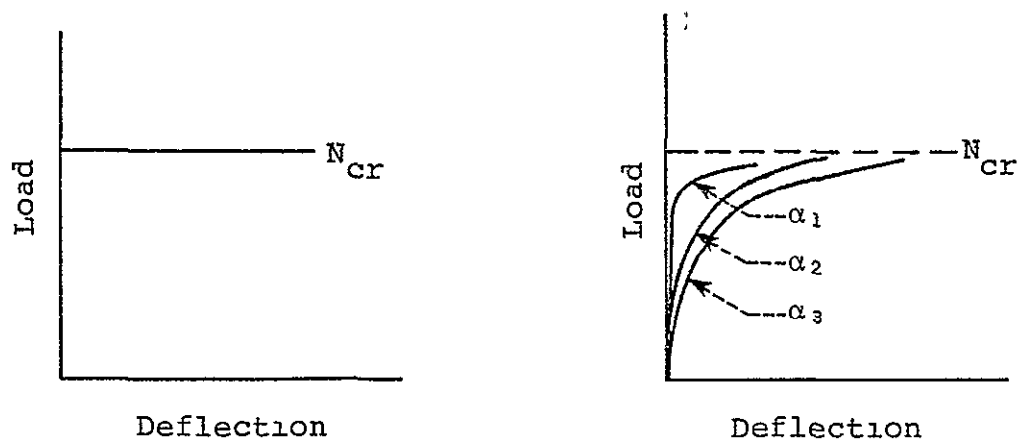of the buckling load for such plots is difficult because the curves do
not exhibit a pronounced change which identifies buckling. In the case
of the beaded panels, the situation is further complicated by the fact
that the elastic buckling mode, as shown in the Moiré fringe photos, has
a lateral component which is perpendicular to the deflection due to the
eccentric loading. The best indication of buckling from the strain gage plots
is given by gages which are mounted on the flats which are relatively
insensitive to out-of-plane deflection (bending), since they are much
closer to the neutral axis of the panel (gages 426 and 428 in figures
A3(q) and (r), for example).

Figure 21 is a plot of the average strains recorded by all of the
gages mounted on the flats (between beads) at the center cross section
of the panel (gages 425, 426, 428, 429, 434, and 437). Up to about
40,000 pounds (177,930 N) the average strain gage response is linear.
This load corresponds to that at which elastic buckling of the center
of the panel occurred as shown in the Moiré fringe photos. The average
strain at 40,000 pounds (177,930 N) from figure 21 is 1600 microinches/
inch and does not increase appreciatively at loads above 40,000 pounds
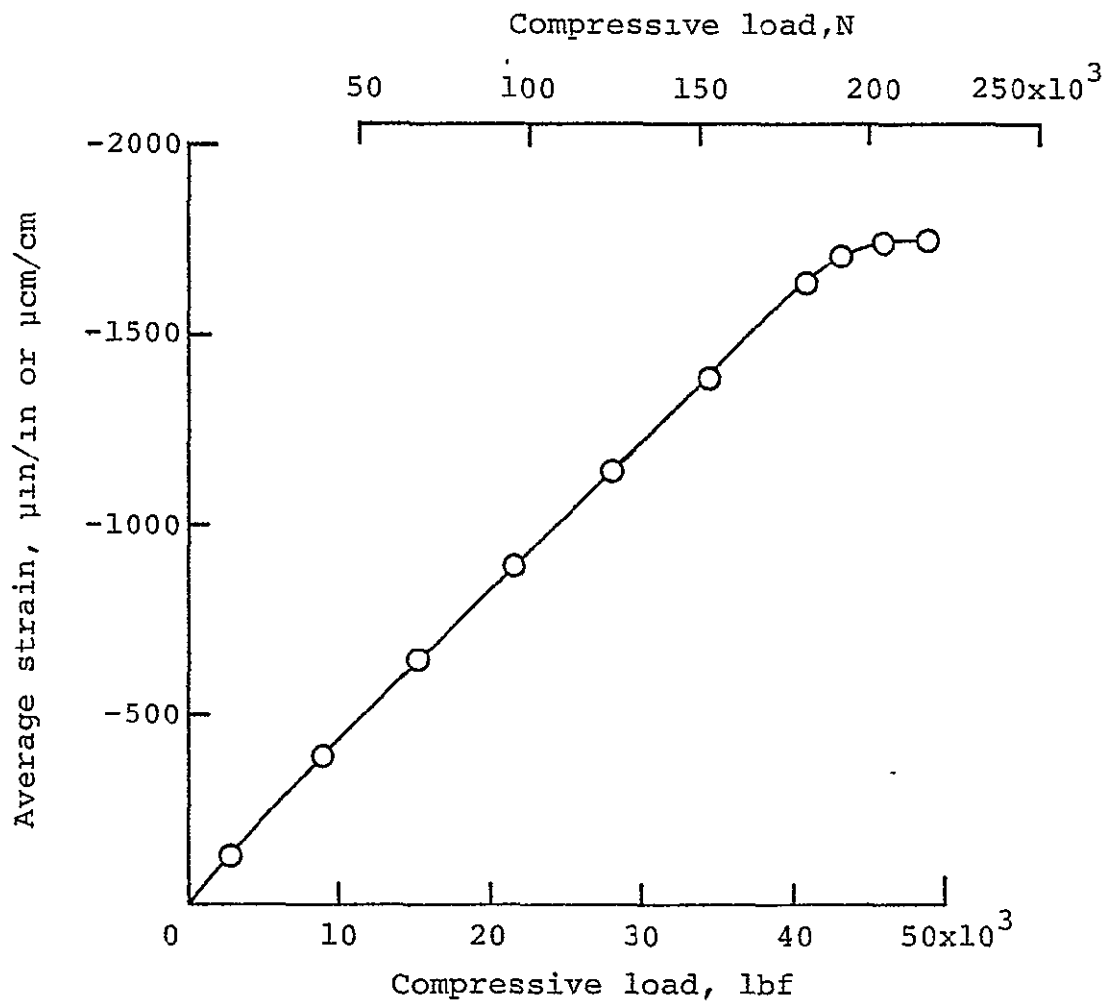(177,930 N).

Figure 21. Average of strains recorded by gages mounted on the flats of the beaded panel at the center cross section.

Force/Stiffness Results

Force/stiffness plots are shown in figures A4(a) through (j).
With the exception of plots (c) and (j), the curves were extrapolated
to indicated failure loads using a second order Lagrange polynomial
(ref. 18). The accuracy of the predictions are affected by the extra-
polation procedure used i.e., linear, second order, third order, etc.
A second order procedure was used for this project since the curves
extrapolated were generally quadratic in nature.

The most important results of this analysis are shown in figures
A4(c) and (j). In these two plots, very pronounced inflections occur
at about 40,000 pounds (177,930 N) as indicated in the figures.
According to reference 11 these inflections indicate changes in the
mode of deflection. More specifically, the inflections are caused by
elastic buckling of the panel which occurred when the flats on either
side of the center bead began moving in the same lateral direction.
Since the inflection points themselves indicate elastic buckling, the
curves were not extrapolated. It should be pointed out that the
significance of these inflections in figures A4(c) and (j) was re-
alized only after correlations between Moiré fringe and strain gage
data were made.

Other results of particular interest are the plots of gages at the
center cross section of the panel. Extrapolations of plots A4(a), (b),
(d), (e), and (f) all intersected the load axis at between 50,850 to
55,000 pounds (226,200 to 240,650 N). These indicated buckling loads
are for the mode of deflection associated with out-of-plane deformation

only. Had the panel not failed elastically at 40,000 pounds (177,930 N) in a mode characterized not only by out-of-plane deflection, but lateral deflection also, it may have supported loads up to the indicated buckling load. Force/stiffness predictions from gages mounted at the 1/4 and 1/3, panel lengths ranged from 53,750 to 61,750 pounds (239,100 to 274,680 N). The larger predictions came from gage pairs mounted at locations which were relatively unaffected by the elastic failure which occurred at the center of the panel. These results point out that the strain gage pairs must be in close proximity of the failure for the most accurate results.

Two points should be made regarding similarities between the experimental results, i.e., modes of deflection, and the modes of instability suggested by the semiclassical analysis (discussed later in this paper). One suggested mode of instability used to analyze the panels, is characterized by a lateral deflection corresponding to the lateral deflection which occurred beginning at 40,000 pounds (177,930 N). In the semiclassical analysis this mode of instability has been called the diagonal mode. Secondly, the out-of-plane deformation of the panel corresponds to one of the suggested instability modes in the semiclassical analysis, known as the general instability mode. The semiclassical analysis section contains a further discussion of the suggested modes of instability.

Edge Stiffener Performance

The edge stiffeners (Z-sections) used to support the edges of the beaded panel were intended to simulate the stiffness of a wing mounted condition. The out-of-plane displacements of the center of the beaded panel edge were compared with similar measurements taken from a panel mounted in the hypersonic wing test structure. The deflection of the beaded panel/Z-section edges were larger than the corresponding HWTS panel edges. Thus, the Z-sections were stiffened with 1x1x42 inch (2.54x2.54x106.68 cm) steel bars which were bolted to the free edges of the Z-sections as shown in figure 22. The out-of-plane displacement of the beaded panel/stiffened Z-section edge (at the center) for a compressive load of 950 lbf/in (1660 N/cm) was 0.015 inches (0.038 cm). The corresponding measurement of the beaded panel mounted in the HWTS was 0.024 inches (0.061 cm).

The reason for the conservative panel/Z-section deflection are two-fold. First, an incorrect load level was taken from the HWTS data and used for comparison purposes. Secondly, the Nastran calculations of out-of-plane deflections were found to be inadequate (see section on computer analysis). However, the edge stiffeners did prevent premature edge failures and in general performed satisfactorily.

It was discovered during the initial tests of the beaded panel, that the free edges of the Z-sections tended to pull away from one another (buckle laterally) under load. To prevent a premature lateral buckling failure of the Z-sections, 0.5x0.25 inch (1.27x0.64 cm) steel straps were used to tie the Z-sections together, as shown in figure 22.
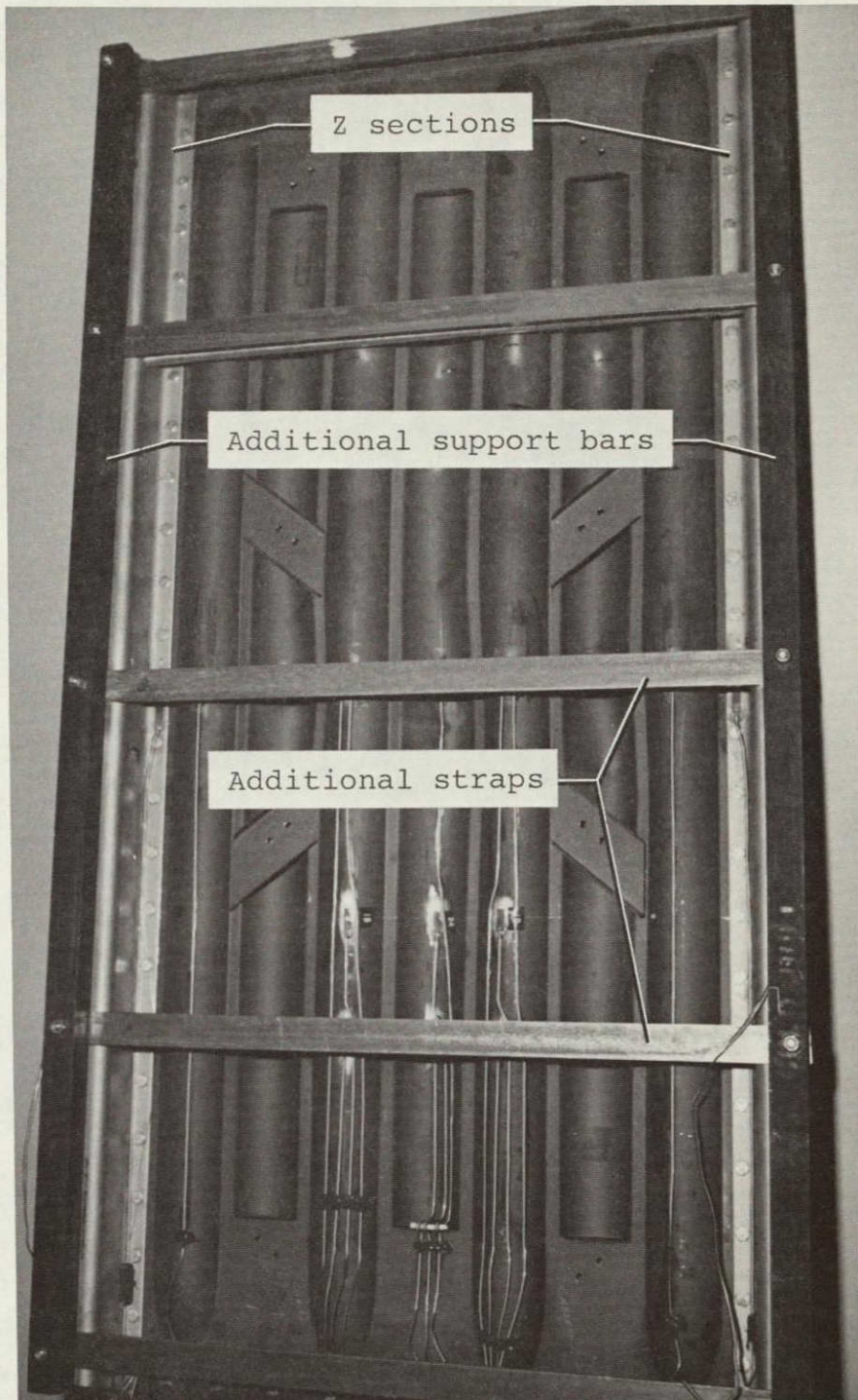
Figure 22. Additional edge support bars and straps mounted on the panel.

NASTRAN COMPUTER MODEL DESCRIPTIONS AND DISCUSSION OF RESULTS

Introduction

Nastran structural analysis (ref. 13) was used as a tool to compute deflections, stresses and the buckling strength of portions of the panel as well as the entire panel. Secondly, Nastran was used as an aid to design the edge stiffeners as previously discussed.

A total of five structural models were made and used in the analysis process. Models EDGE2 and EDGE3 were 1/4 and 1/2 panel models, respectively. Each of these models were used to determine the strength, deflection and buckling characteristics of the beaded panels. The 1/2 panel model EDGE3 was made after the results of the buckling analysis done with the 1/4 panel model EDGE2 were found to be inadequate. The remaining three models entitled BEAD, FLAT and DIAG, were used to analyze instability modes suggested in the semiclassical analysis classified as bead, flat and diagonal modes of instability, respectively.

The results of the computer analysis done with models EDGE2 and EDGE3 will be compared with the experimental results previously discussed. The other three models, BEAD, FLAT and DIAG will be compared to the semiclassical analysis only.

Finite Element Model EDGE2:   Description

and Results of Analysis

Figure 23 is a computer generated plot of model EDGE2. It is a
quarter panel model, and takes advantage of the two lines of symmetry
of the beaded panel. It consisted of 306 elements, 298 grid points and
1443 degrees of freedom. EDGE2 utilized dimensions and thicknesses of
the panel as determined by direct measurements. In addition, the eccen-
tricities which were measured after the edge stiffeners and end supports
had been mounted were also incorporated into the model.

Figure 23 also shows the direction of the loads applied to model
EDGE2. The letters along the sides of the model indicate the restricted
degrees of freedom. For example; x indicates that translation in the
X-direction is restricted, Rx indicates rotation about the X-axis is
restricted. The boundary conditions along the right and lower sides of
the panel were relatively straight forward to define, since the panel
attaches to spar and rib caps at these boundaries. However, the boundary
conditions along the cut edges (lines of symmetry) were not as easy to
formulate. This was especially true of the instability or buckling
analysis. The mode shape prior to testing was expected to be the gen-
eral instability mode (See semiclassical analysis section). Therefore,
the boundary conditions along the cut edges of the panel model were
varied in a trial and error procedure until plots of the buckled shape
resembled the general instability mode.

The results of the buckling analysis performed by model EDGE2 were
poor. An elastic buckling load of 31,700 pounds (141,000 N) was calcu-
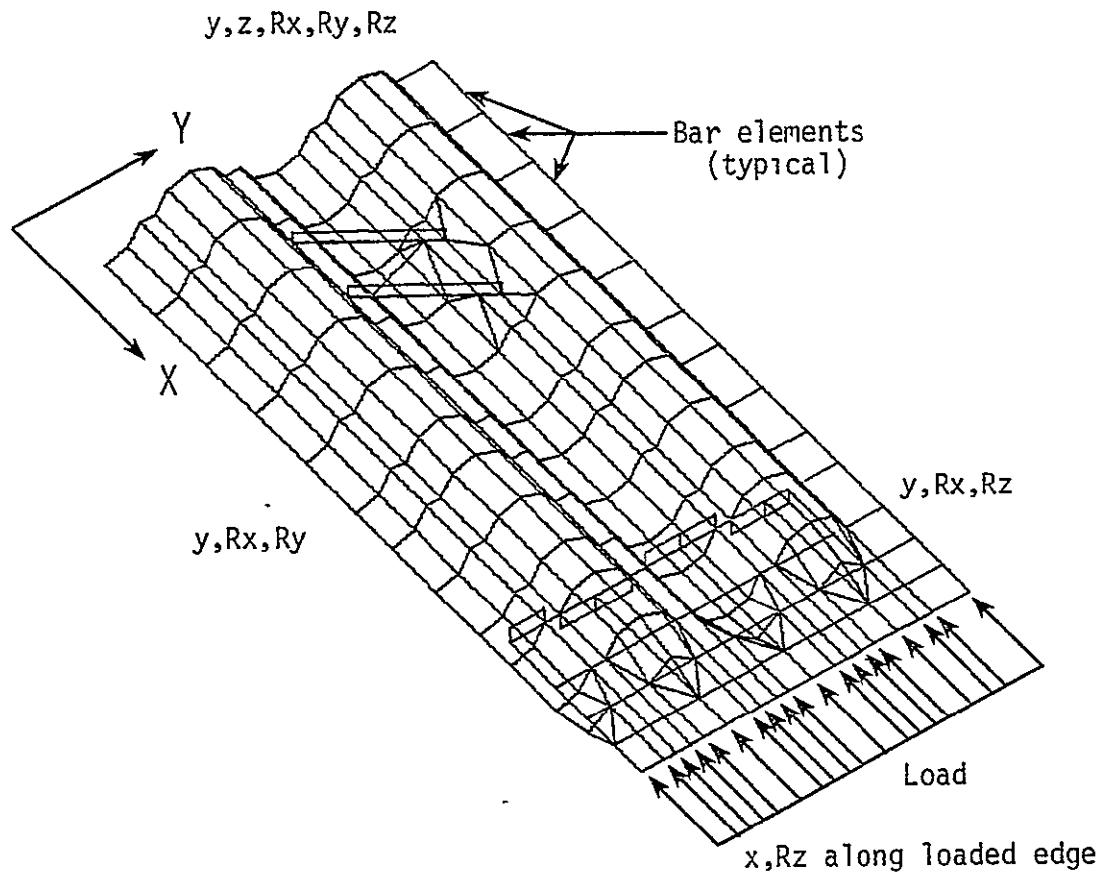lated which compares with an actual elastic buckling load of about

Figure 23. *Finite element buckling model EDGE2. The restricted degrees of freedom indicated along the sides of the model are for buckling analysis only.*

40,000 lbs (177,930 N). The predicted load was 26% lower than the actual failure load. This large descrepancy prompted the development of the 1/2 panel model, EDGE3. The reason for the large difference between the results of the buckling analysis utilizing model EDGE2 and the experimental results is very probably caused by the problems associated with prescribing boundary conditions along the cut edge of the model (i.e., the line of symmetry parallel to the center bead).

It should be noted that initially the analysis done with model EDGE2 was done assuming a perfectly flat structure, i.e., with no eccentricities. However, the difference in results between the analysis including eccentricities and the analysis without eccentricities was insignificant.

Finite Element Model EDGE3· Description
and Results of Analysis

Model EDGE3 shown in figure 24 was a full half panel model consisting of 920 elements, 842 grid points and 4591 degrees of freedom. As in model EDGE2, the dimensions and thicknesses used in model EDGE3 were measured directly from the panel. Measured eccentricities were not included since previous experience with model EDGE2 had shown that inclusion of the eccentricities had an insignificant effect on the results of the analysis.

Figure 24 also shows the direction of the loads which were applied to the panel and the restricted degrees of freedom. The same degrees of freedom used in model EDGE2 were also used in EDGE3.

The buckling analysis using EDGE3 gave an elastic buckling load
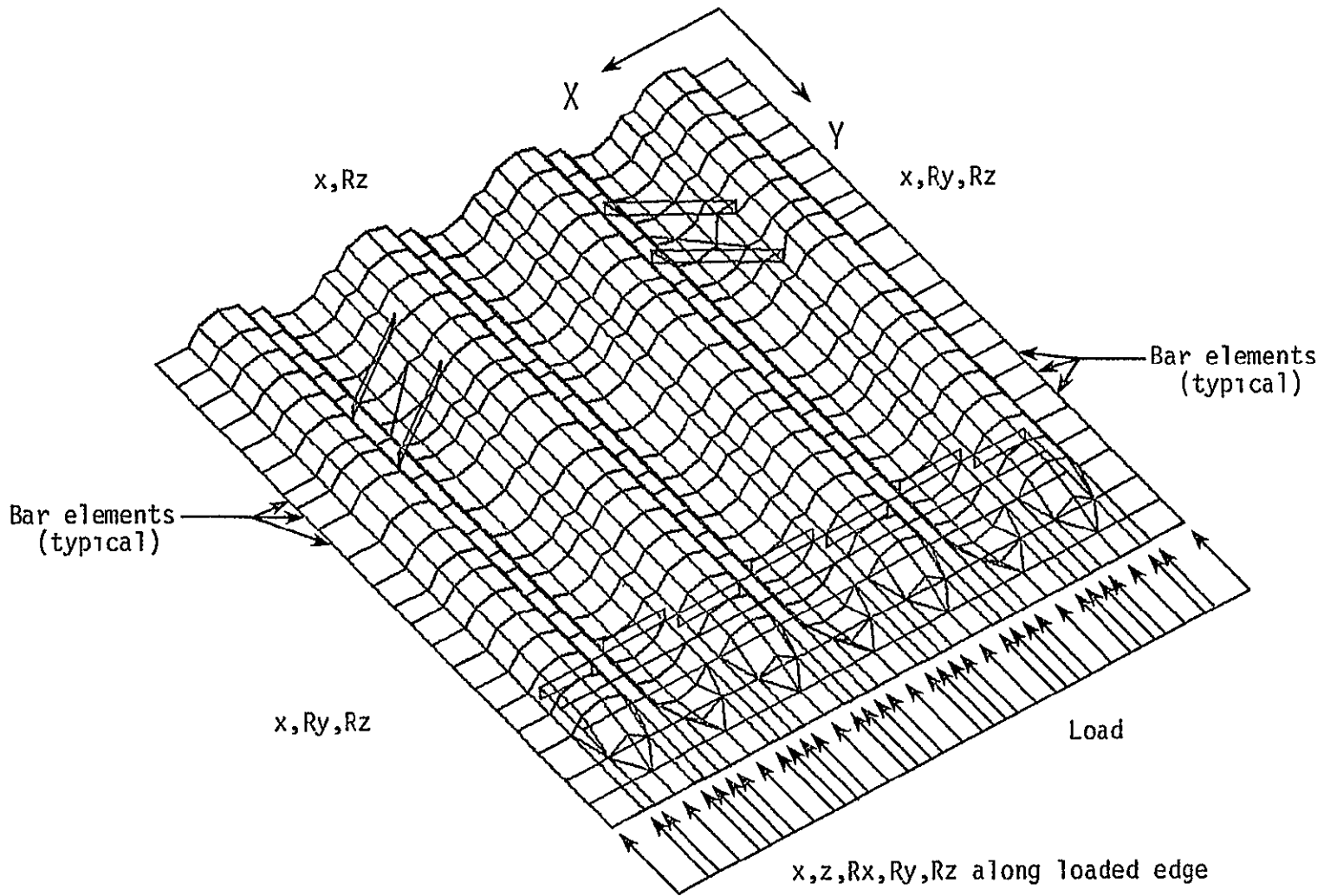
Figure 24. Finite element buckling model EDGE3. The restricted degrees of freedom indicated along the sides of the model are for buckling analysis only.

of 50,000 pounds (222,400 N). This calculated load compared to an actual elastic buckling load of about 40,000 pounds (177,930 N) representing an error of 25%. The magnitude of the error reflects the accuracy of the model for the buckling analysis.

The Nastran static analysis program exhibited an inability to account for the nonlinear effects of out-of-plane bending with loads applied in the plane of the panel. Thus comparisons of calculated and experimental stresses across the entire panel, could only be made at relatively low loads, where the effects of bending were small. In addition, stress comparisons at higher loads could only be made on the flats where the effects of bending were not predominant. For example, figure 25(a) is a plot of the stresses at the center cross section of the panel, at a load of 10,000 pounds (44,480 N) using models EDGE2 and EDGE3 as well as the experimentally derived stresses. At 10,000 pounds (44,480 N) a good correspondence exists between the analysis and experimental results across the entire panel. However, the experimentally derived stresses on the beads of the panel are noticeably affected by out-of-plane bending whereas the computer analysis results are not. Figures 25(b) and (c) are plots of the stresses at the center cross section at 24,000 and 36,000 pounds (106,760 and 160,140 N), respectively. Pronounced bending effects can be seen in the experimental results; these effects are not accounted for by Nastran static analysis (with applied in-plane loads). On the flats, where bending has less effect, good comparisons are possible even at the higher loads.

The results of the analysis using these finite element models point out the need for further research in the area of finite element buckling analysis for the beaded panels. The development of a full panel model would be one possibility for further study.
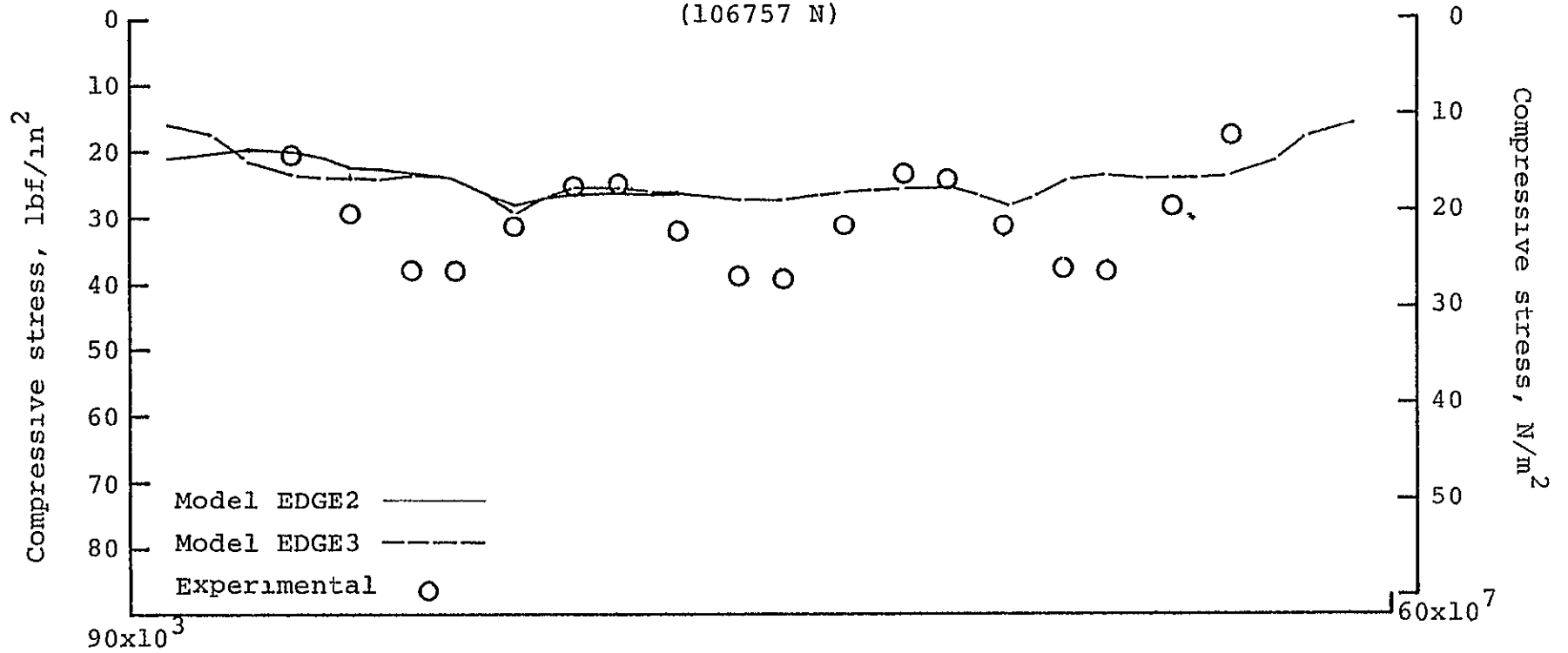
Beaded panel computer model cross section

10000 lbf

(44482 N)

Model EDGE2 ————
Model EDGE3 — — —
Experimental   O
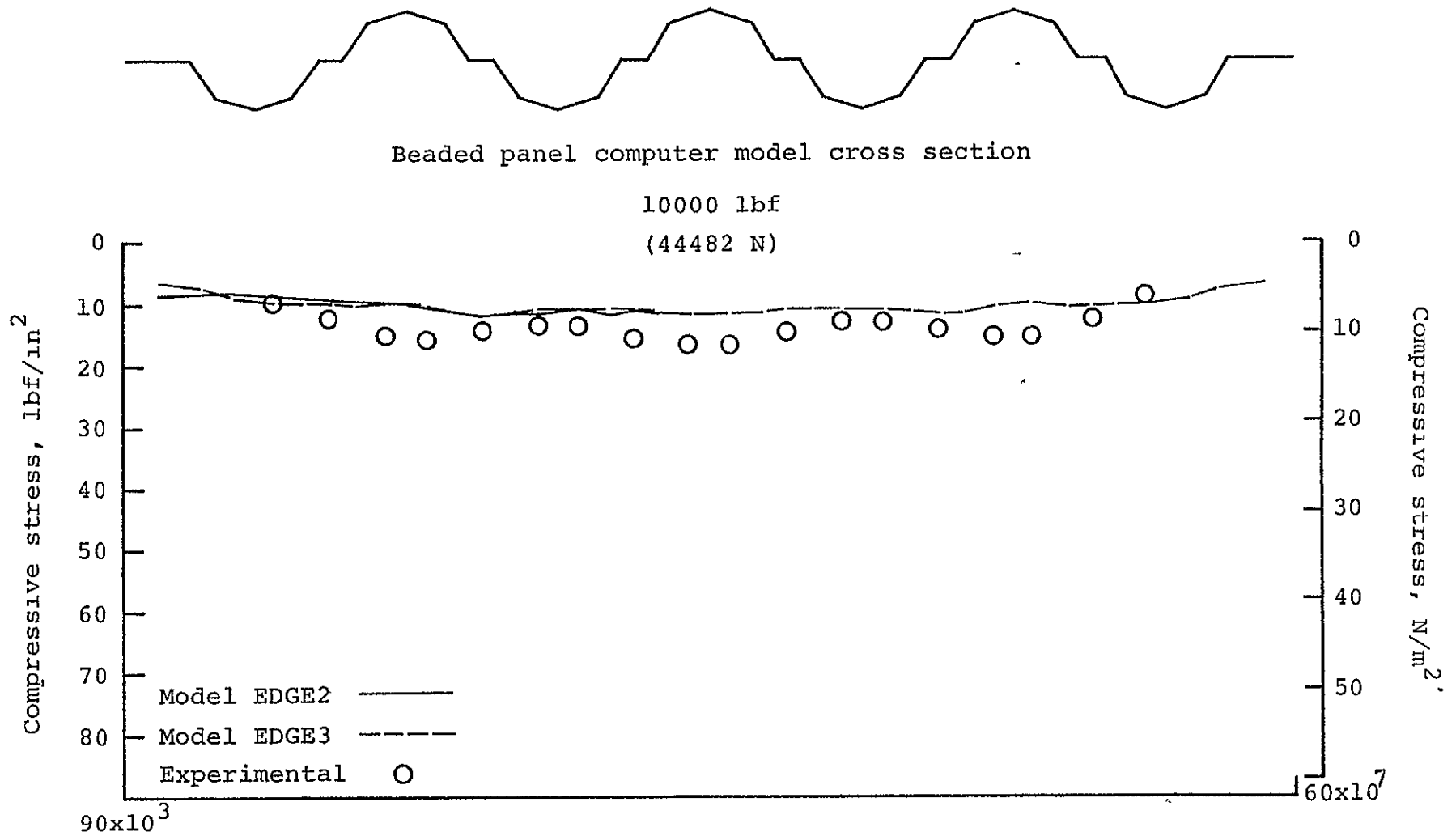
(a)

Figure 25.   Comparisons of static stresses computed by finite element models EDGE2 and EDGE3 with experimental results.
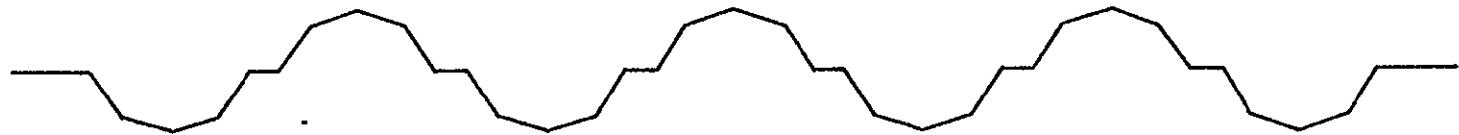
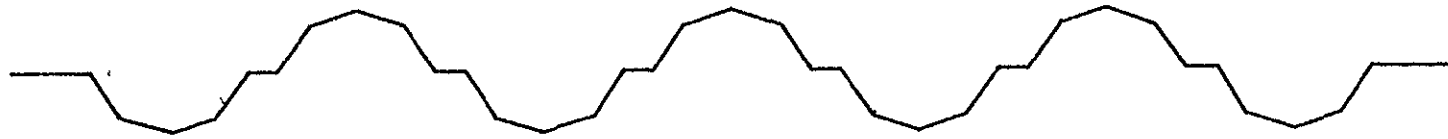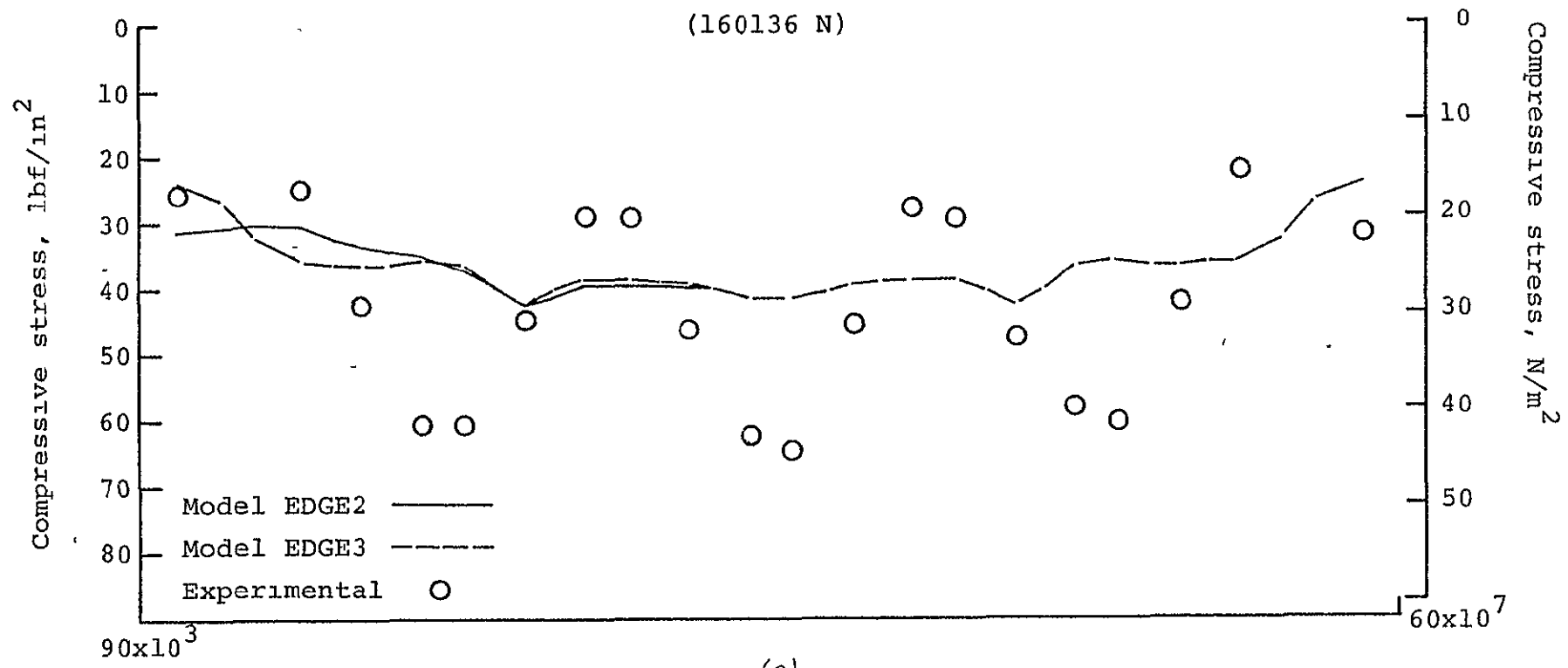Beaded panel computer model cross section

24000 lbf

(106757 N)

Model EDGE2 ————
Model EDGE3 — — —
Experimental   O

(b)

Figure 25. Continued

Beaded panel computer model cross section

36000 lbf

(160136 N)

Figure 25. Continued

Finite Element Models BEAD, FLAT and DIAG:

Descriptions and Results of Analysis.

The remaining three Nastran structural models, BEAD, FLAT and
DIAG, were models of an individual panel bead, a flat between beads,
and of a cross section from approximately peak to peak of two adjacent
beads, respectively. These models were used only for comparison pur-
poses with semiclassical analysis.

The finite element model BEAD is shown in figure 26. It con-
sisted of 447 elements, 497 grid points and 1347 degrees of freedom.
Boundary conditions for BEAD were prescribed to simulate simply sup-
ported edges. The restricted degrees of freedom and direction of the
applied loads are shown in figure 26.

The Nastran model FLAT was a model of the flat between two beads.
It was a very simple model consisting of 84 elements, 170 grid points
and 344 degrees of freedom. The boundary conditions used were identical
to those shown along the edges of the model BEAD shown in figure 26 and
represented simply supported edges.

The last of the three section models was DIAG which is shown in
figure 27. It consisted of 320 elements, 374 grid points and 1694
degrees of freedom. As in the case of models BEAD and FLAT, the bound-
ary conditions on the edges of DIAG represented simply supported edges.
Each of the foregoing models was loaded in compression parallel to their
long axis.

The results of the analysis using these three section models were
compared to semiclassical results only, (which will be discussed later)
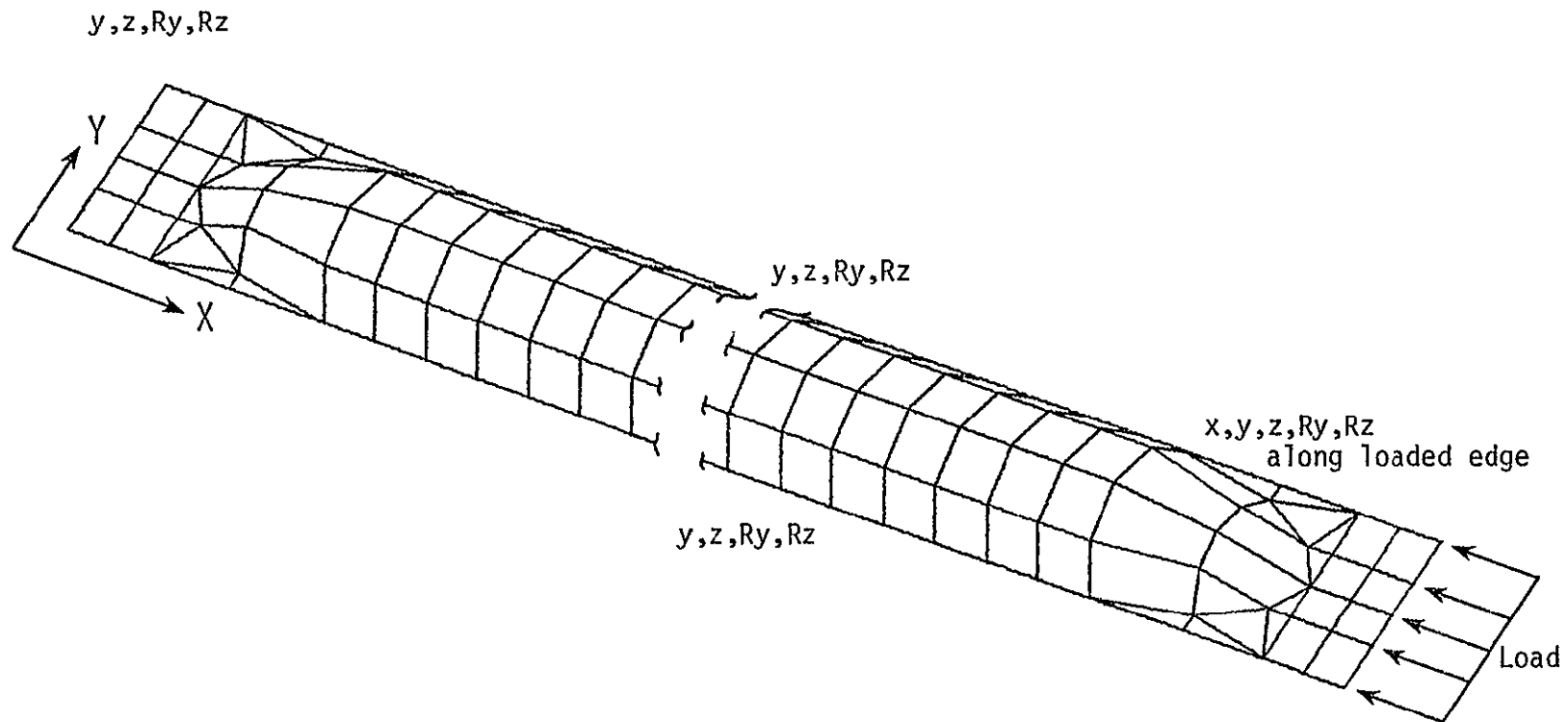since no individual section tests were performed. The comparisons are

Figure 26. *Finite element buckling model BEAD. The restricted degrees of freedom indicated represent simply supported edges.*
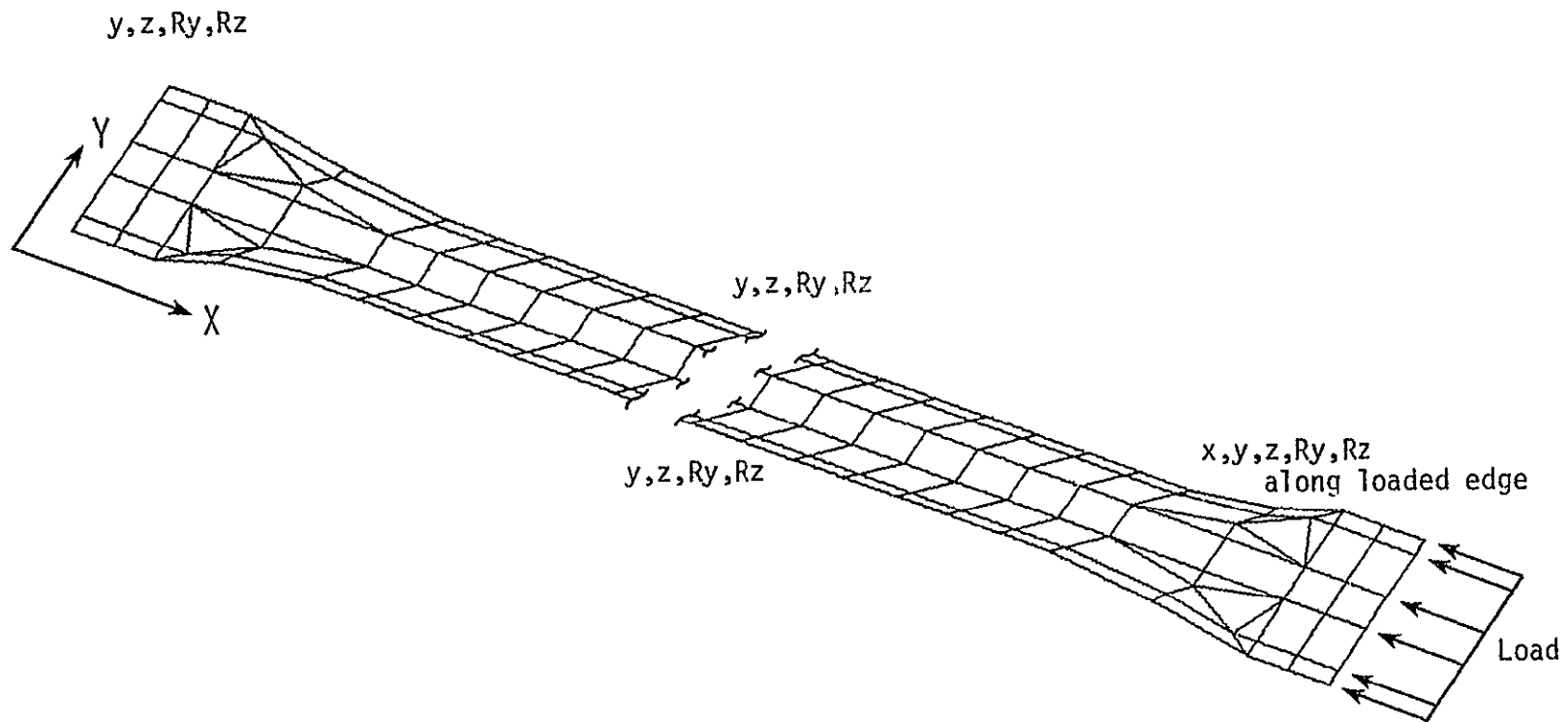
Figure 27.   Finite element buckling model DIAG.   The restricted degrees of freedom indicated represent simply supported edges.

summarized in table 5   The best comparison occurs with the flat in-
stability modewith a difference of 16%. The bead and diagonal modes
exhibit differences of 23% and 58%, respectively. The reason for these
poor comparisons is not known.

Table 5. Comparison of section model buckling results with semi-
classical analysis.

Instability mode	Semiclassical buckling load	Nastran model buckling load	Percent difference
Bead	343,200 lbf/in^2 (236,600 N/cm^2)	264,600 lbf/in^2 (182,400 N/cm^2)	23
Flat	687,000 lbf/in^2 (473,600 N/cm^2)	579,700 lbf/in^2 (399,700 N/cm^2)	16
Diagonal	42,700 lbf (190,000 N)	67,400 lbf (299,700 N)	58

SEMICLASSICAL ANALYSIS

Introduction

The purpose of this section is to present a summary of the semi-classical analysis of the beaded panel buckling characteristics given in references 2, 3, and 4. The four beaded panel buckling modes which were identified in the references include general instability, flat instability, bead instability and diagonal instability. The diagonal mode of instability is a localized instability between the peaks of adjacent beads. In all four instances, semiclassical buckling theory assuming simply supported edges was used in the analysis. The use of this simplified approach on a problem with the complexity of a beaded panel is questionable.

Since this project is concerned solely with compressive loads on the panels just the pertinent equations will be presented. A more detailed analysis may be found in references 2, 3 and 4.

Section Properties of the Panel

Prior to examining the four instability modes of the panel, it is necessary to define a number of section properties to be used in the various buckling equations. The first of these properties are the flexural rigidities of the beaded panel with respect to the X, Y and ξ axis shown in figure 28. The equations of flexural rigidity for bending moments along the X and Y axes and twisting of the XY plane are:

$$R = 1.045 \ \text{in} \qquad a = 1.239 \ \text{in}$$
$$(2.654 \ \text{cm}) \qquad \qquad (3.147 \ \text{cm})$$

$$C = .8190 \ \text{in} \qquad t = .0285 \ \text{in}$$
$$(2.080 \ \text{cm}) \qquad \qquad (.0724 \ \text{cm})$$

$$b = .4380 \ \text{in} \qquad \theta_1 = 77.5°$$
$$(1.113 \ \text{cm})$$

$$t_F = .0345 \ \text{in}$$
$$(.0876 \ \text{cm})$$

Figure 28. Section parameters of the beaded panel

$$D_1 = \frac{a}{s_a} \frac{Et^3}{12(1 - \nu^2)}$$

$$D_2 = E\, I_{xx} \qquad\qquad\qquad (1)$$

$$D_3 = \frac{s_a}{a} \frac{Et^3}{12(1 + \nu)}$$

where I_{xx} is defined as:

$$I_{xx} = \frac{tR^3}{a} \{(0.5 + \cos^2 \theta_1)\theta_1 - 0.75(\sin 2\theta_1)\} \qquad (2)$$

The diagonal mode of instability occurs at a critical value of θ_2, shown in figure 28, where the area moment of inertia of the diagonal section is minimum. The flexural rigidity equations about the ξY plane for buckling across the diagonal defined by angle θ_2 are:

$$D_I = E\hat{I}_{\xi\xi}$$

$$D_{II} = \frac{\delta}{s_\delta} \frac{Et^3}{12(1 - \nu^2)} \qquad\qquad\qquad (3)$$

$$D_{12} = \frac{s_\delta}{\delta} \frac{Et^3}{12(1 + \nu)}$$

$\hat{I}_{\xi\xi}$ in equation 3 includes only the material within the dimensions

63

of δ and is defined by:

$$\hat{I}_{\xi\xi} = \frac{1}{\delta} (\hat{I}_{XX} \cos^2\theta_3 + \hat{I}_{ZZ} \sin^2\theta_3 - \hat{I}_{XZ} \sin 2\theta_3) \qquad (4)$$

and $\hat{I}_{XX}$, $\hat{I}_{ZZ}$, and $\hat{I}_{XZ}$ are defined as:

$$\hat{I}_{XX} = aI_{XX} - tR^3\{(0.5 + \cos^2\theta_1)\theta_2 - \sin \theta_2(2 \cos \theta_1 - 0.5 \cos \theta_2)\}$$

$$\hat{I}_{ZZ} = tR\{(\frac{R^2}{2} + a^2)(\theta_1 - \theta_2) - \frac{R^2}{4} (\sin 2\theta_1 - \sin 2\theta_2) +$$

$$+ 2aR(\cos \theta_1 - \cos \theta_2) \quad \frac{t_F b^3}{24} \qquad (5)$$

$$I_{XZ} = tR^2\{a(\sin \theta_1 - \sin \theta_2) - \frac{R}{2}(\sin^2 \theta_1 - \sin^2 \theta_2) -$$

$$- R \cos \theta_1(\cos \theta_1 - \cos \theta_2) - (\theta_1 - \theta_2)a \cos \theta_1\}$$

Numerical values for equations 1 through 5 are summarized in table 6.

Table 6. Numerical values of the beaded panel cross section parameters

Section Property	Numerical Value	Section Property	Numerical Value
D_1	49.286 lbf·in (5.569 N·m)	D_I	5,415 lbf·in (611.8 N·m)
D_2	33.75×10^4 lbf·in (38.13×10^4 MN·m)	D_{II}	59.51 lbf·in (6.72 N·m)
D_3	59102 lbf·in (6.67 N·m)	D_{12}	48.88 lbf·in (5.52 N·m)
I_{xx}	1.109×10^{-2} in^4/in (.462 cm^4/cm)	$\hat{I}_{xx}$	9.256×10^{-3} in^4/in (.039 cm^4/cm)
$\hat{I}_{zz}$	1.164×10^{-2} in^4/in (.484 cm^4/cm)	$\hat{I}_{\xi\xi}$	1.780×10^{-4} in^4/in (7.409×10^{-3} cm^4/cm)
$\hat{I}_{xz}$	1.029×10^{-2} in^4/in (.428 cm^4/cm)		

Semiclassical Buckling Analysis for Pure Compression

Stability equations for the beaded panel may now be summarized. It is important to reiterate that the equations which follow are based upon simplified classical theory.

General instability is analyzed by assuming that the entire panel is a simply supported wide column under compressive load. From reference 2 the critical axial buckling load is given by:

$$N_{YCr} = \frac{-\pi^2 D_2}{L^2} \qquad (6)$$

Diagonal instability, a local instability (of the simply supported panel cross section) between the peaks of adjacent beads is given as follows:

$$N_{YDCr} = \frac{-\pi^2}{2\delta^2} \{(D_I D_{II}) + D_{12}\} \frac{\delta}{s_\delta} \frac{s_a}{s} \qquad (7)$$

The critical diagonal buckling load occurs when the diagonal cross section has a minimum moment of inertia. The angle θ_2 in figure 28 which defines the boundaries of the diagonal cross section, was varied from 0 to 77.5 degrees in small increments and the critical buckling load calculated. The results are shown in figure 29 which is a plot of the diagonal buckling load versus angle θ_2. Given the geometry of the beaded panel used in this project, the angle θ_2 is about 12.875 degrees from the peak.

Instability of the flats between the beads is the third mode to be considered. From reference 2, the compressive buckling formula

for flat instability, assuming simply supported edges, is given by:

$$F_{CF} = \frac{-4\pi^2 E}{12(1 - \nu^2)} \frac{t_F^2}{b} \tag{8}$$

Instability of a single simply supported bead cross section is the final mode to be analyzed. Consideration must be made for the critical axial compressive stress as well as the critical compressive stress due to bending. The equations which define this mode (ref. 2) are respectively:
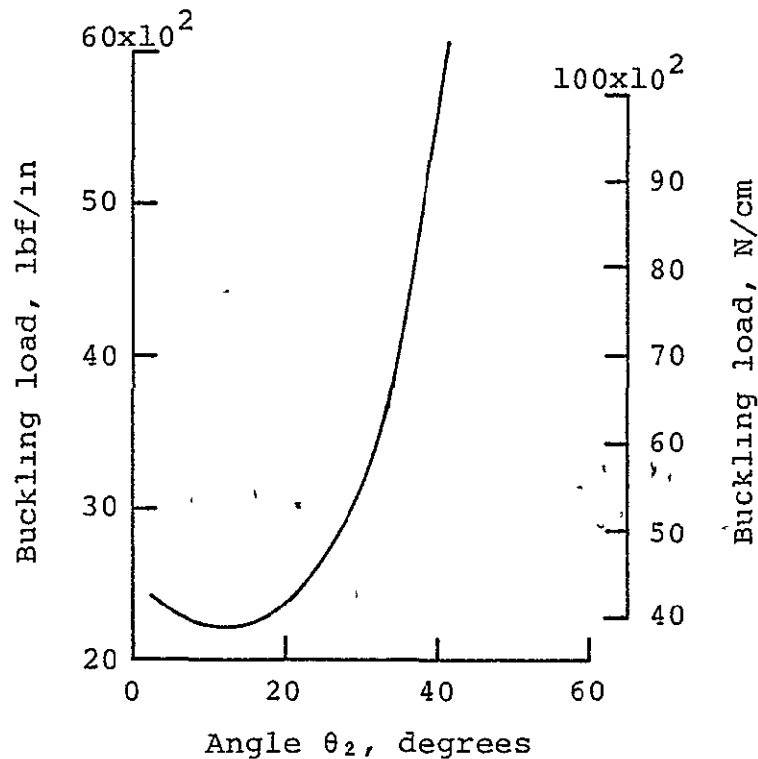
Figure 29. Effects of varying angle θ_2 on the diagonal mode of instability.

$$F_{Cb} = -0.82 \ E(t/R)^{1.19} \tag{9}$$

$$F_{Bb} = -0.77 \ E(t/R)^{1.15} \tag{10}$$

On the basis of these equations, the critical buckling loads for the beaded panel were determined and are presented in table 7.

Table 7. Semiclassically derived buckling loads

Instability mode	Load lbf/in (N/cm)	Total load
General - N_{YCr}	1818 (3200)	34,700 lbf (154,350 N)
Diagonal - N_{YDCr}	2240 (3920)	42,700 lbf (190,000 N)
Flat - F_{CF}	- - - -	687,000 lbf/in^2 (473,700 N/cm^2)
Bead ' Axial - F_{Cb}	- - - -	343,200 lbf/in^2 183,400 N/cm^2)
Bending - F_{Bb}	- - - -	372,200 lbf/in^2 (256,600 N/cm^2)

COMPARISONS OF EXPERIMENTAL RESULTS

WITH SEMICLASSICAL ANANLSIS

Comparisons can be made between the results of experimental test-
ing and semiclassical analysis. As previously discussed, the critical
elastic buckling load derived from semiclassical analysis was 1,818
LBf/in (3,200 N/cm), the critical mode being general instability.
However, the semiclassical analysis ignores the restraint at the ends
of the panel which the doublers provide. Furthermore, the semiclassi-
cal analysis assumes a constant cross-sectional thickness along the
panel length. Because of these simplifications, it is probable that
the actual buckling load should be higher. The results of the force/
stiffness analysis support that assertion. From figures A4(a), (b),
(d), (e), and (f) the indicated buckling load for general instability
was found to be between 2,660 to 2,880 LBf/in (4,660 to 5,040 N/cm) or
about 37% higher.

The results of the experimental analysis has shown that it was
not general instability which was the critical mode, but a mode which
was similar to the diagonal mode. The buckling load for diagonal in-
stability calculated using the semiclassical analysis was 42,700 pounds
(190,000 N). The results of the test show that the panel underwent
elastic buckling at about 40,000 pounds (177,930 N) in a mode similar
to that assumed by the semiclassical diagonal mode analysis. However,
the test results show that the buckled shape of the beads did not match
the edge conditions assumed in the semiclassical analysis (i.e., the
edges did not remain straight). Therefore, the fairly close agreement
of the buckling loads for this particular panel cannot indicate the

general validity of the semiclassical diagonal mode analysis.

The inadequacies of the semiclassical analyses, point out the need of more sophisticated analysis such as Nastran or more realistic semiclassical theory.

SUMMARY OF RESULTS

For purposes of comparison, the primary experimental results will
be reiterated at this point along with a summary of the results of the
finite element and semiclassical analysis.

Experimental Results

1.   The panel was eccentrically loaded (due to panel geometry) as
     verified by the experimental data.

2.   Elastic buckling occurred at a load of about 40,000 pounds
     (177,930 N). The critical axial force per unit width of the
     panel was 1,680 LBf/in (2,940 N/cm). The elastic buckling load
     involved out-of-plane deformation in addition to a lateral de-
     flection characteristic of the diagonal mode of instability.

3.   The ultimate strength of the panel/side stiffener assembly was
     48,600 pounds (216,180 N).

Finite Element and Semiclassical Analysis Results

1.   An elastic buckling load of 31,700 pounds (141,000 N) was cal-
     culated using finite element model EDGE2, 26% lower than the
     actual failure load.

2.   An elastic buckling load of 50,000 pounds (222,400 N) was cal-
     culated using finite element model EDGE3, 25% higher than the
     actual failure load.

3.   Both of the models used for static analysis exhibited an inability
     to account for the nonlinear effects of out-of-plane bending
     with loads applied in the plane of the panel.

4.   The results of the finite element buckling analysis done with

models BEAD, FLAT and DIAG, compared poorly with the semiclassi-

cal results.

5. Elastic buckling loads of 34,700 and 42,700 pounds (154,350 and

190.000 N) were calculated for the general and diagonal modes of

instability, respectively. These values are based upon simplified

semiclassical theory.

CONCLUSIONS AND RECOMMENDATIONS

The semiclassical analysis used to design the beaded panels is based upon some simplifying assumptions. First, the sections used in the semiclassical analysis were assumed to be simply supported. However, the test results show that the buckled shape of the panel did not match the assumed edge conditions used in the semiclassical analysis. Secondly, significant restraint is ignored in the semi-classical analysis by assuming a constant cross-sectional thickness along the panel length. Therefore, the fairly close agreement in the buckling loads, for the diagonal mode in particular, cannot indicate the general validity of the semiclassical analysis.

The experimental results suggest that the semiclassical analysis is conservative. It can therefore be concluded that the panel was conservatively designed and thus heavier than necessary.

On the basis of the results of the semiclassical and finite element analysis the following recommendations are made:

1. The inadequacies of the semiclassical analysis point out the need for more sophisticated analyses. The analysis should include realistic edge support assumptions as well as the use of accurate cross-sectional thicknesses in the analyses.

2. The results of the finite element buckling analysis compared poorly with the experimental and semiclassical results. The reason for the poor comparisons is not precisely known, but is certainly an area for further research. One possible area for investigation would be the development of a full panel model for buckling analysis.

Finally, several concluding remarks should be made about the test monitoring techniques used during the tests. The force/stiffness technique provided unconservative predictions of the elastic buckling strength of the panel. Furthermore, for the best results the gages should be in close proximity to the location of the elastic failure. Secondly, the Moiré fringe·technique proved to be extremely useful as an aid in identifying the mode shapes of the panel. Furthermore, the Moiré fringe technique made it possible to identify mode shape changes which might have gone unnoticed based upon strain gage results alone. The technique also provided an accurate means of measuring out-of-plane displacements of the entire panel.

APPENDIX A

EXPERIMENTAL DATA

Strain gage locations are indicated on all of
strain gage plots presented in this section, by
two symbols. A closed circle (•) is used to
indicate gages on the side of the panel shown.
An open circle (○) is used to indicate gages
on the opposite side of the panel.
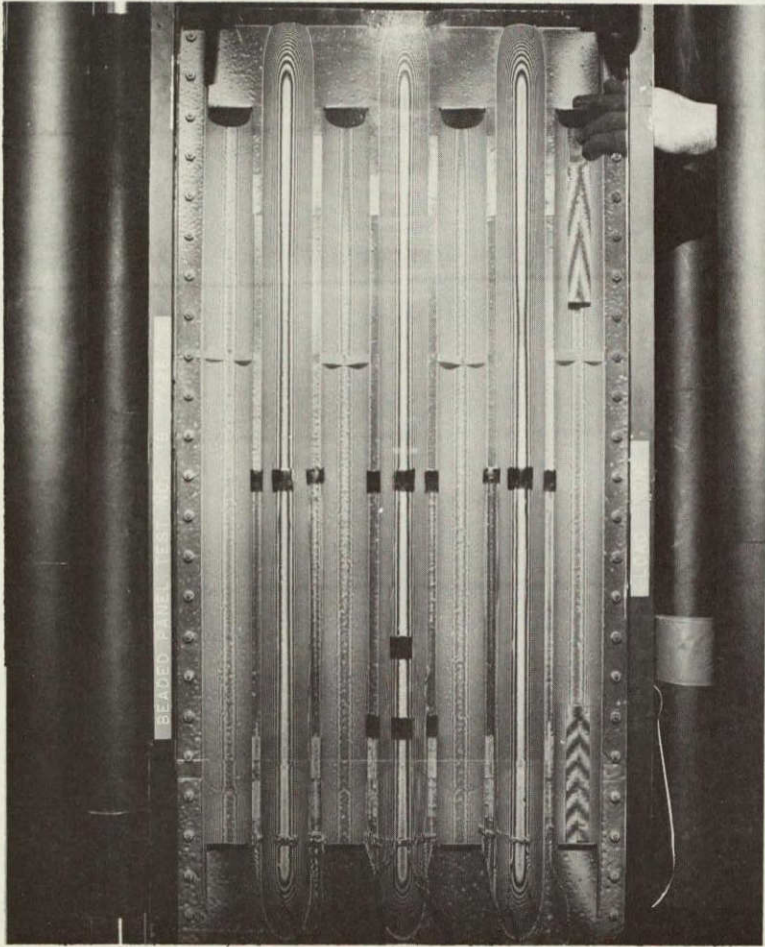
(a) Calibration photo (No load).   (b) 24,000 pounds (106,760N) load.
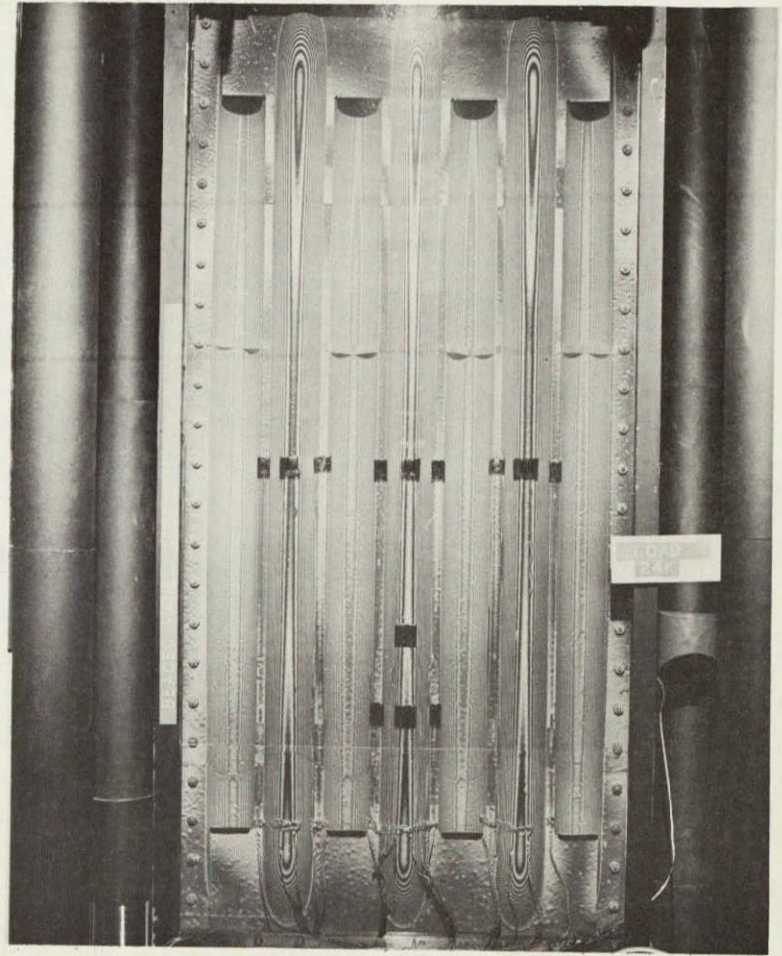
Figure A1. Moiré fringe photographs.
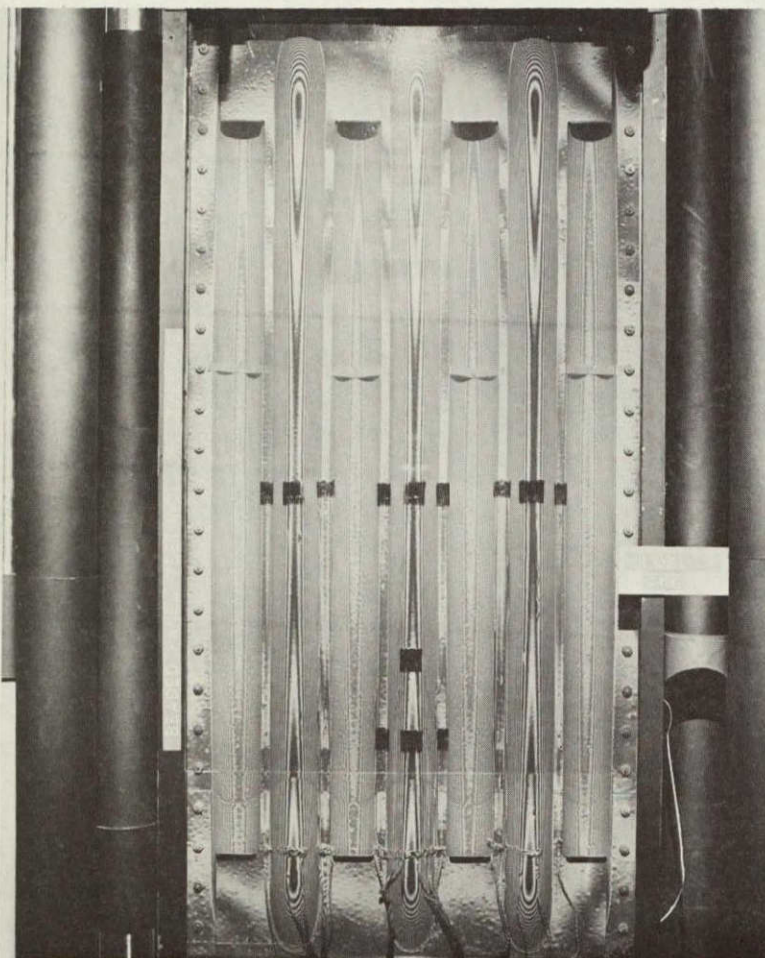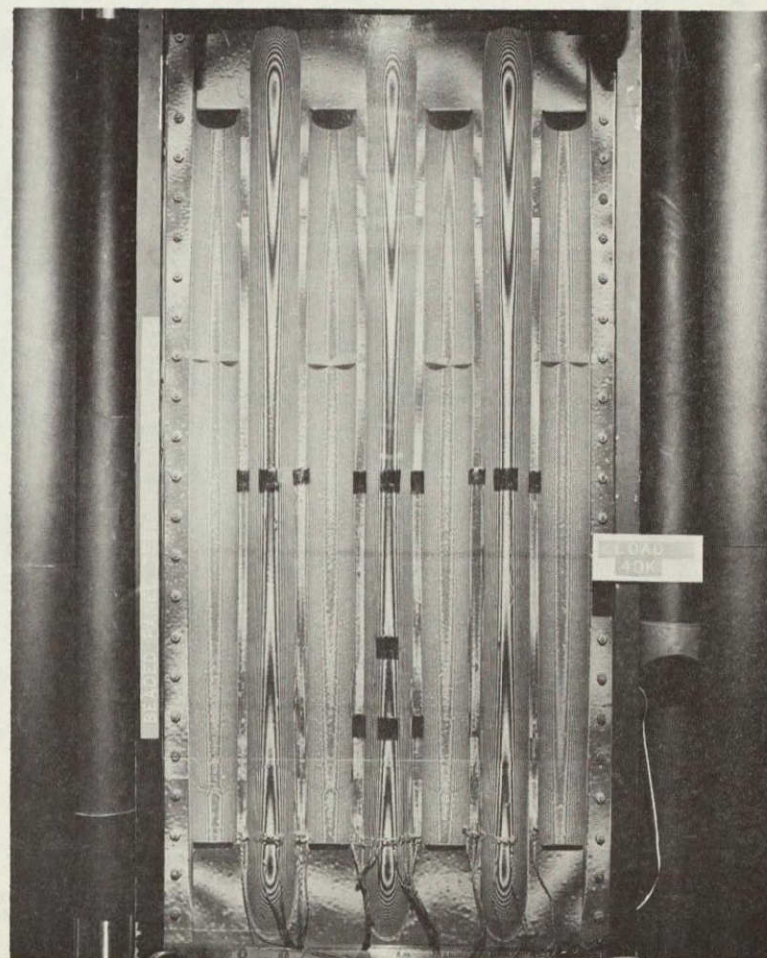
(c) 36,000 pounds (160,140N) load.　　　　　　　　　　(d) 40,000 pounds (177,930N) load.

Figure A1. (continued) Note differences in curvature
of center two flats of the panel in (c) and (d).
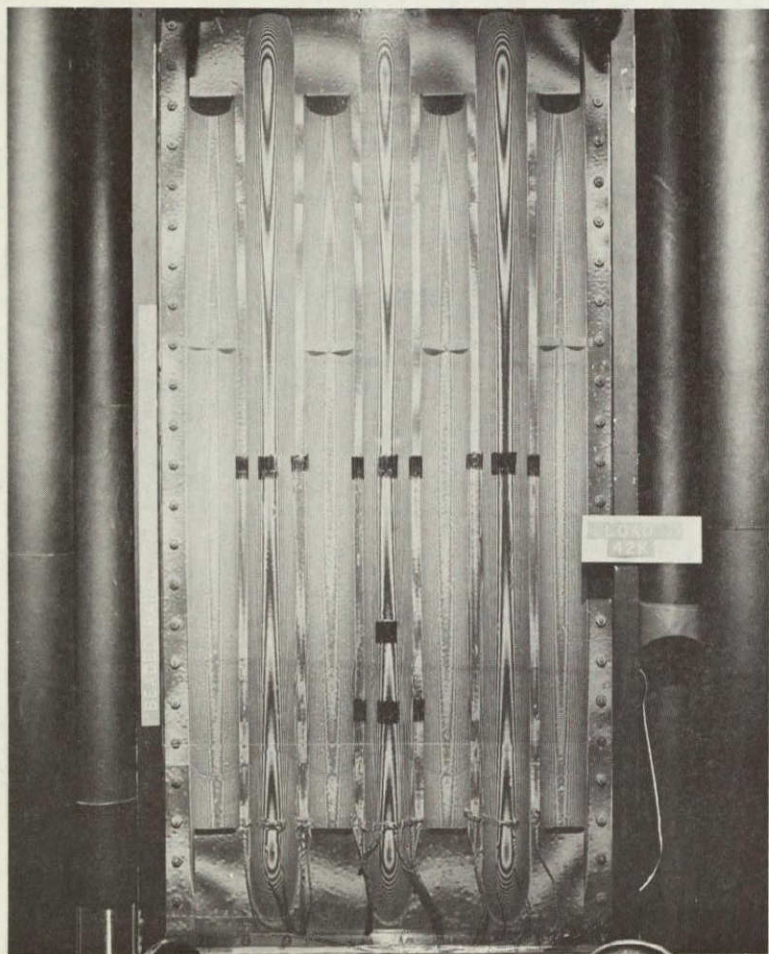
(e) 42,000 pounds (186,825N) load.   *(f) 44,000 pounds (195,720N) load.*
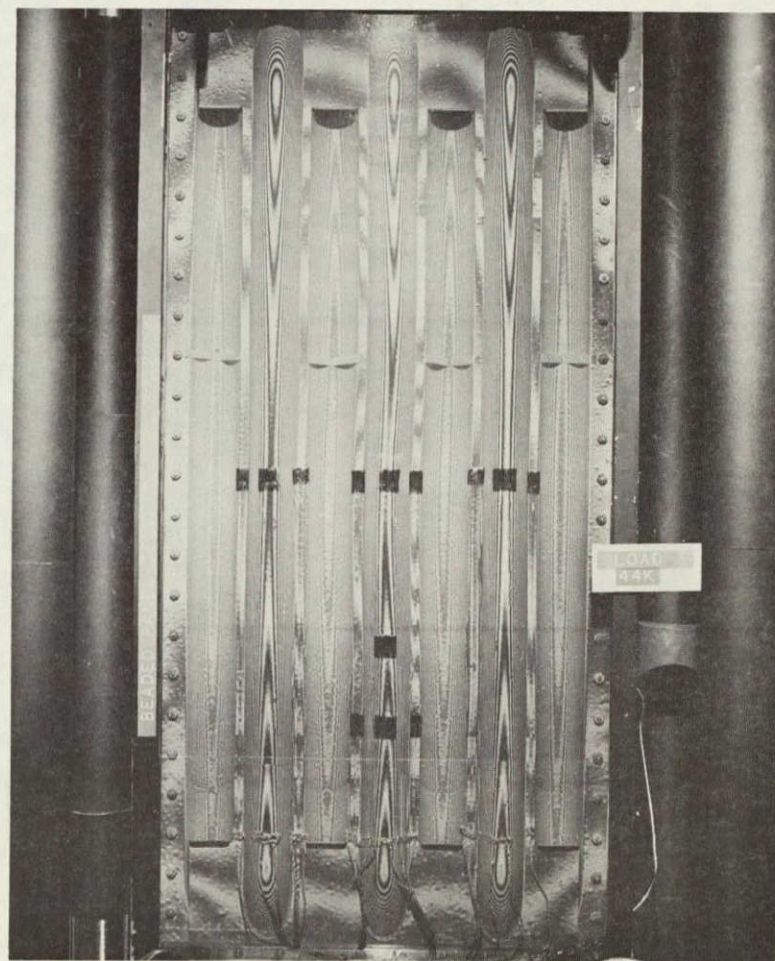
Figure A1.   (continued)
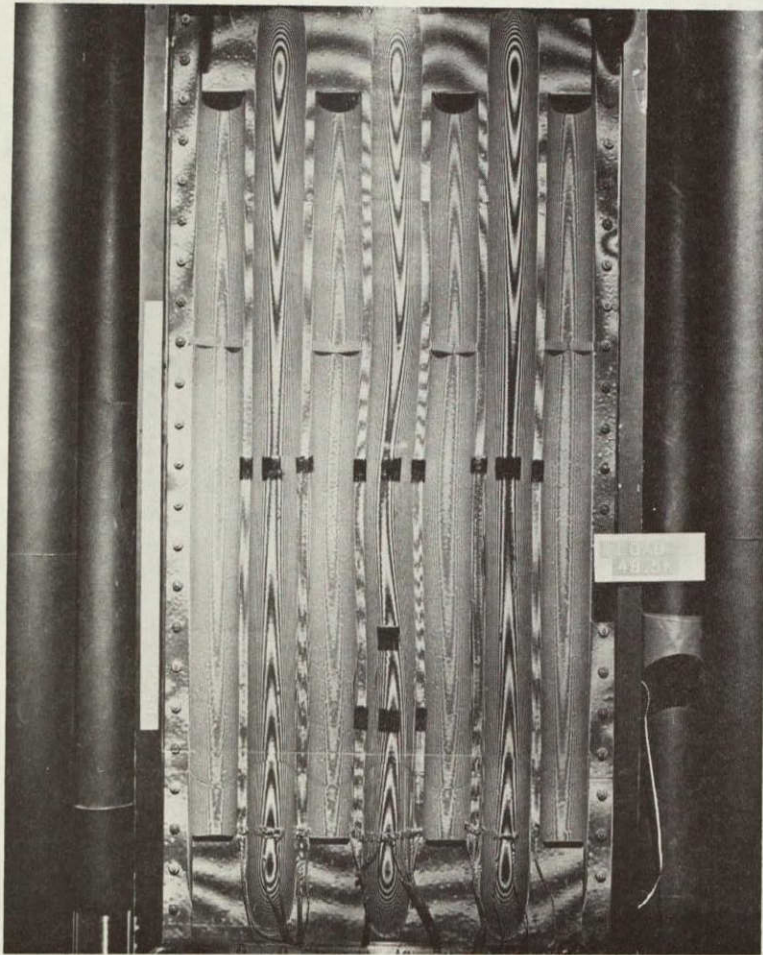
(g) 48,500 pounds (215,750N) load.
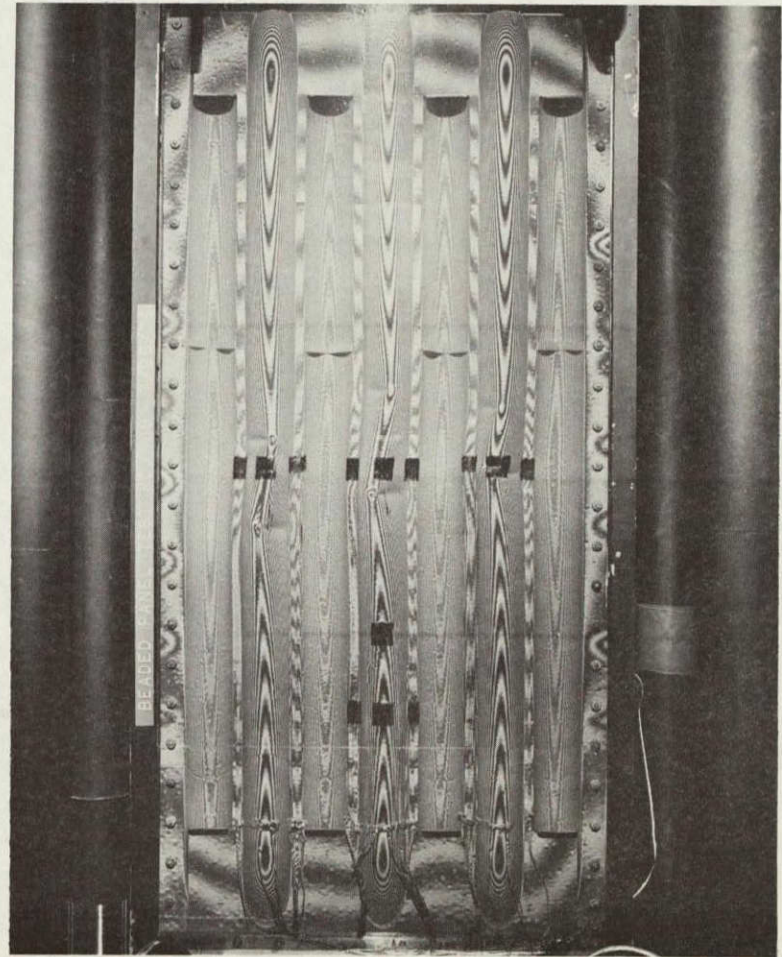
(h) The panel after failure, no load.

Figure A1. (continued)

(i)

Figure A1.   (continued)   The panel after failure
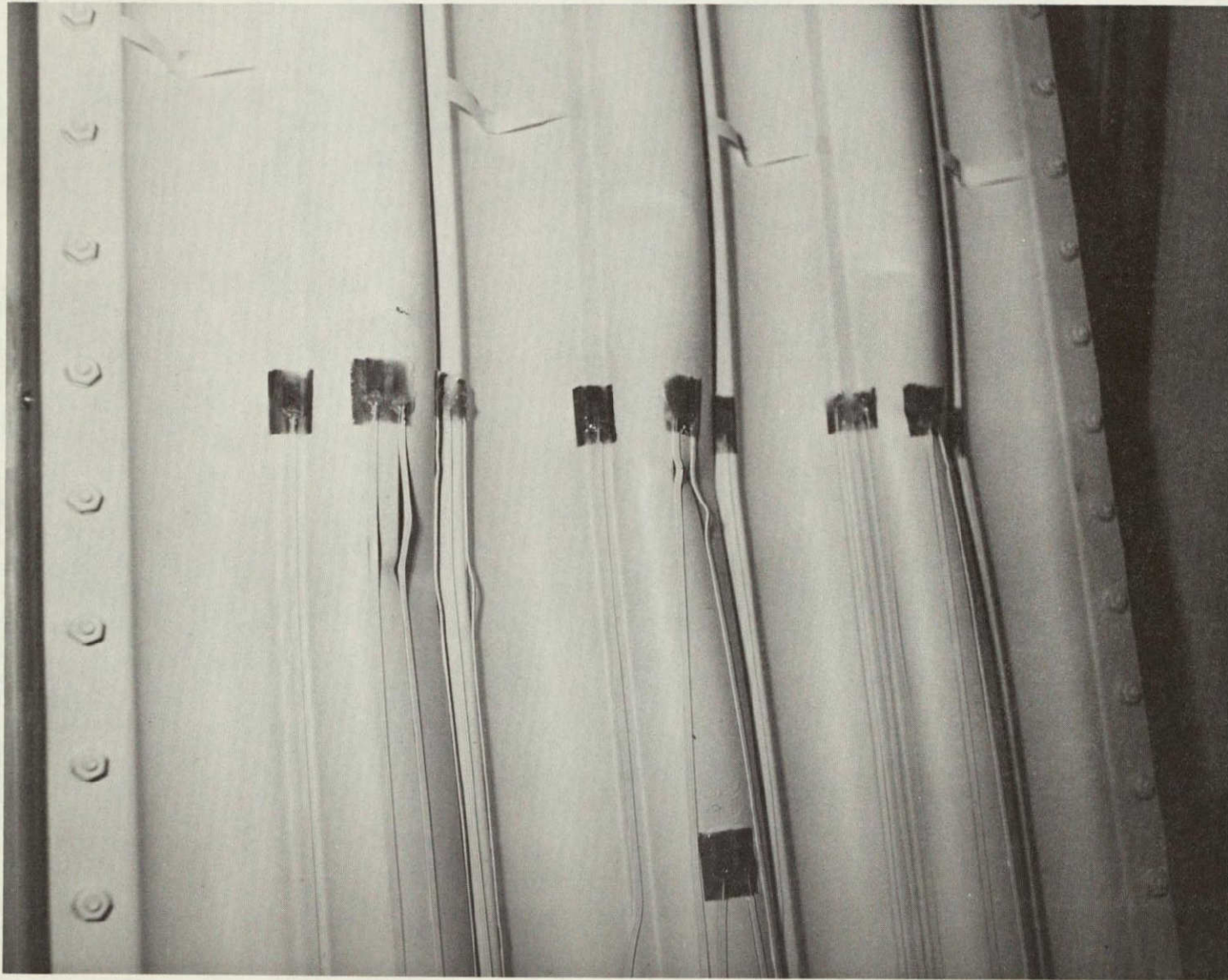
(j)

Figure A1. (continued) The panel after failure.

Panel length, cm
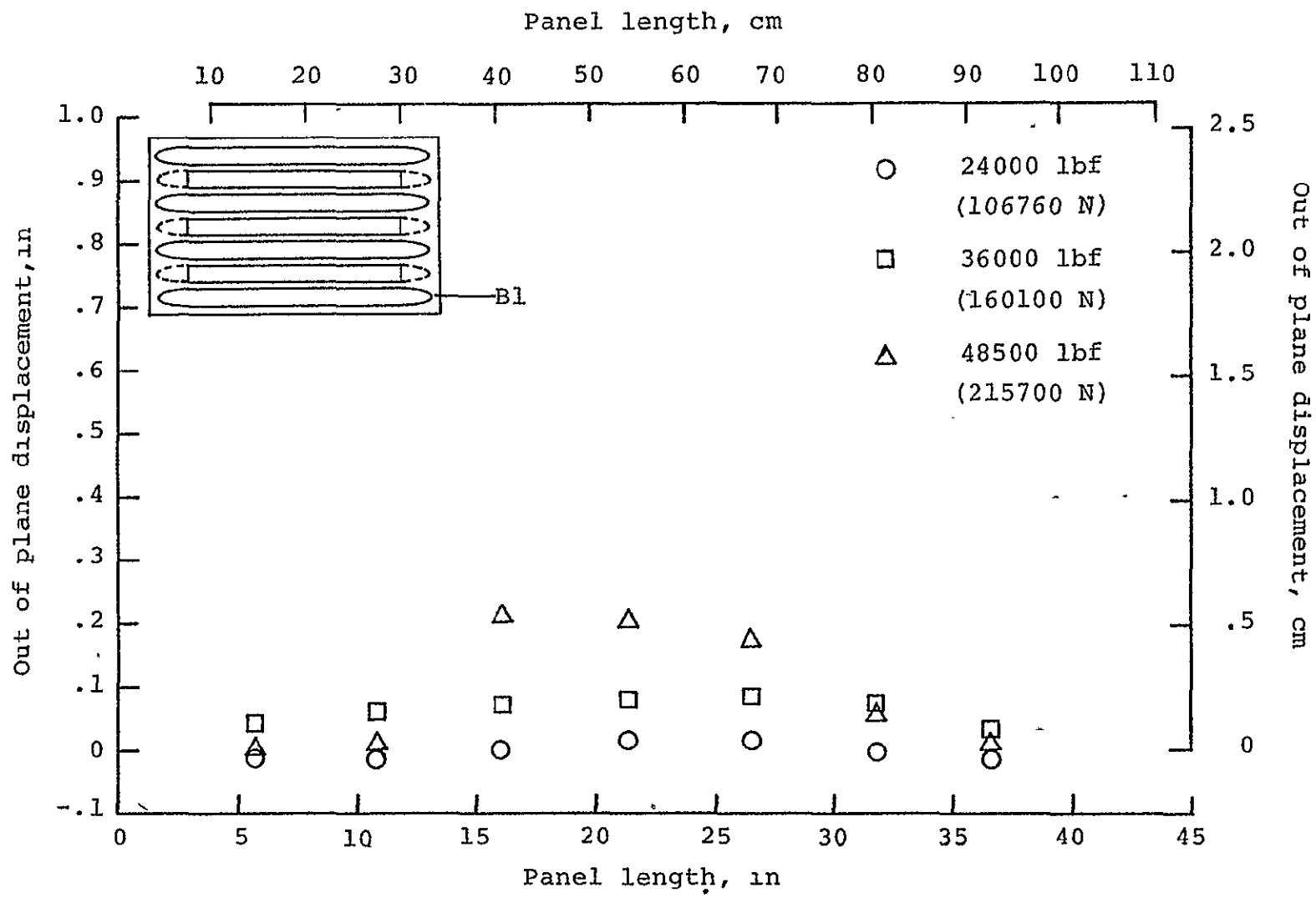
(b)

Figure A2.   Moiré fringe measurements.
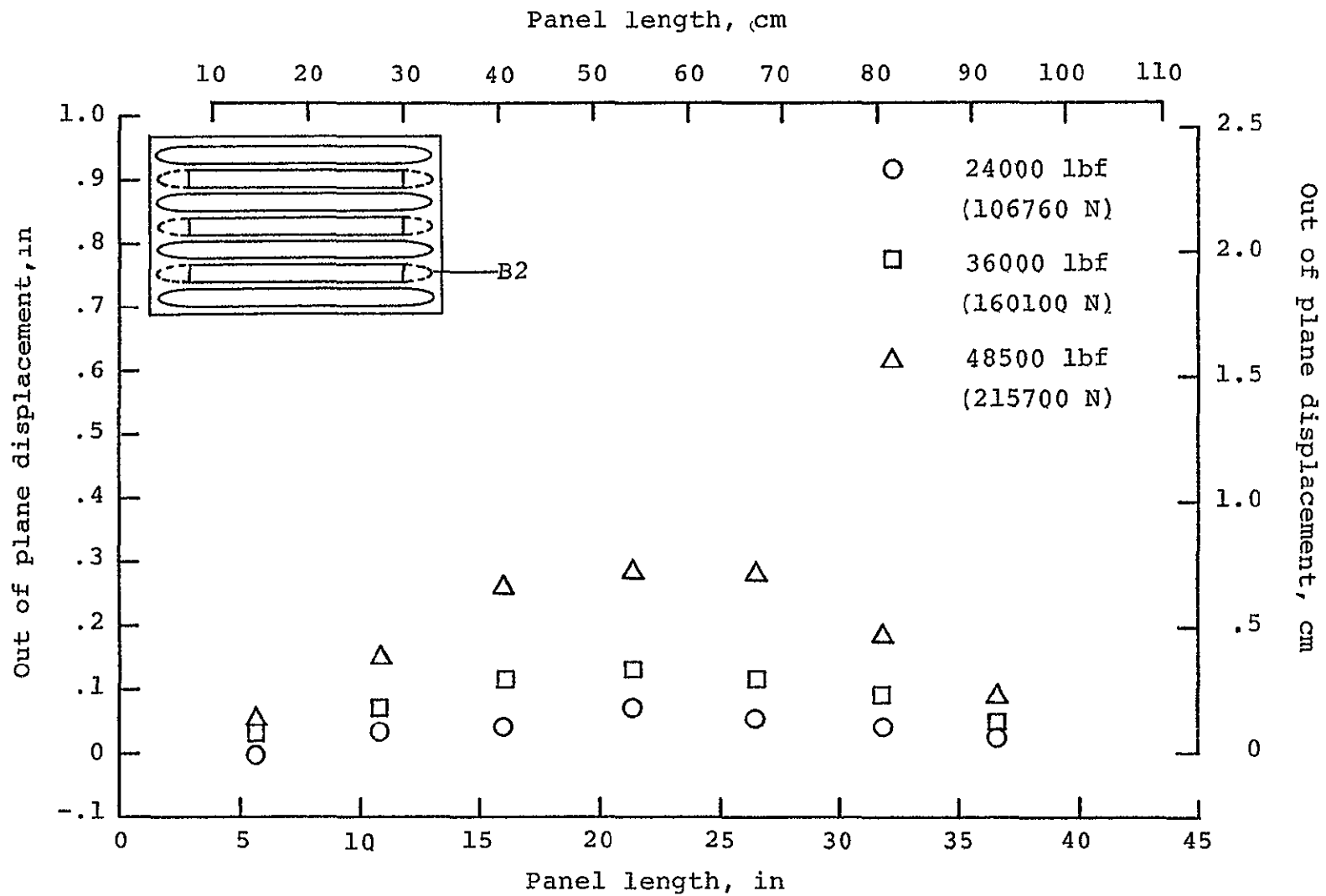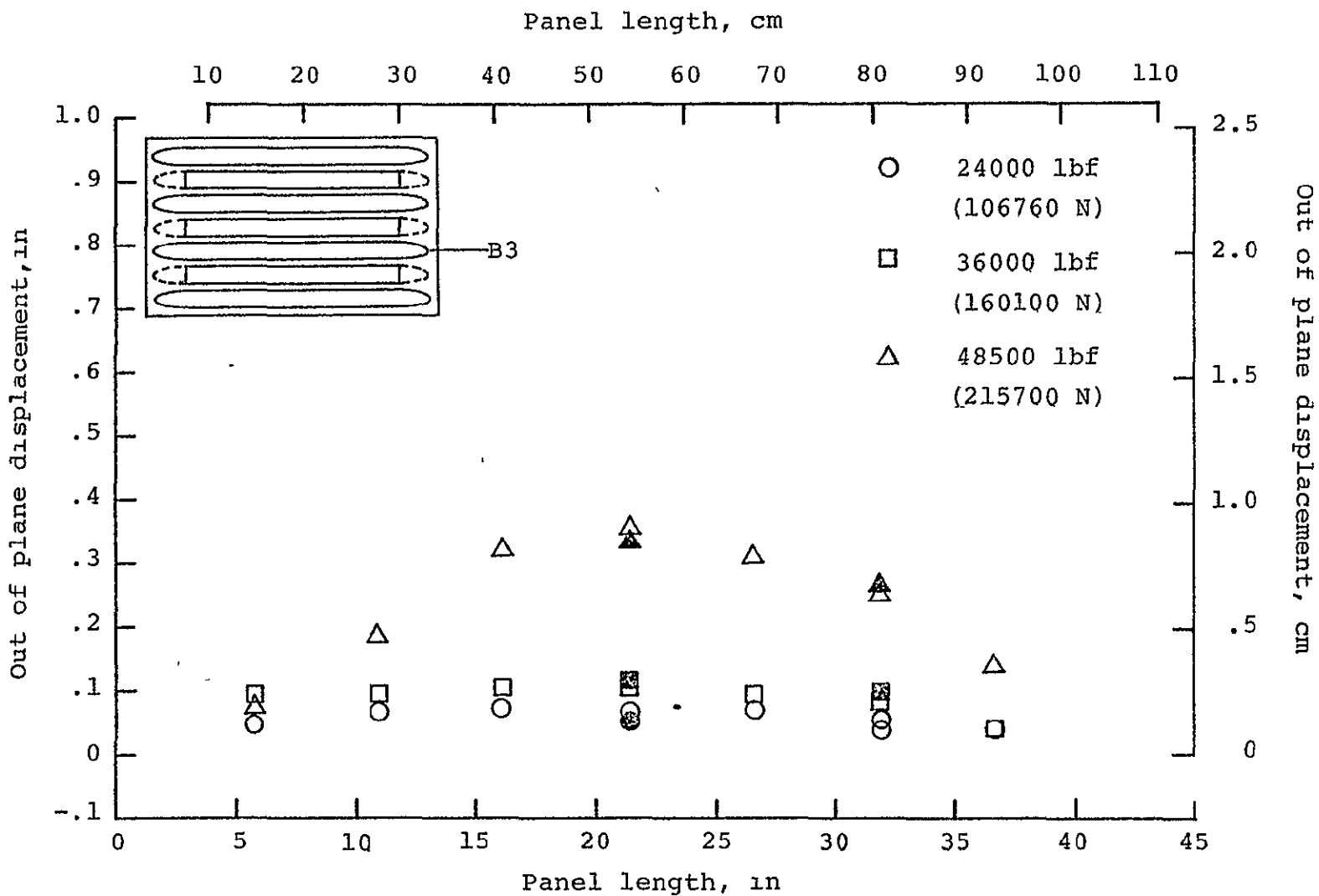
83

Figure A2. Continuted

Figure A2.   Continued
Solid symbols denote DT data.

(d)

Figure A2.   Continued
Solid symbols denote DT data.

Panel length, cm

Figure A2. Continued
Solid symbols denote DT data.

(g)
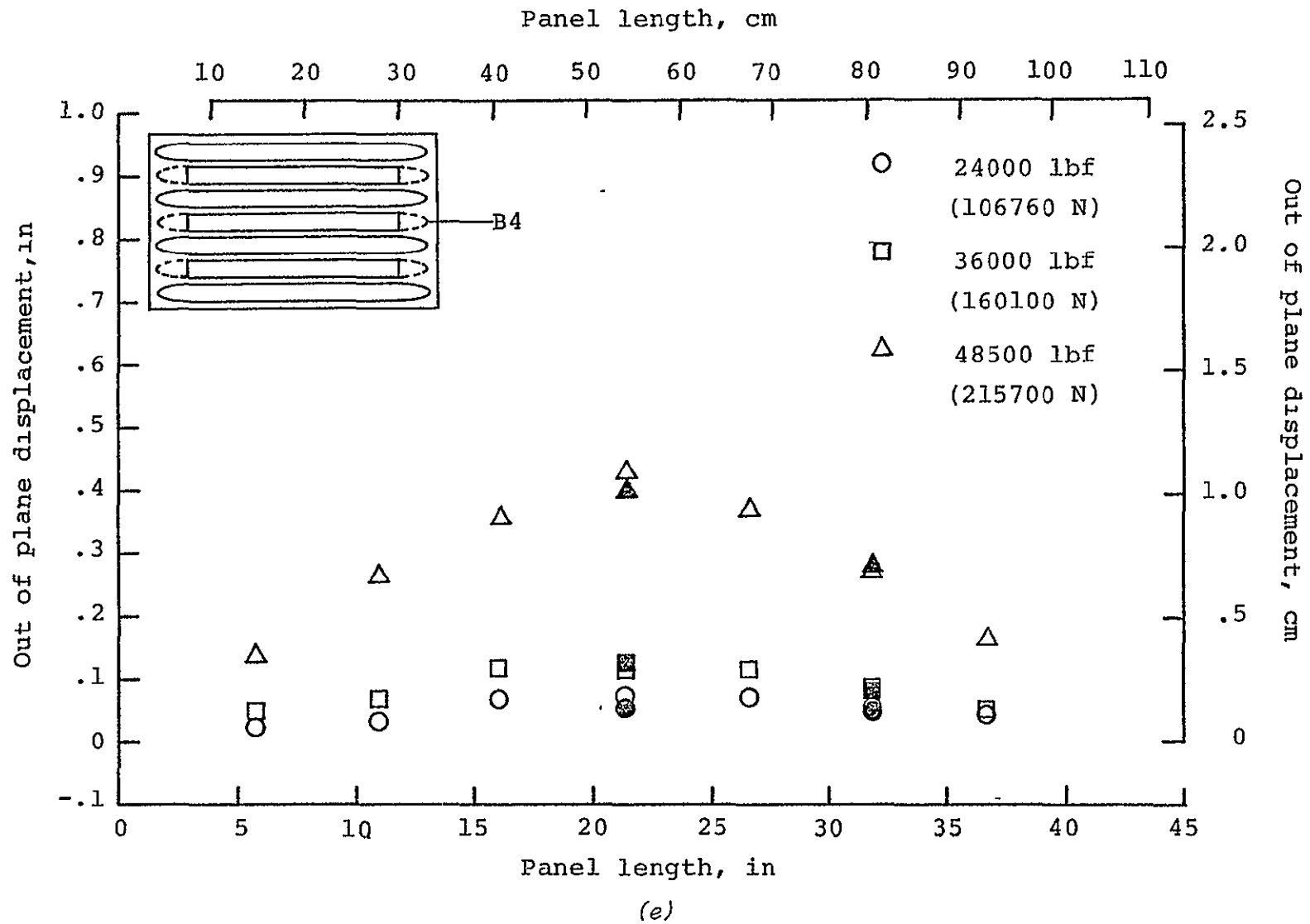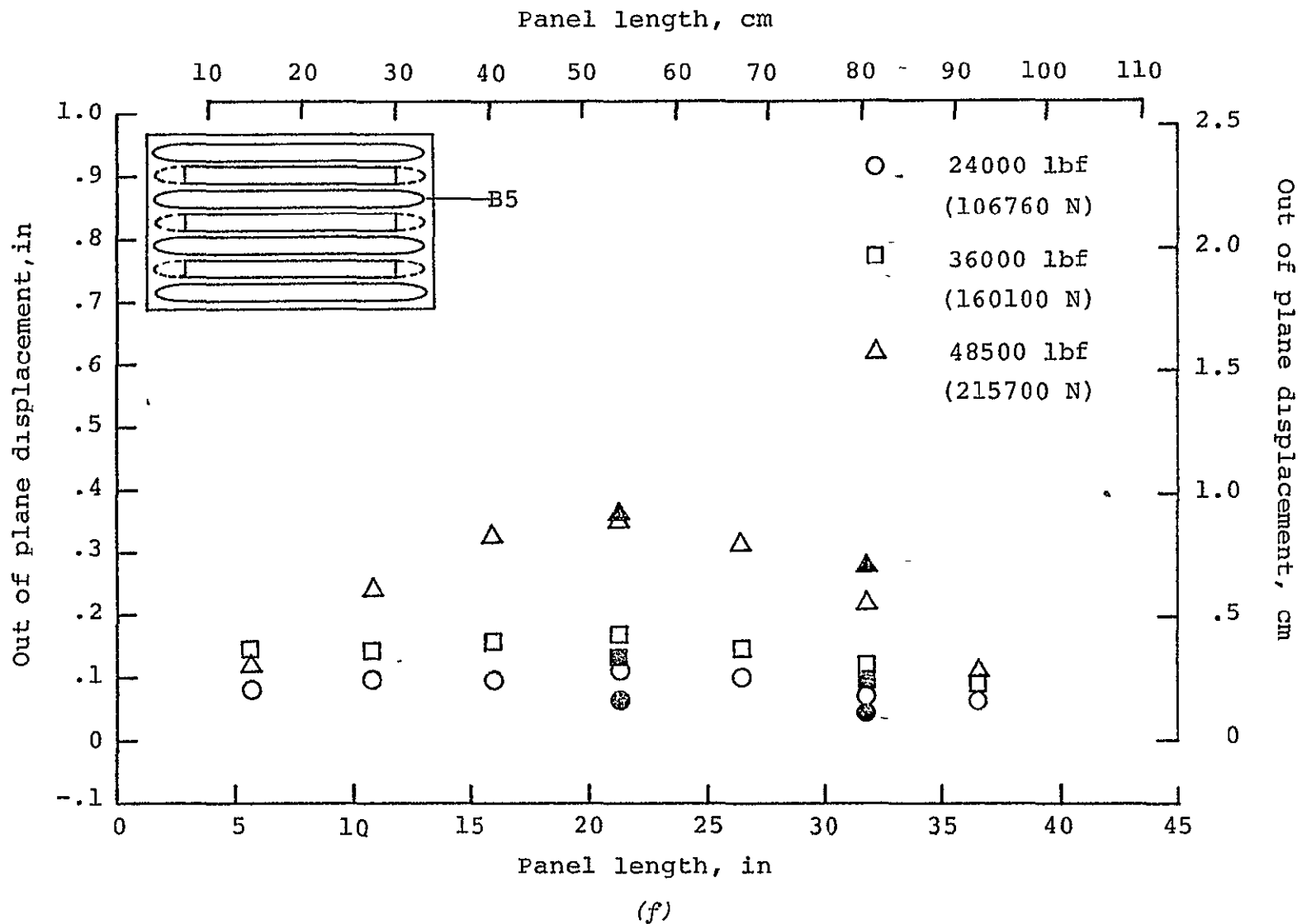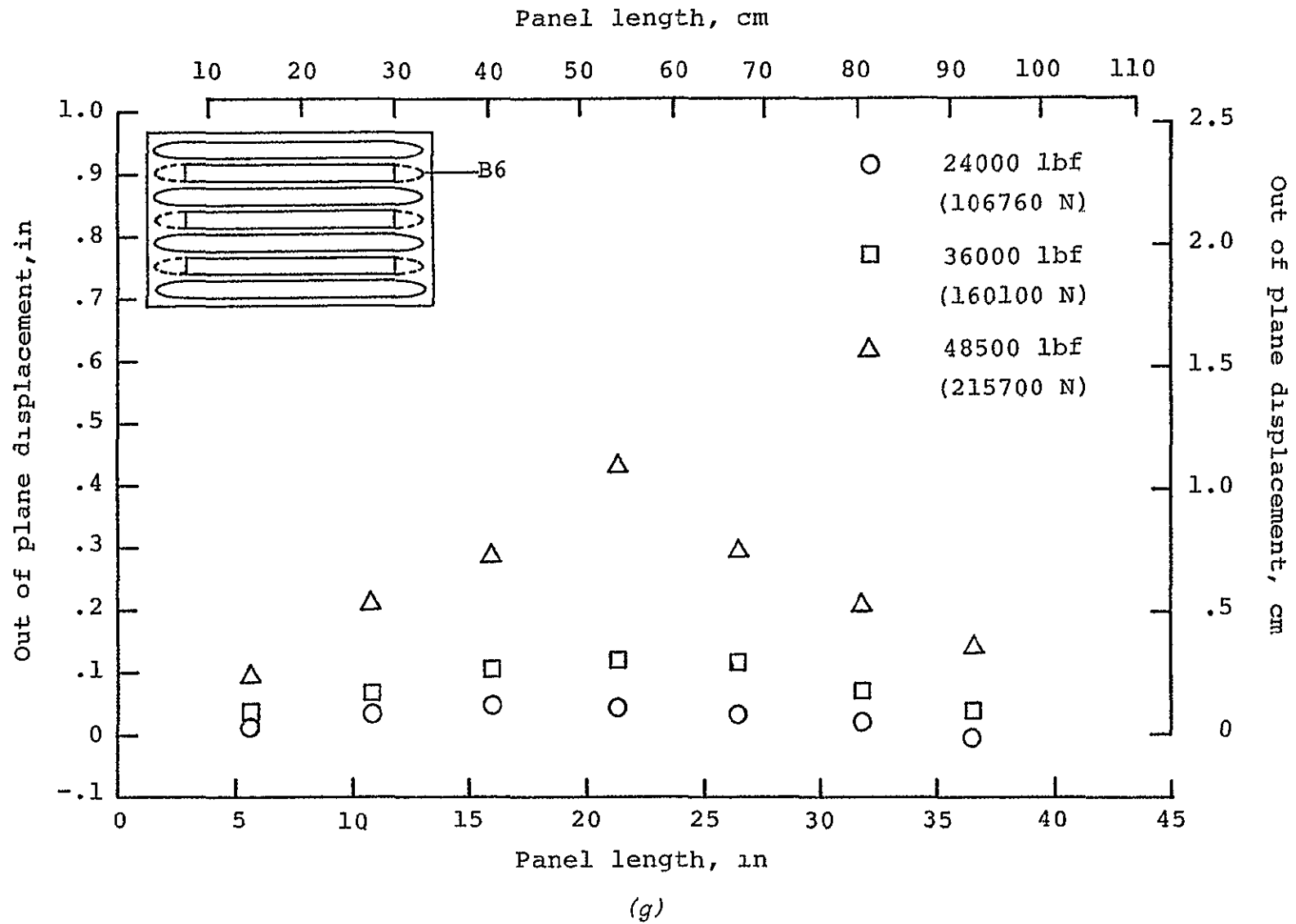
Figure A2. Continued
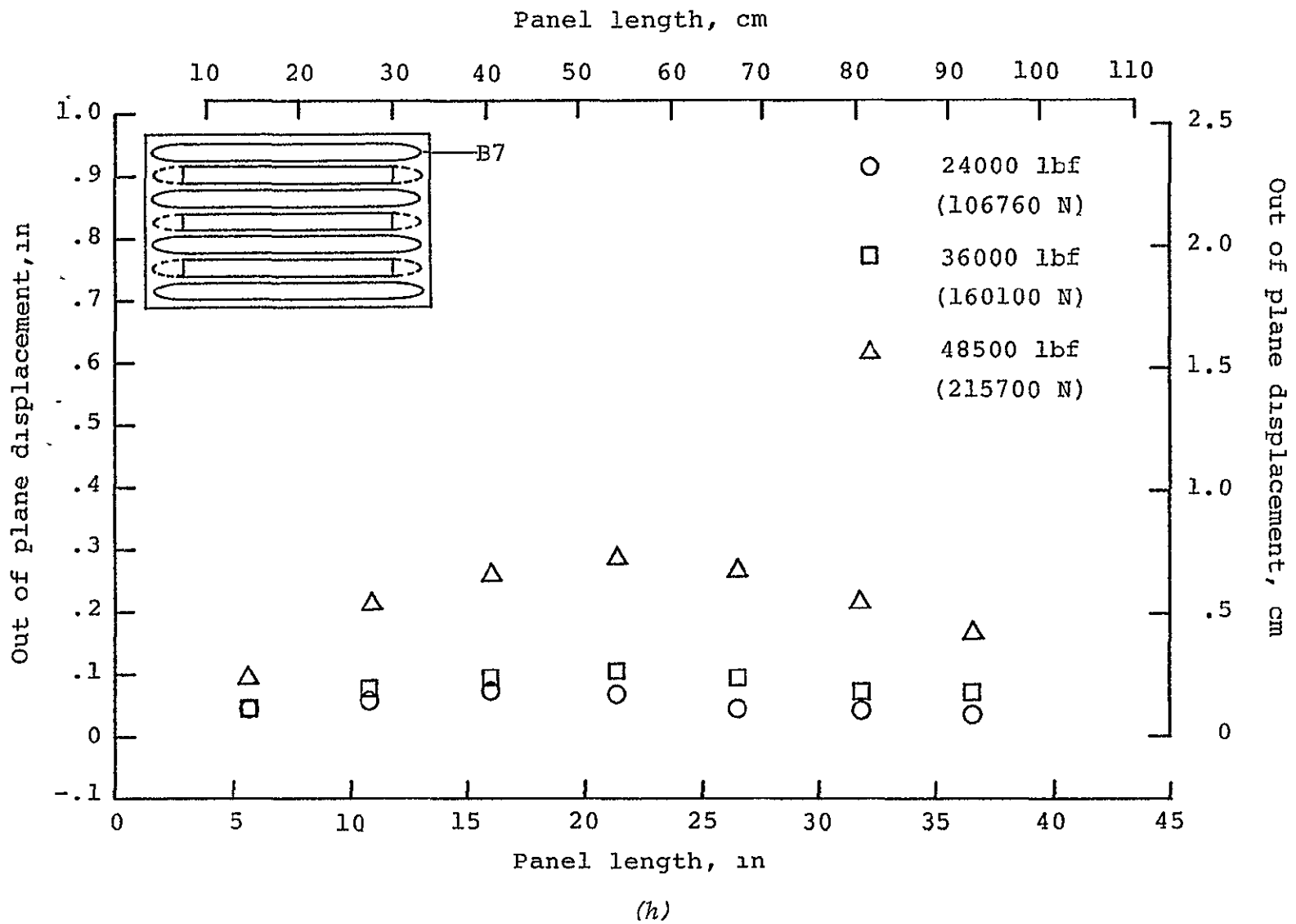
Figure A2.   Continued
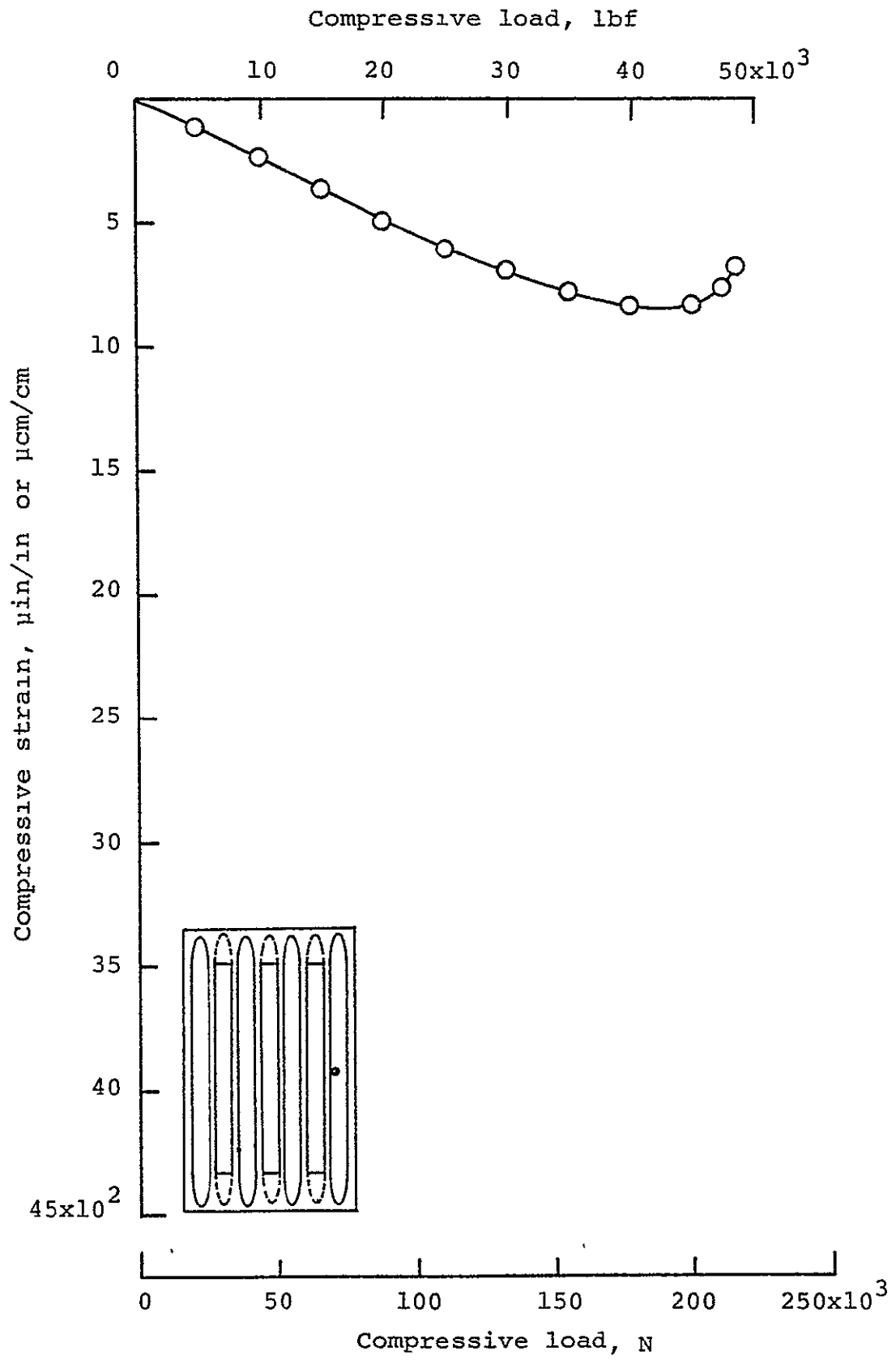
(a) Strain gage 401.

Figure A3. Strain gage plots.
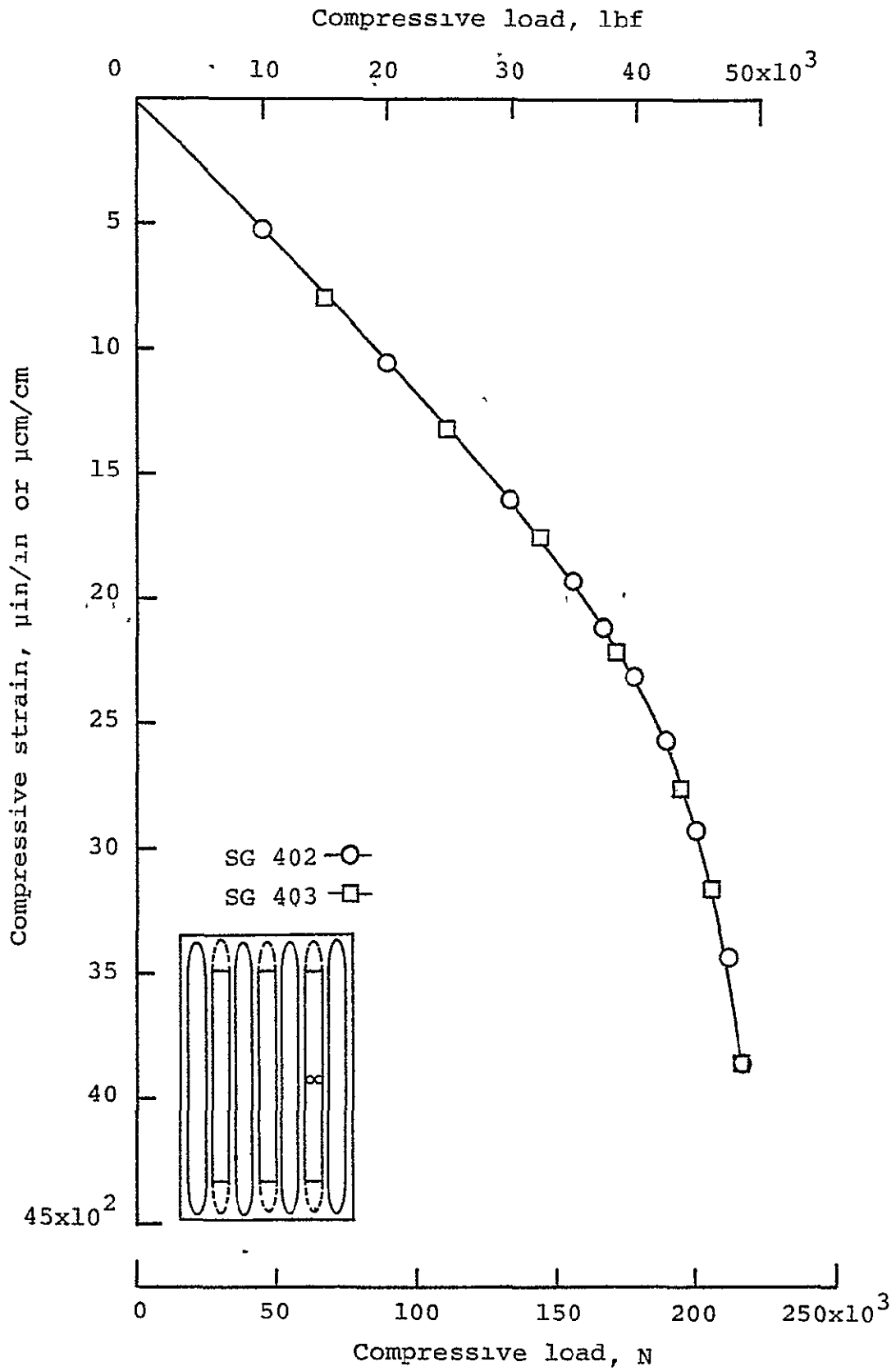
(b)   Strain gages 402 and 403.

Figure A3.   Continued
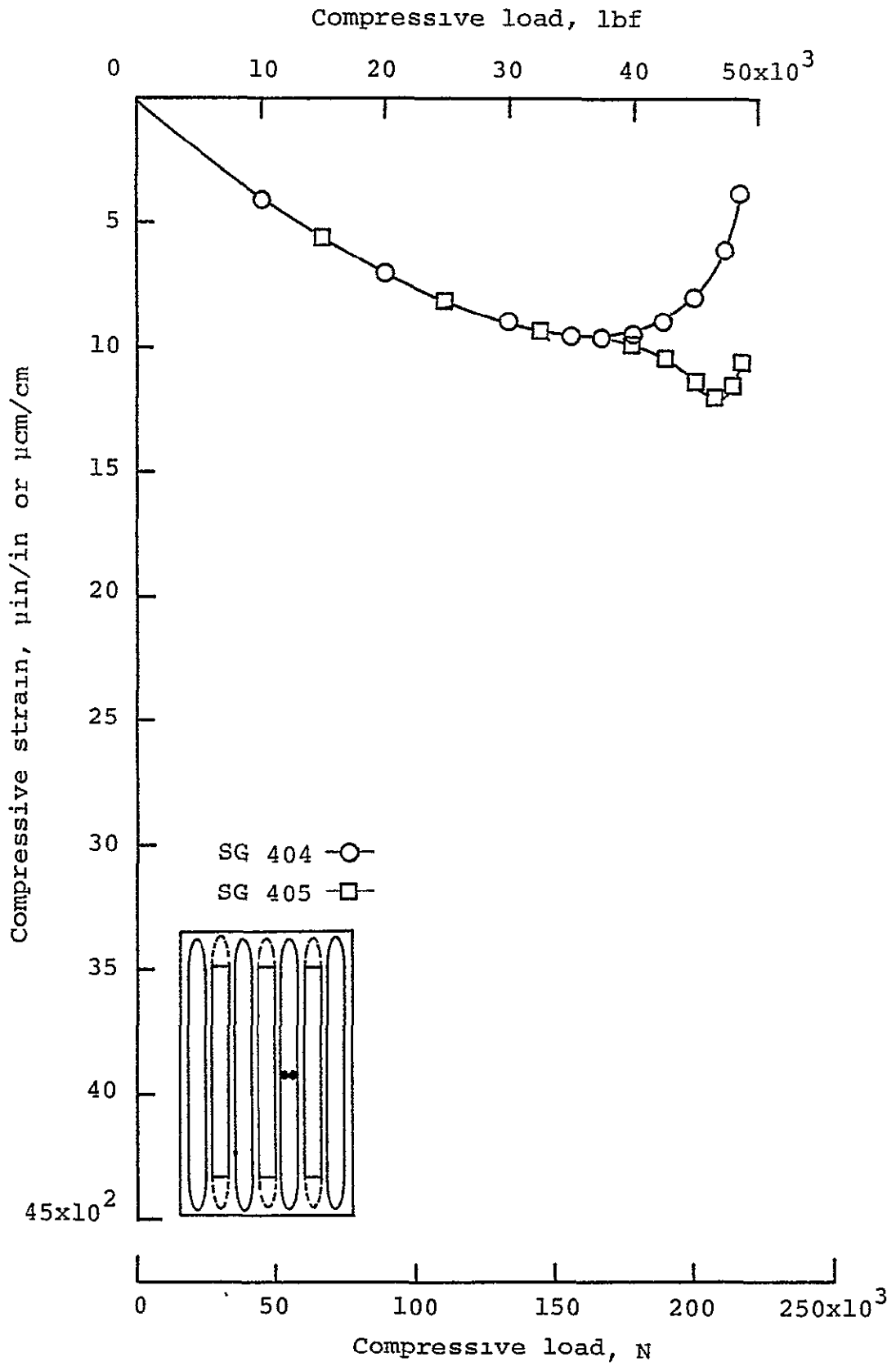
(c) Strain gages 404 and 405.

Figure A3. Continued
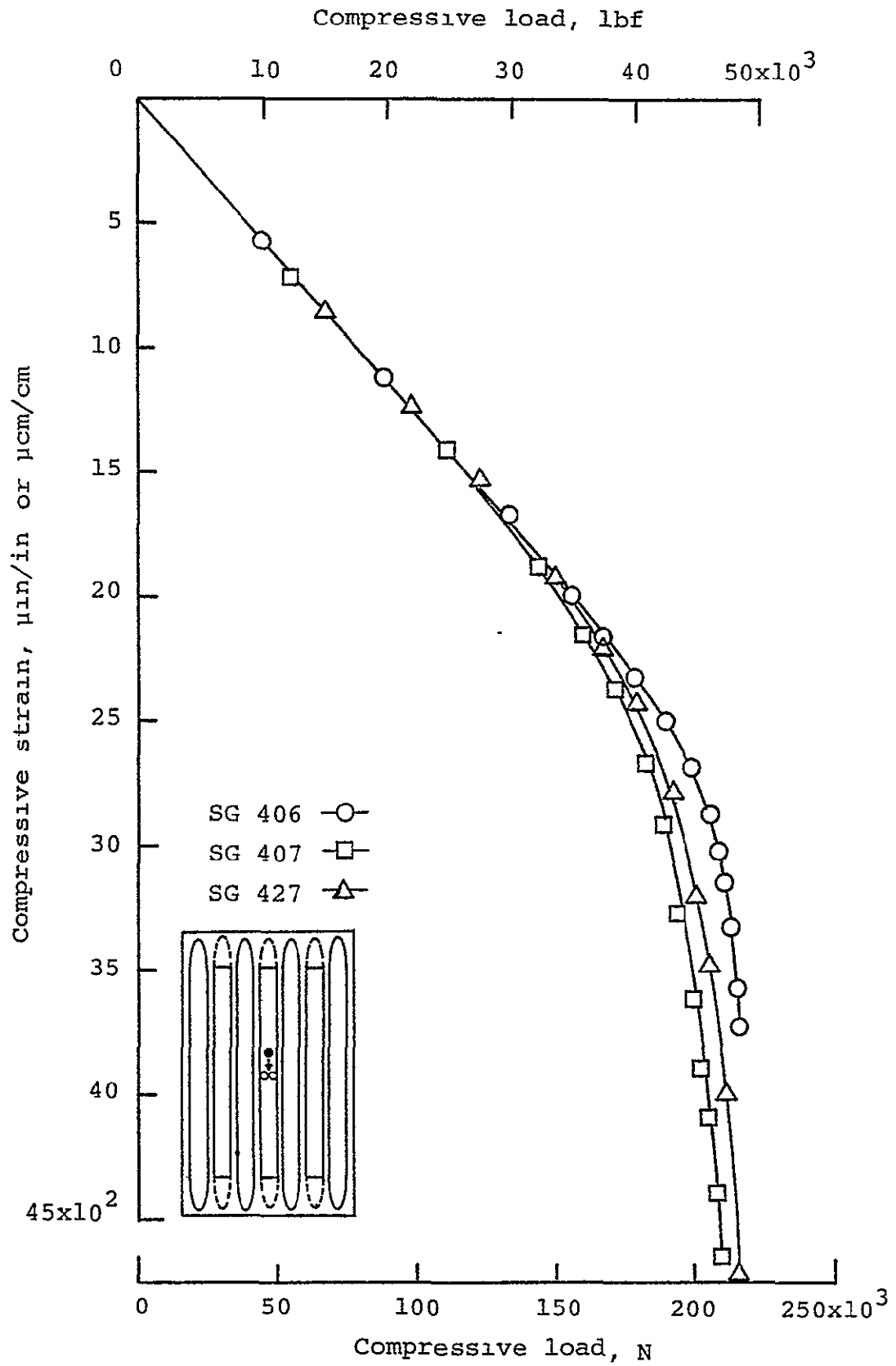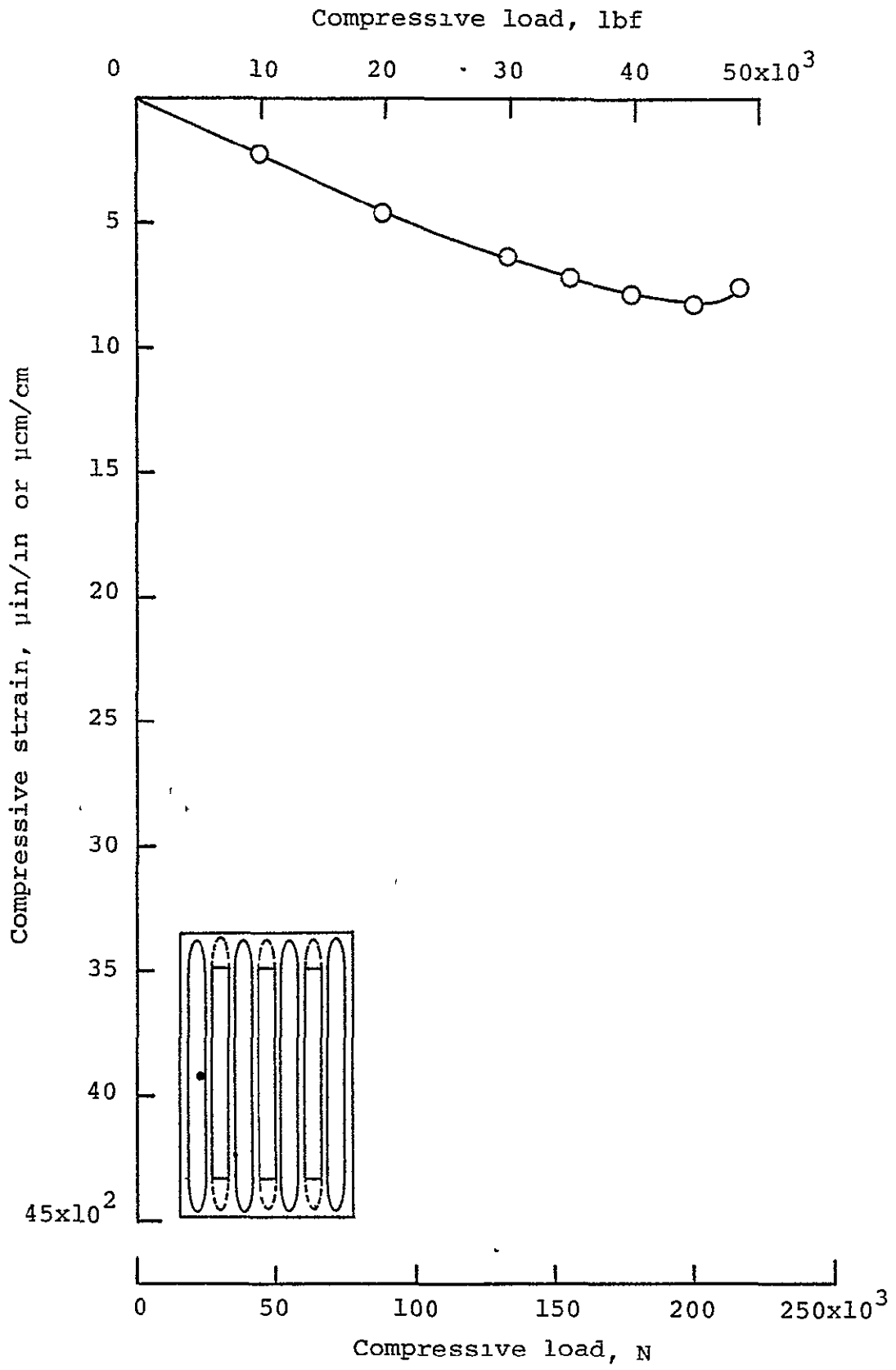
(d)   Strain gages 406, 407 and 427.

Figure A3.   Continued
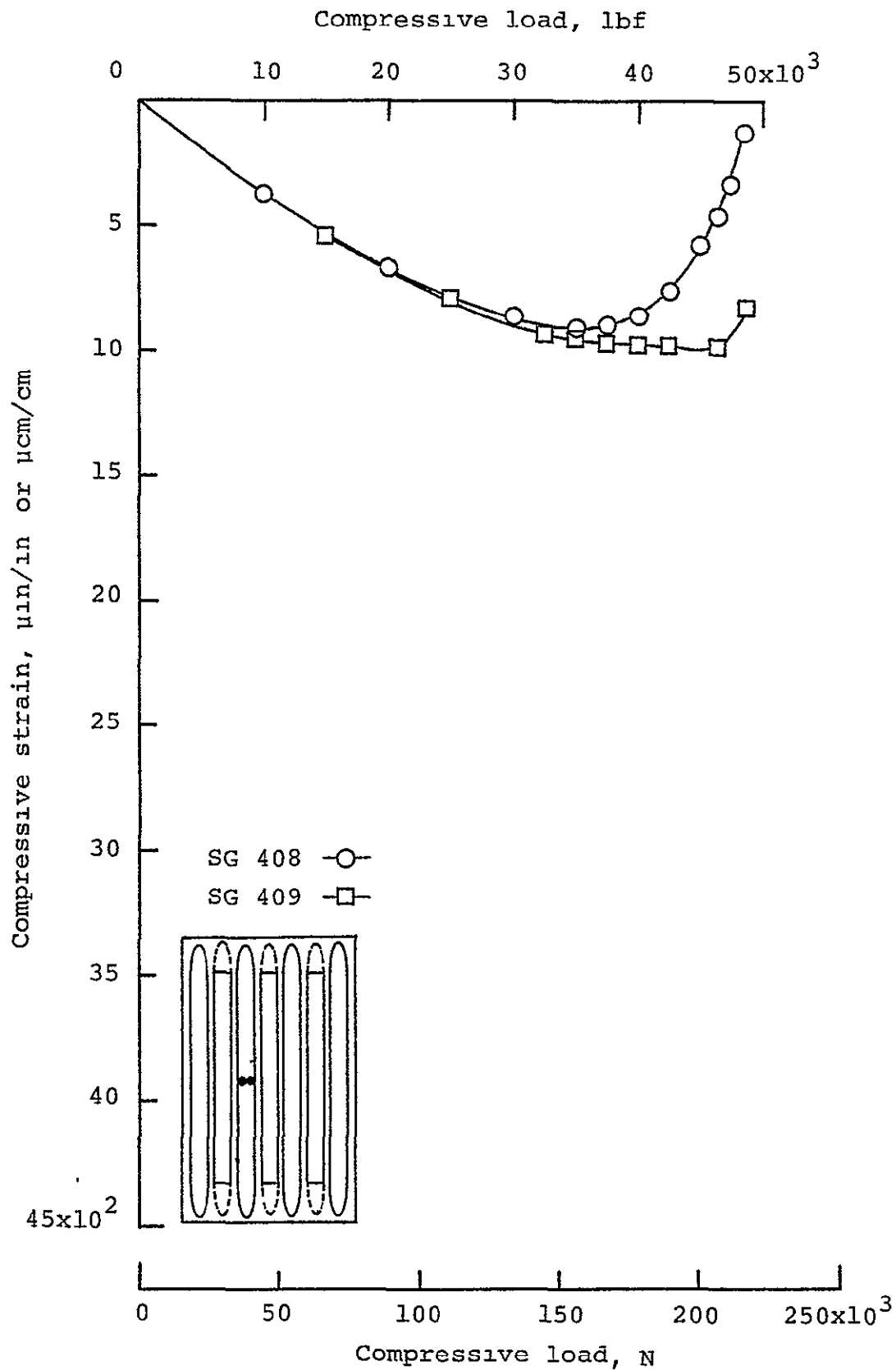
(e)   Strain gages 408 and 409.
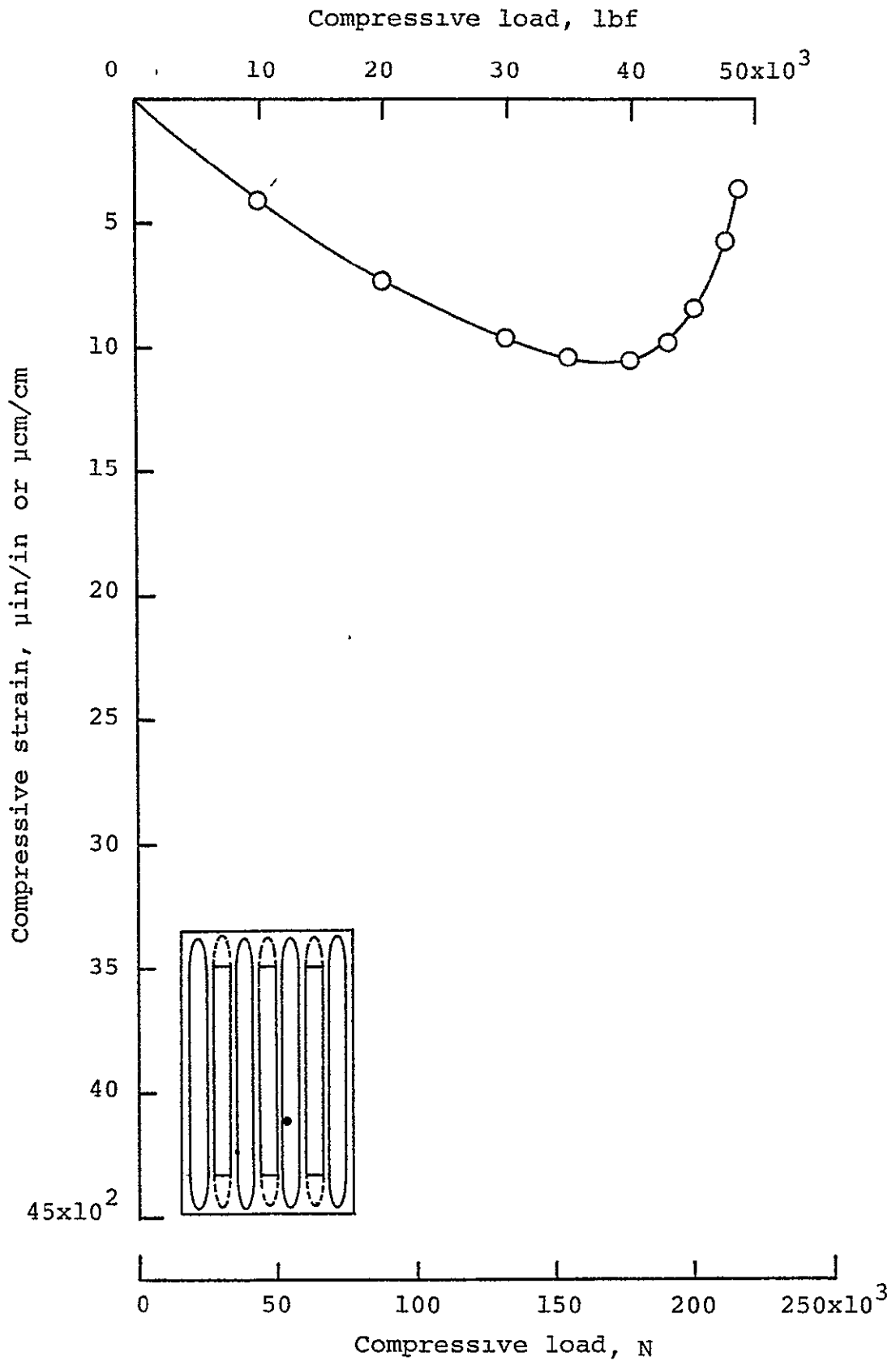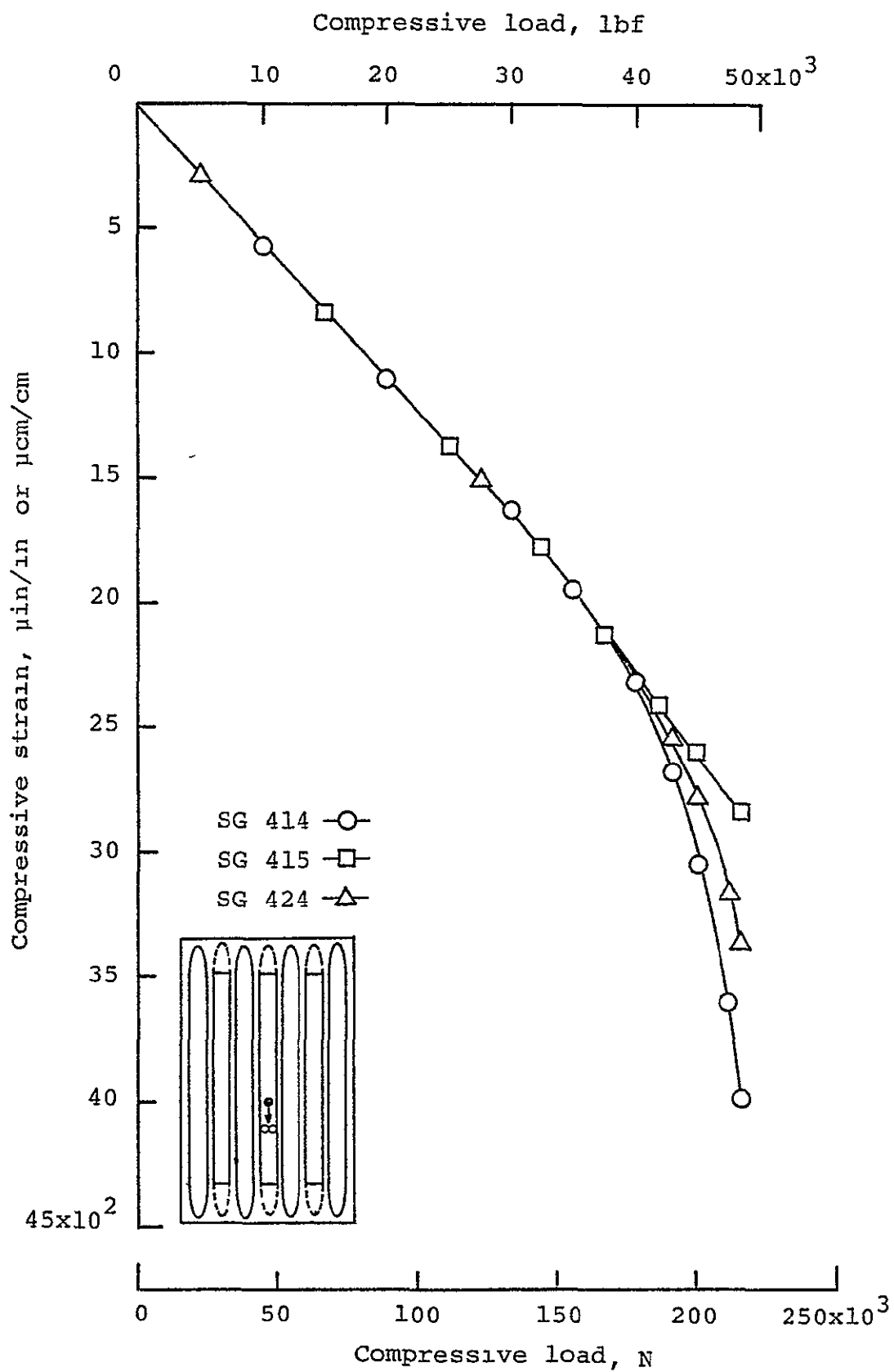
Figure A3.   Continued

Compressive load, lbf

0   10   20   30   40   50x10³

Compressive strain, µin/in or µcm/cm

5

10

15

20

25

SG 410 —O—
SG 411 —□—

30

35

40

45x10²

0   50   100   150   200   250x10³

Compressive load, N
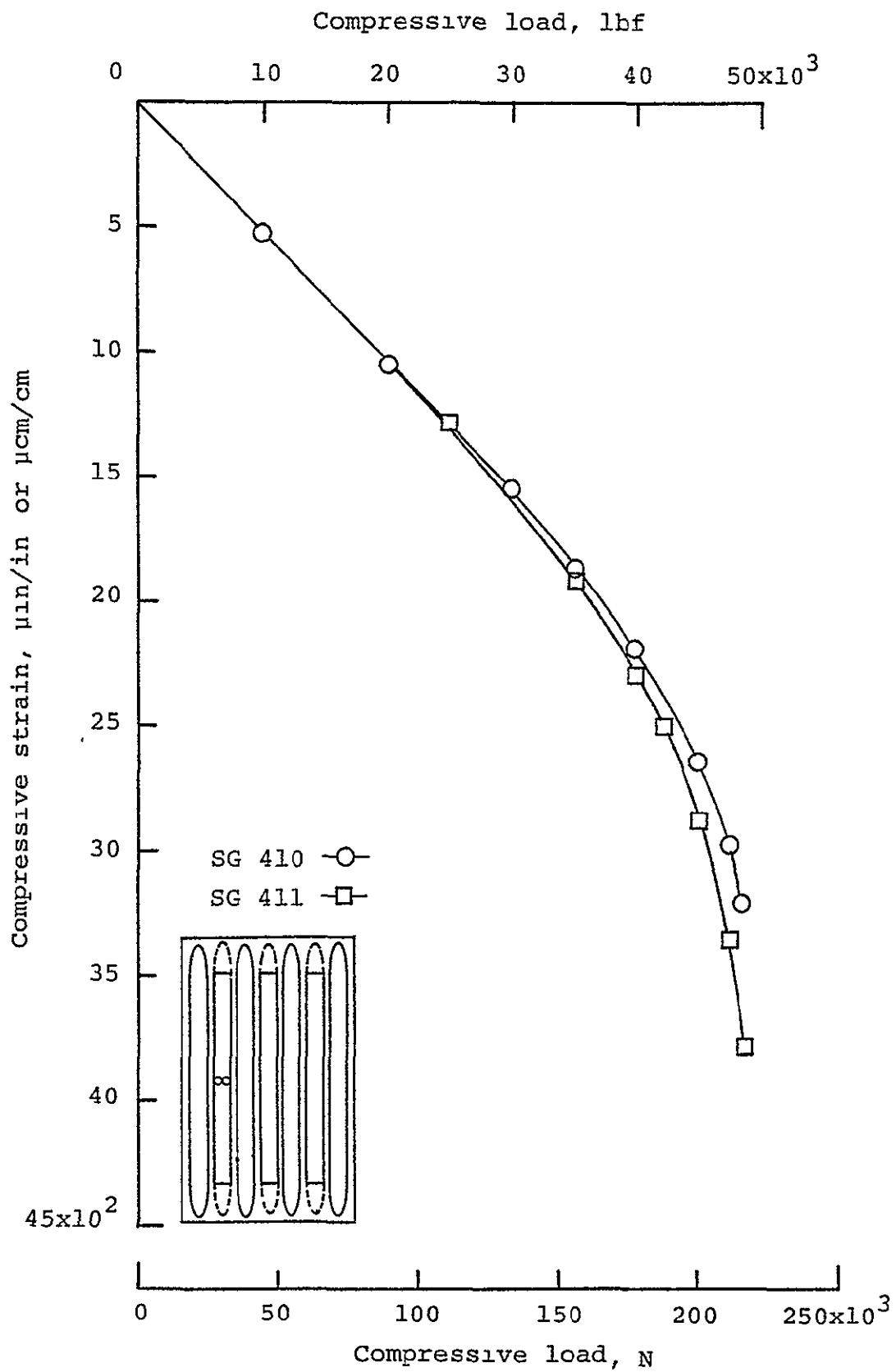
(f)   Strain gages 410 and 411.

Figure A3.   Continued

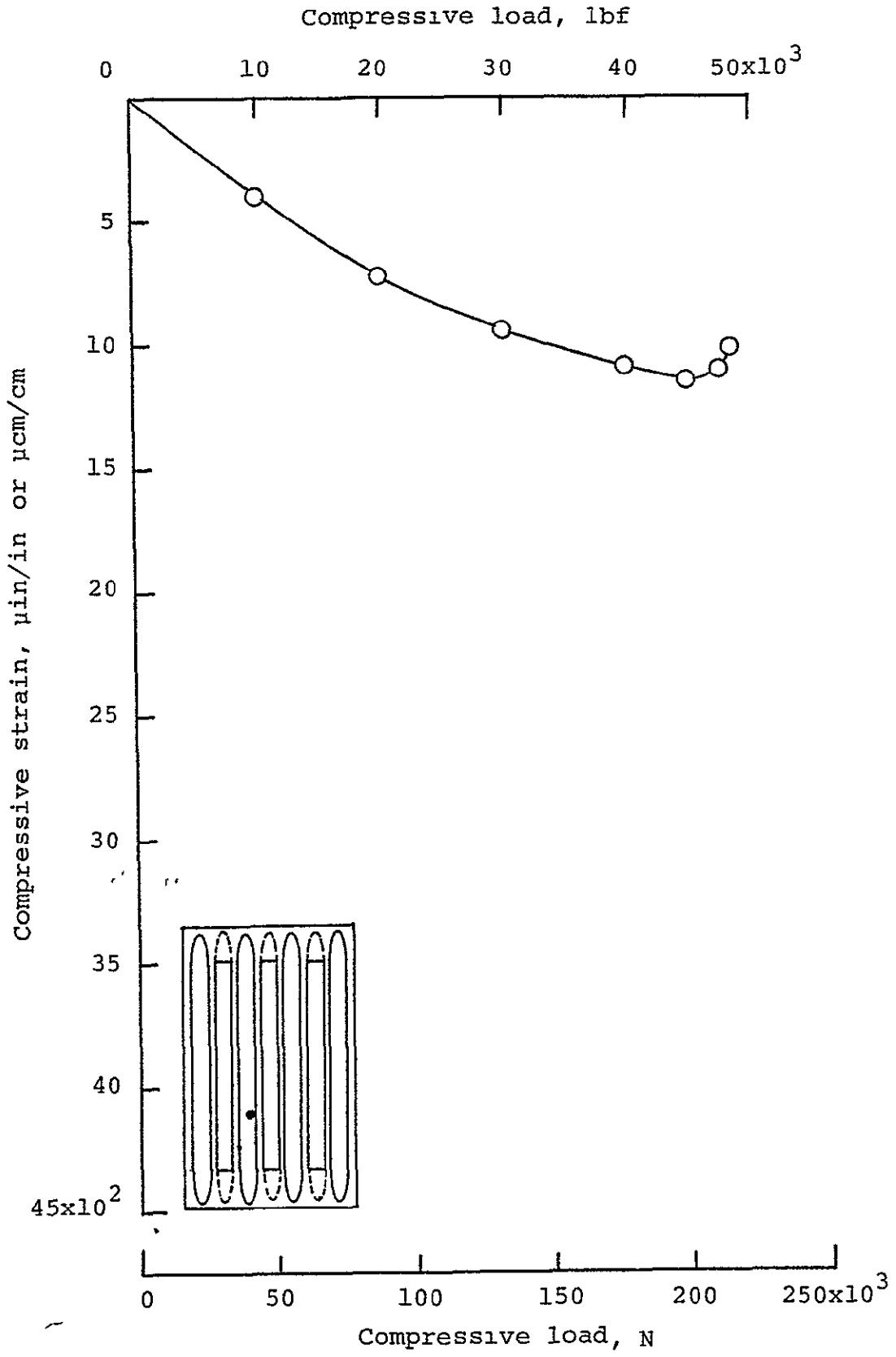(g) Strain gage 412.

Figure A3. Continued

(h) Strain gage 413.
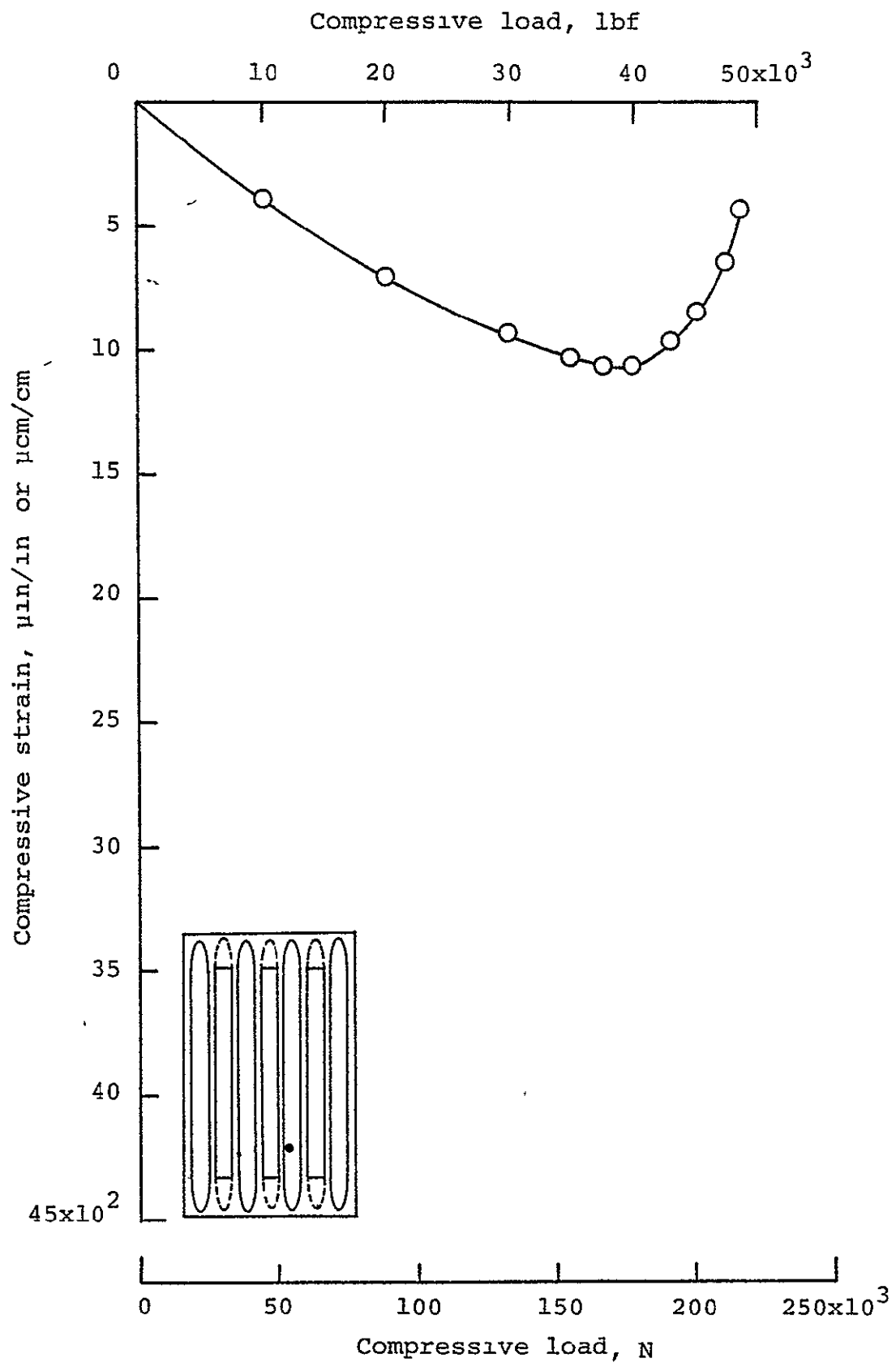
Figure A3. Continued

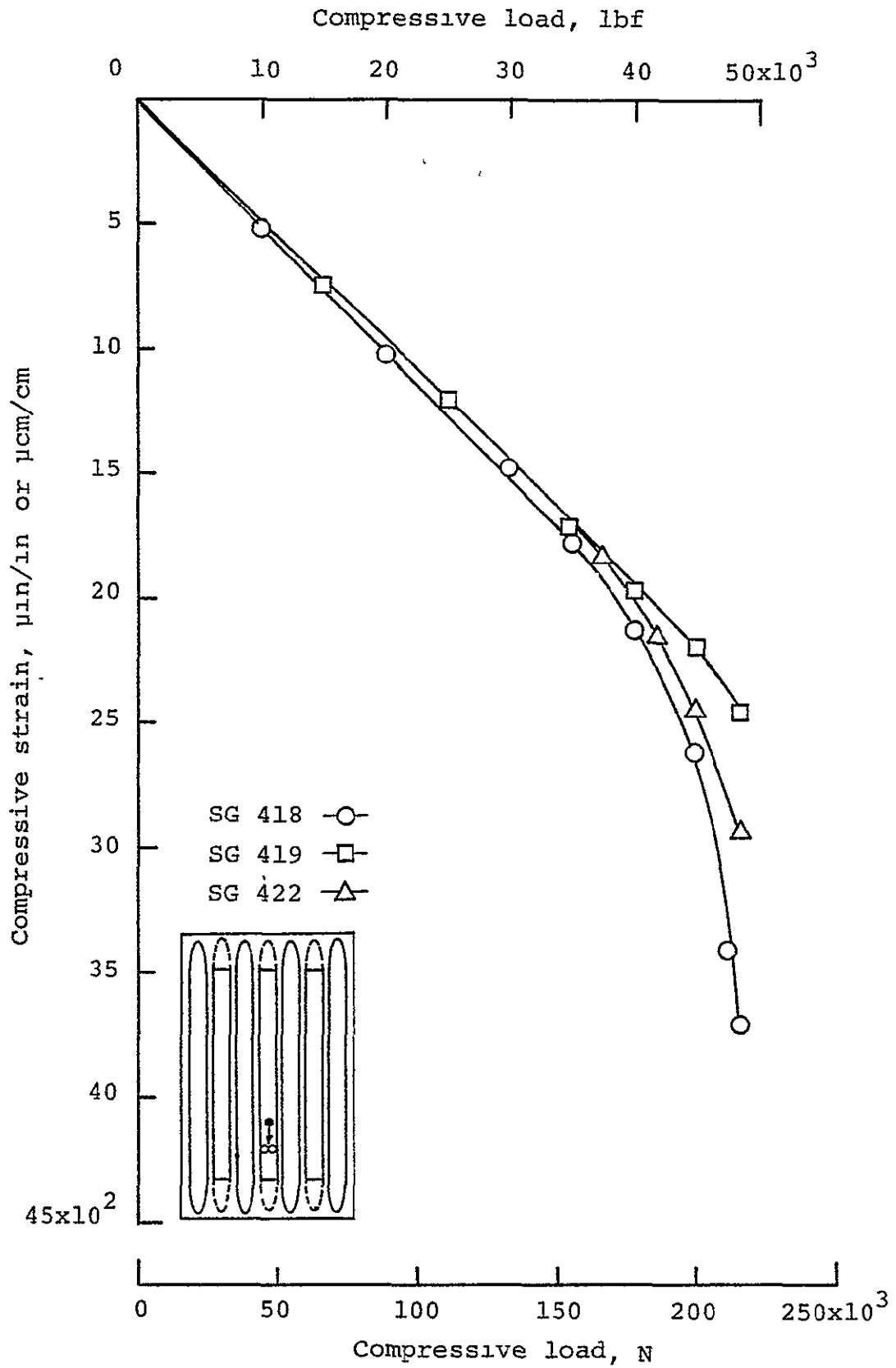(1)   Strain gages 414, 415 and 424.

Figure A3.   Continued

(j)   Strain gage 416.
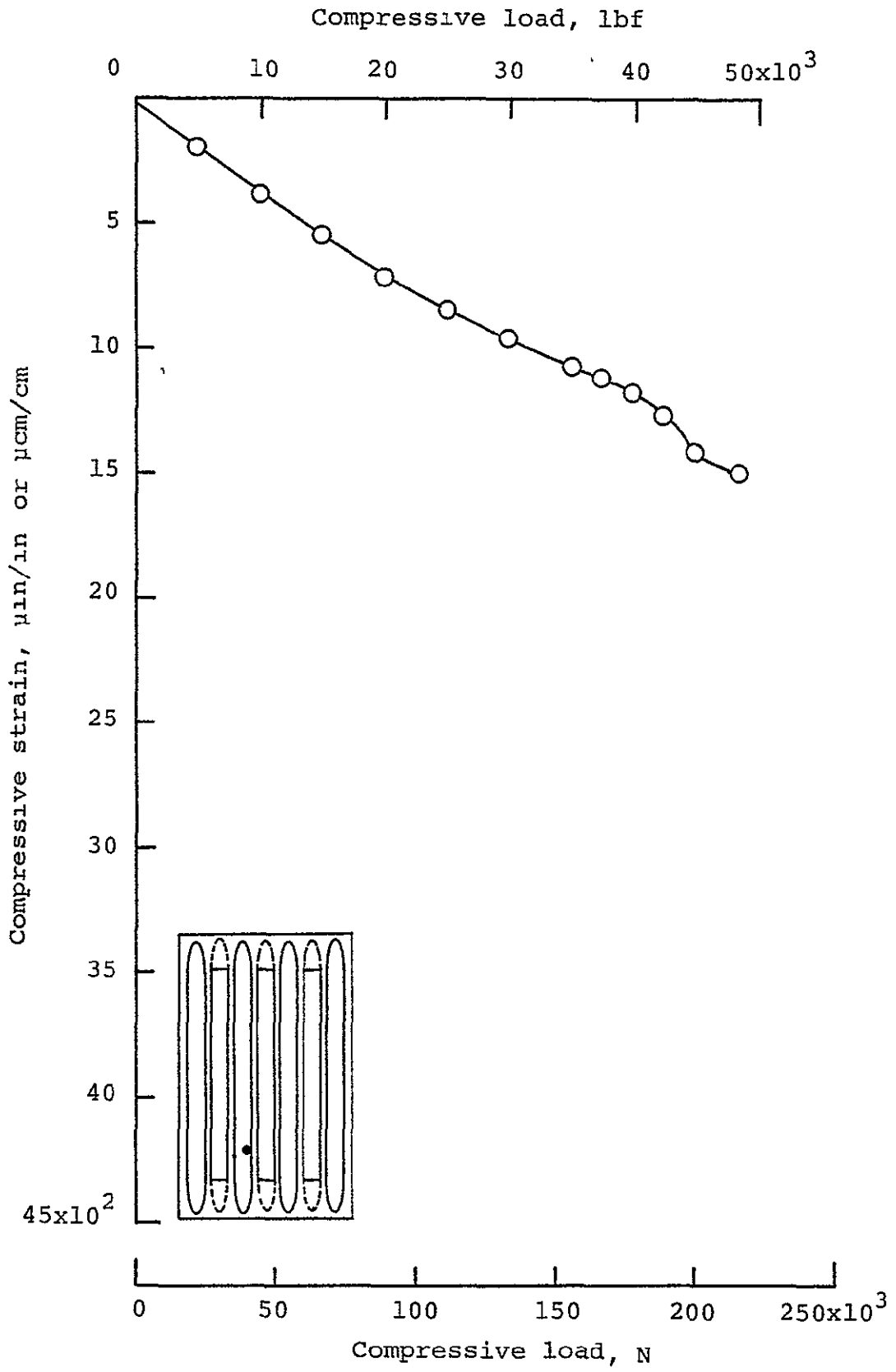
Figure A3.   Continued

99

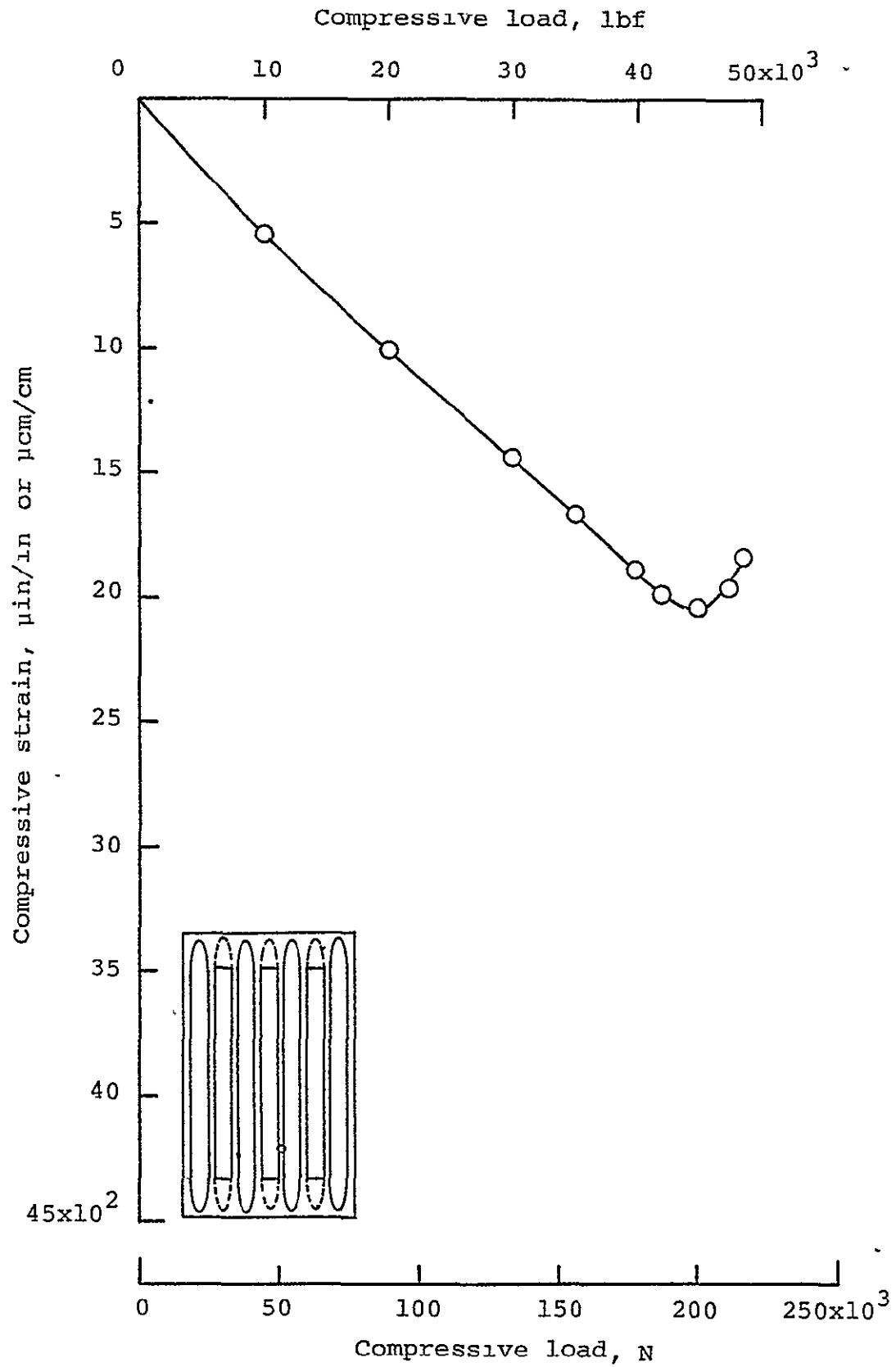(k)   Strain gage 417.

Figure A3.   Continued

(1)   Strain gages 418, 419 and 422.

Figure A3.   Continued
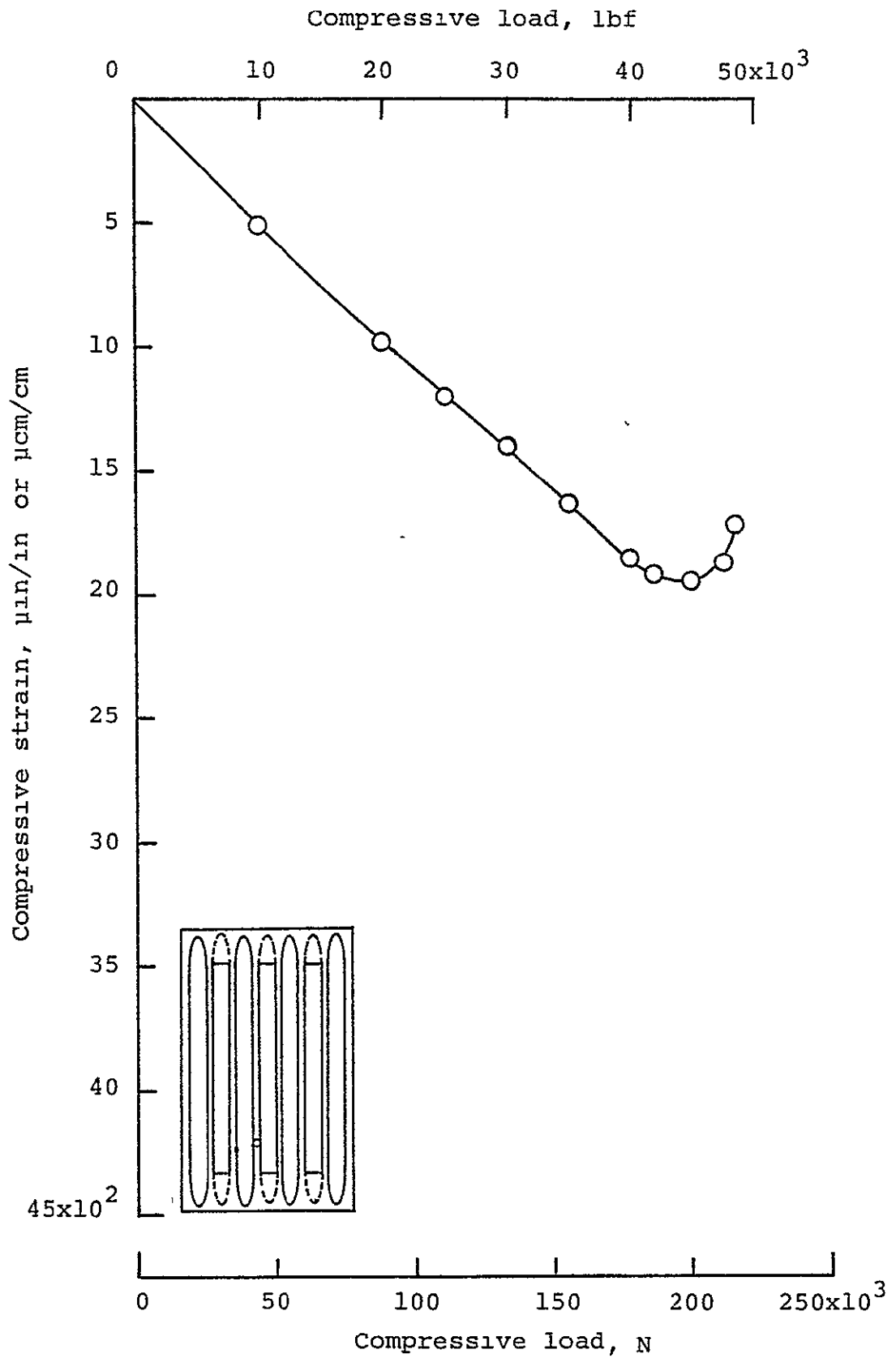
(m) Strain gage 420.

Figure A3. Continued

Compressive load, lbf

Compressive strain, μin/in or μcm/cm

Compressive load, N

(n) Strain gage 421.

Figure A3. Continued

103

(o)   Strain gage 423
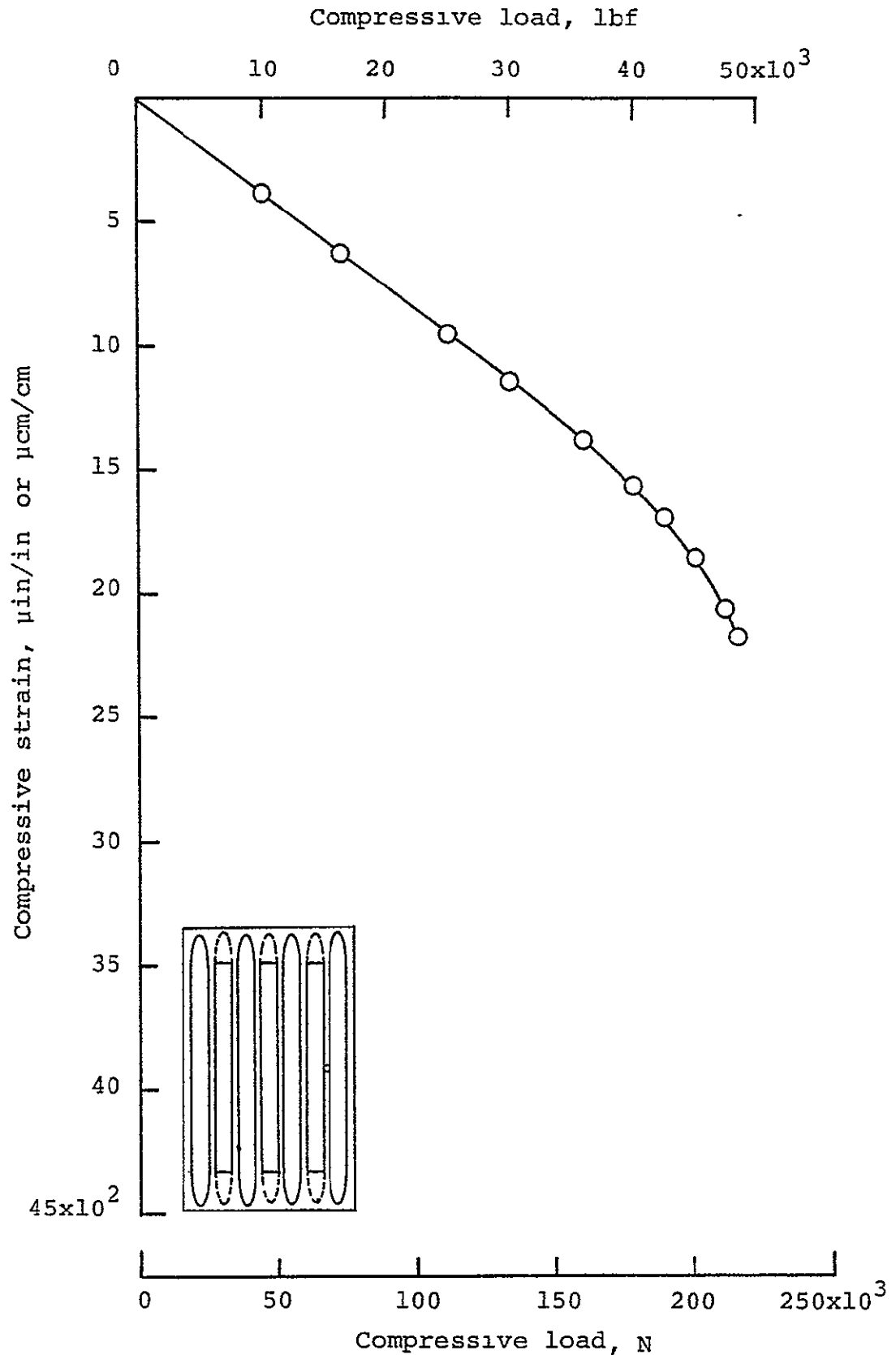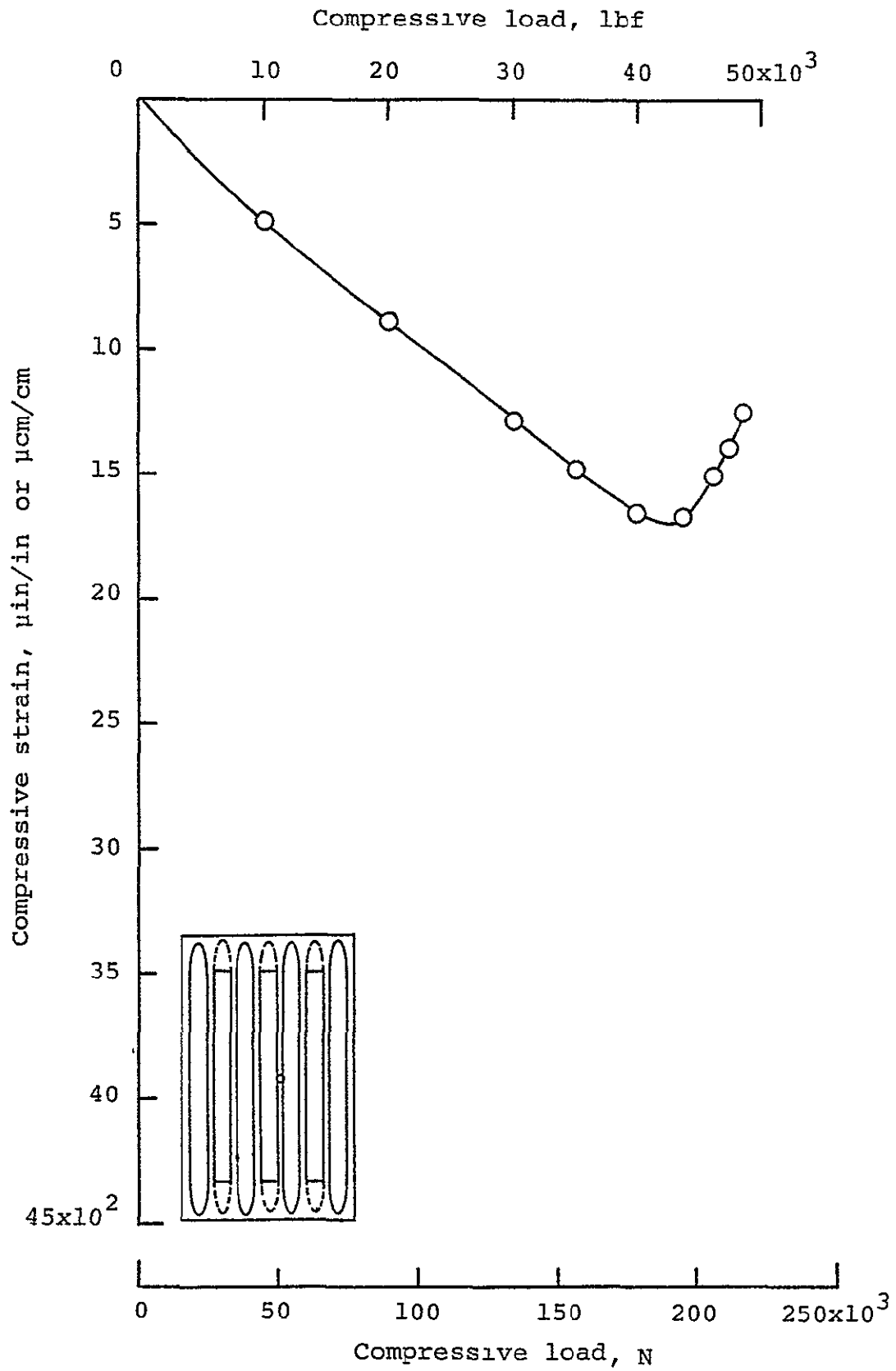
Figure A3.   Continued

104

(p) Strain gage 425.

Figure A3. Continued

(q)   Strain gage 426.

Figure A3.   Continued

(r)   Strain gage 428.

Figure A3.   Continued

(s)   Strain gage 429.

Figure A3.   Continued

Compressive load, lbf

0   10   20   30   40   50x10³

Compressive strain, μin/in or μcm/cm

5

10

15

20

25

30

35

40

45x10²

SG 430 —○—
SG 432 —□—

Note: Gages mounted on Z-section
       edge stiffener

0   50   100   150   200   250x10³

Compressive load, N
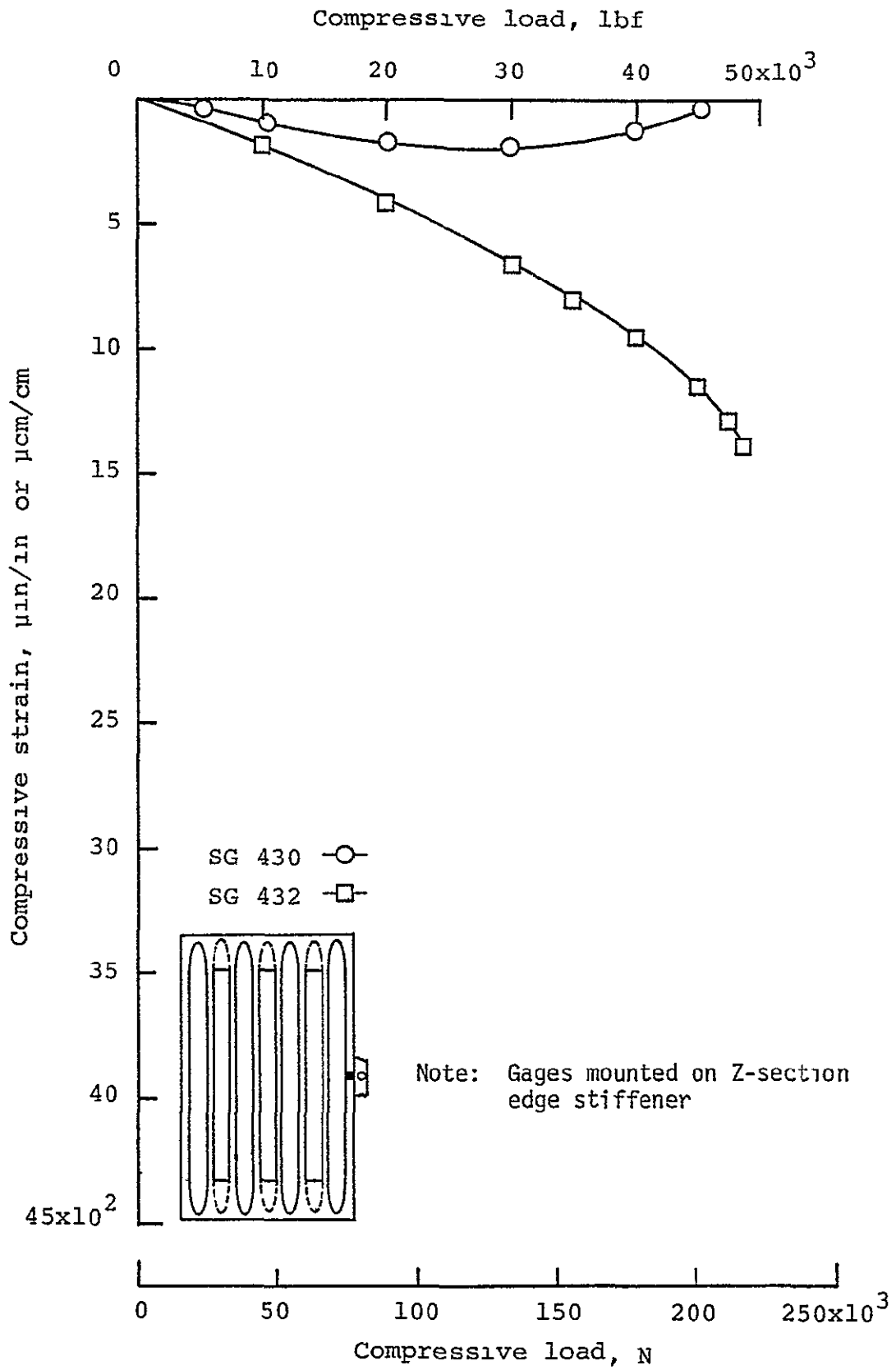
(t) Strain gages 430 and 432.

Figure A3. Continued

Compressive load, lbf

Compressive strain, μin/in or μcm/cm

SG 431 —O—
SG 433 —□—

Note: Gages mounted on Z-section
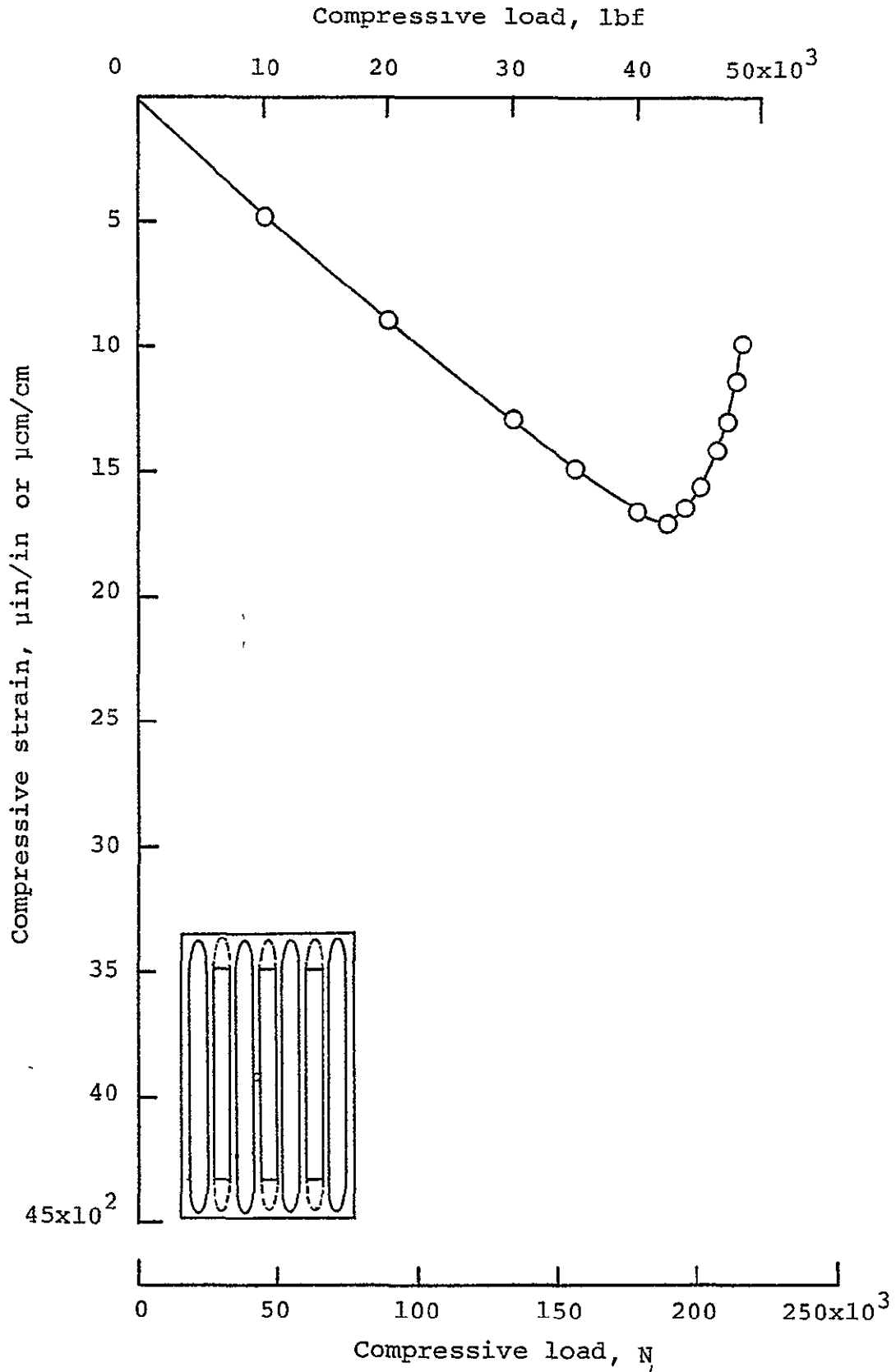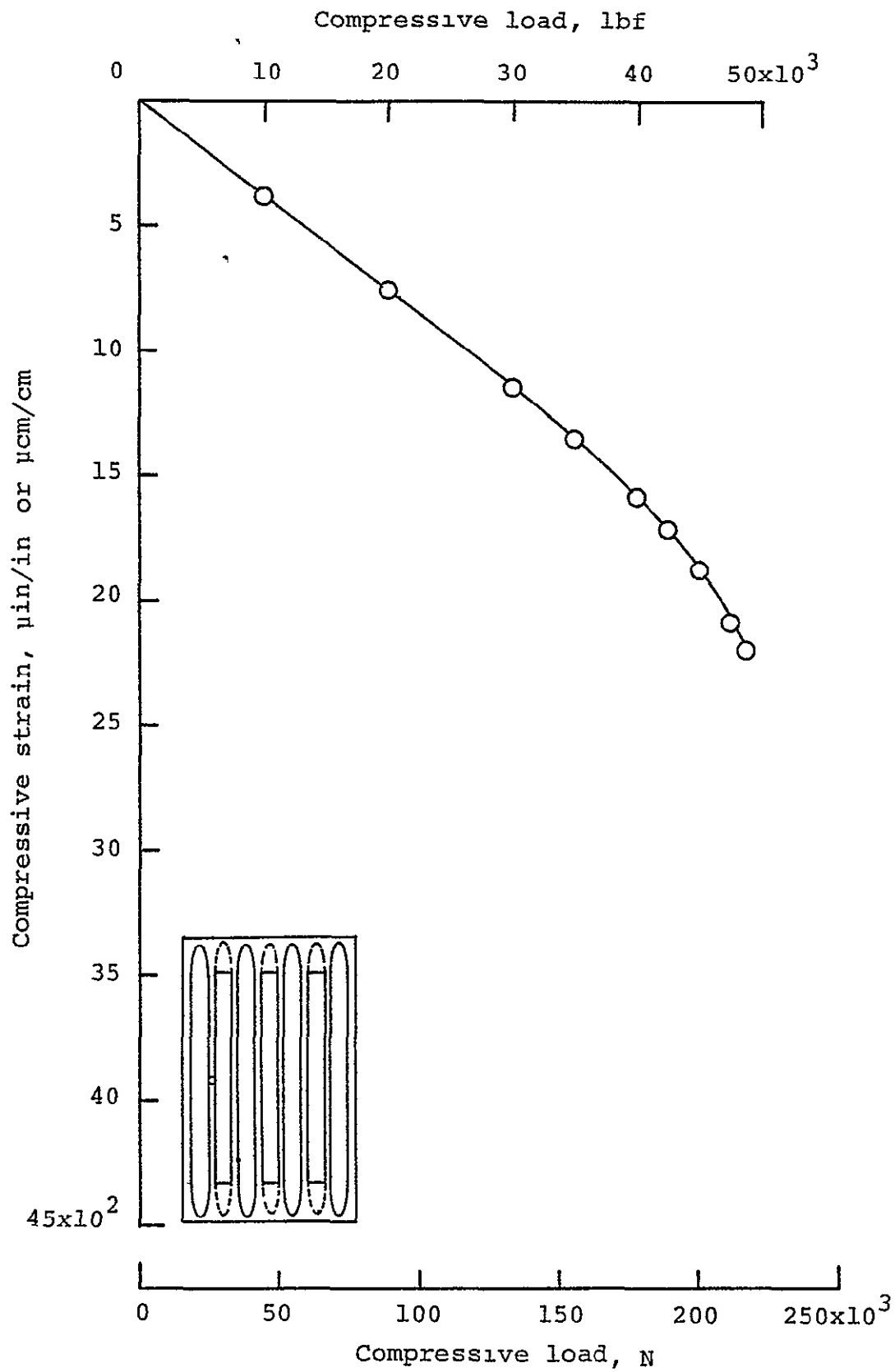edge stiffener.

Compressive load, N
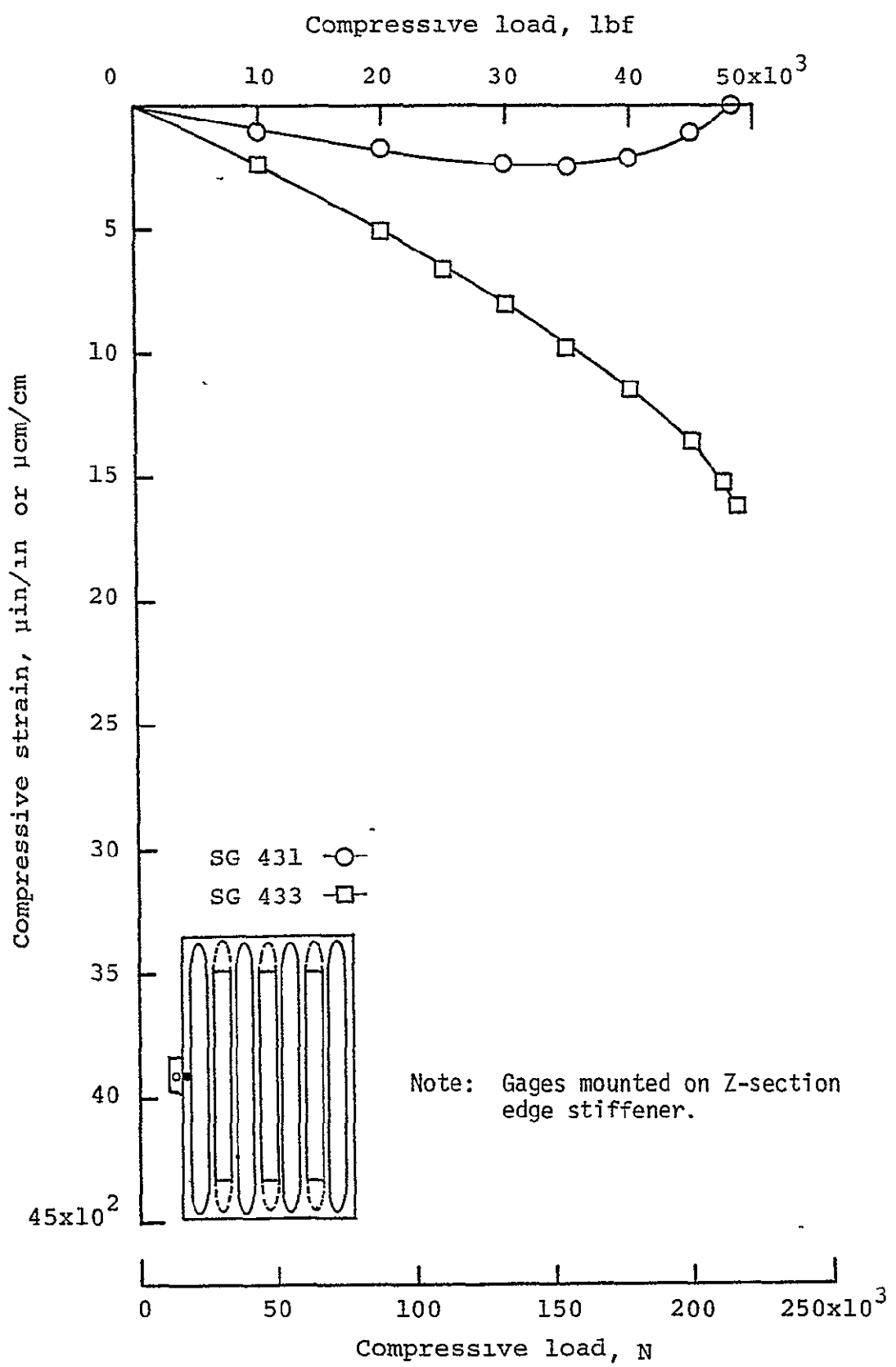
(u) Strain gages 431 and 433.

Figure A3. Continued
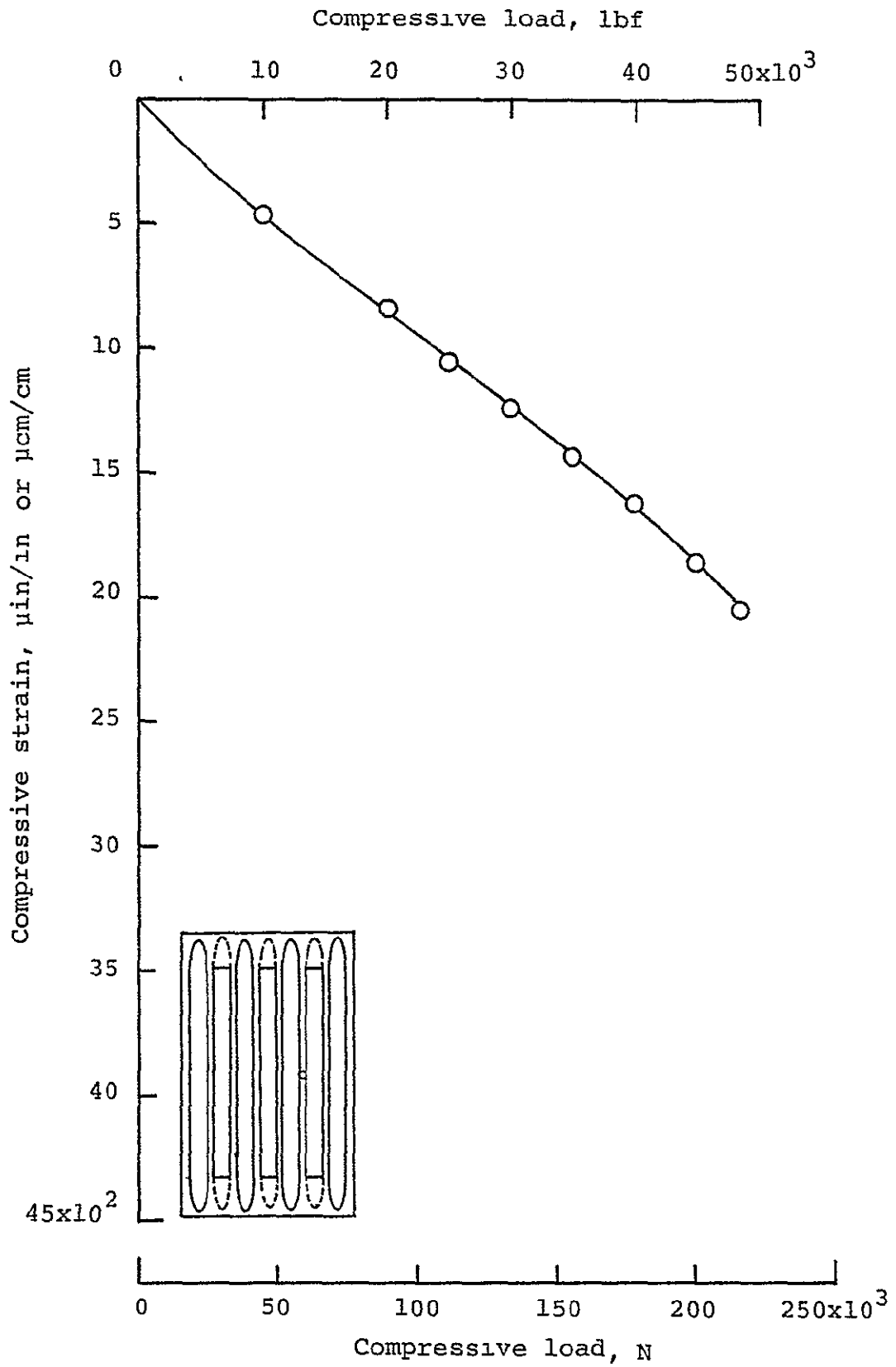
(v)   Strain gage 434.

Figure A3. Continued
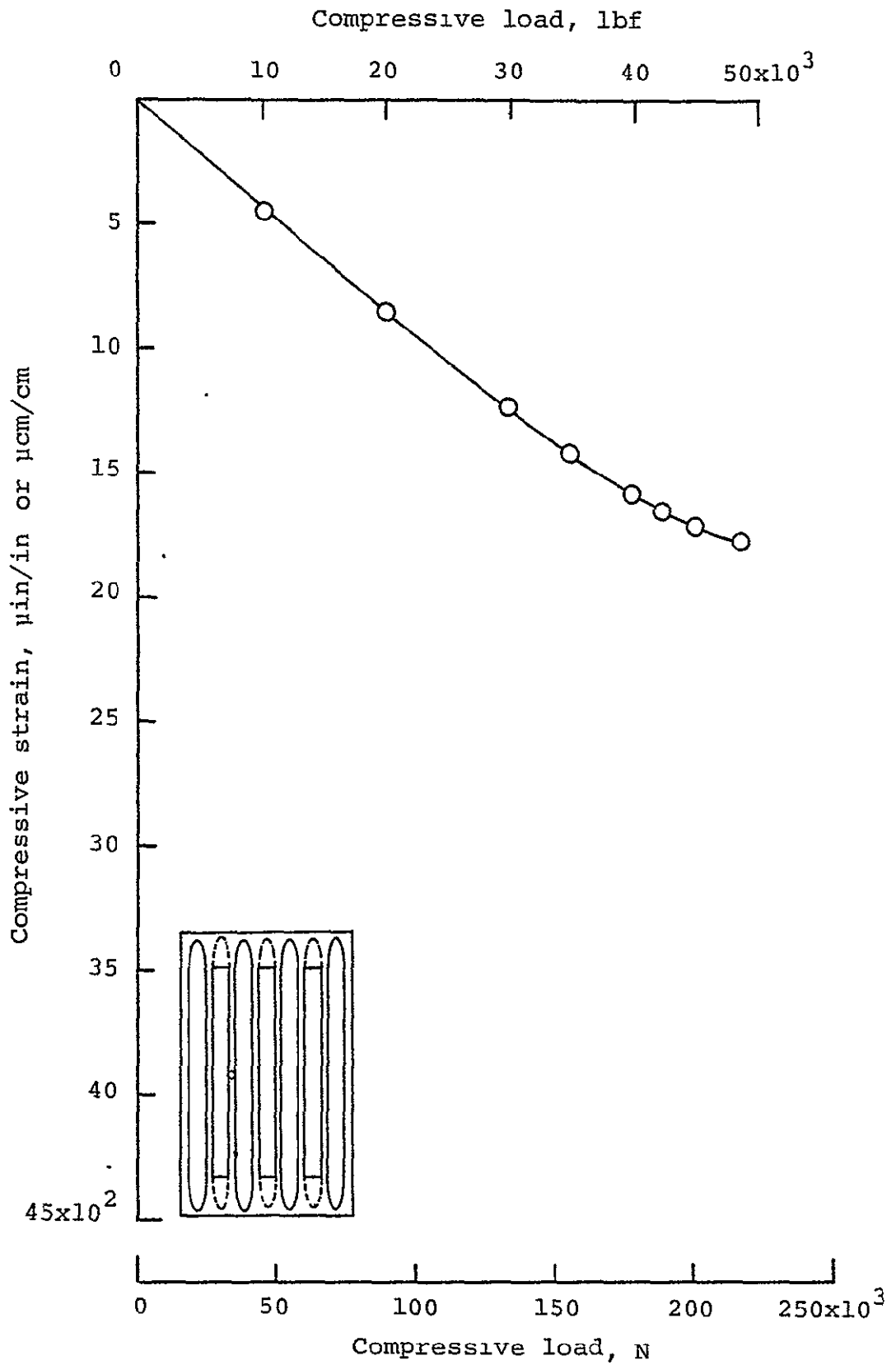
(w) Strain gage 437.

Figure A3. Continued
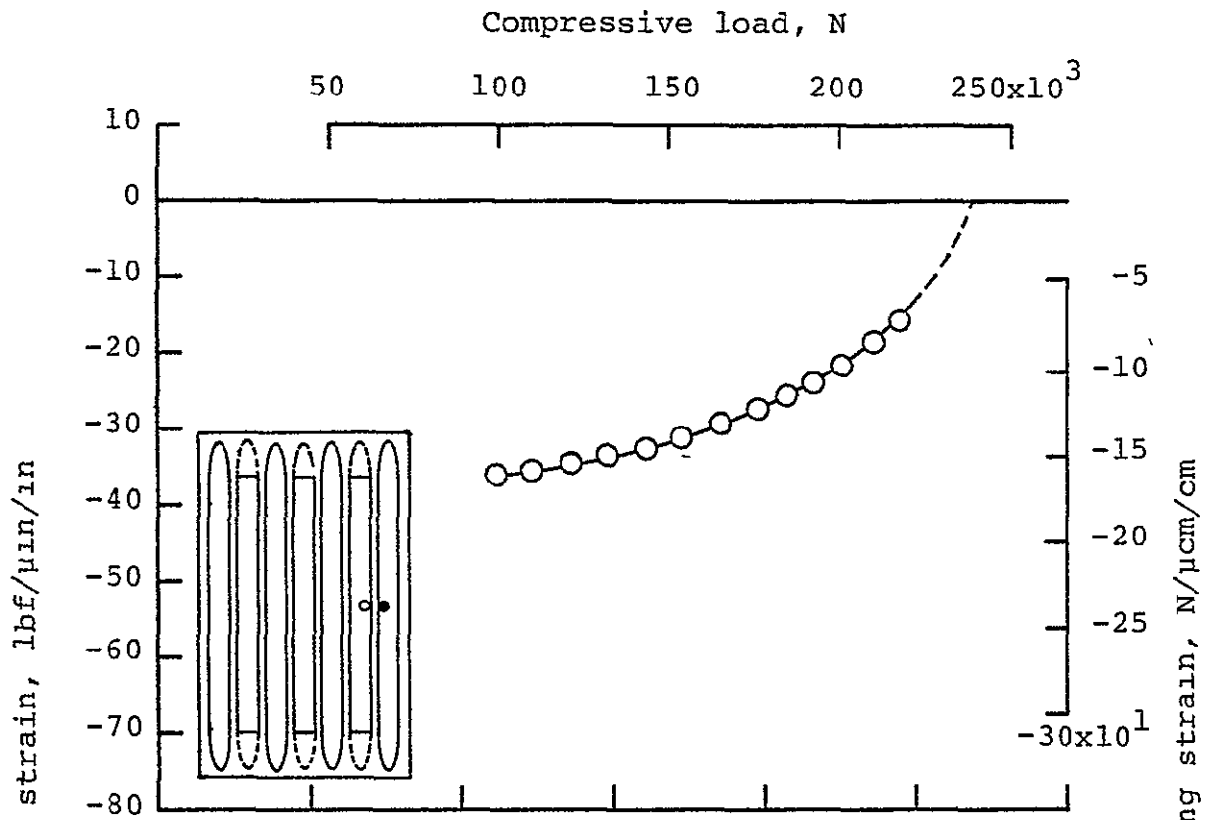
(a)   Strain gages 401 and 402.
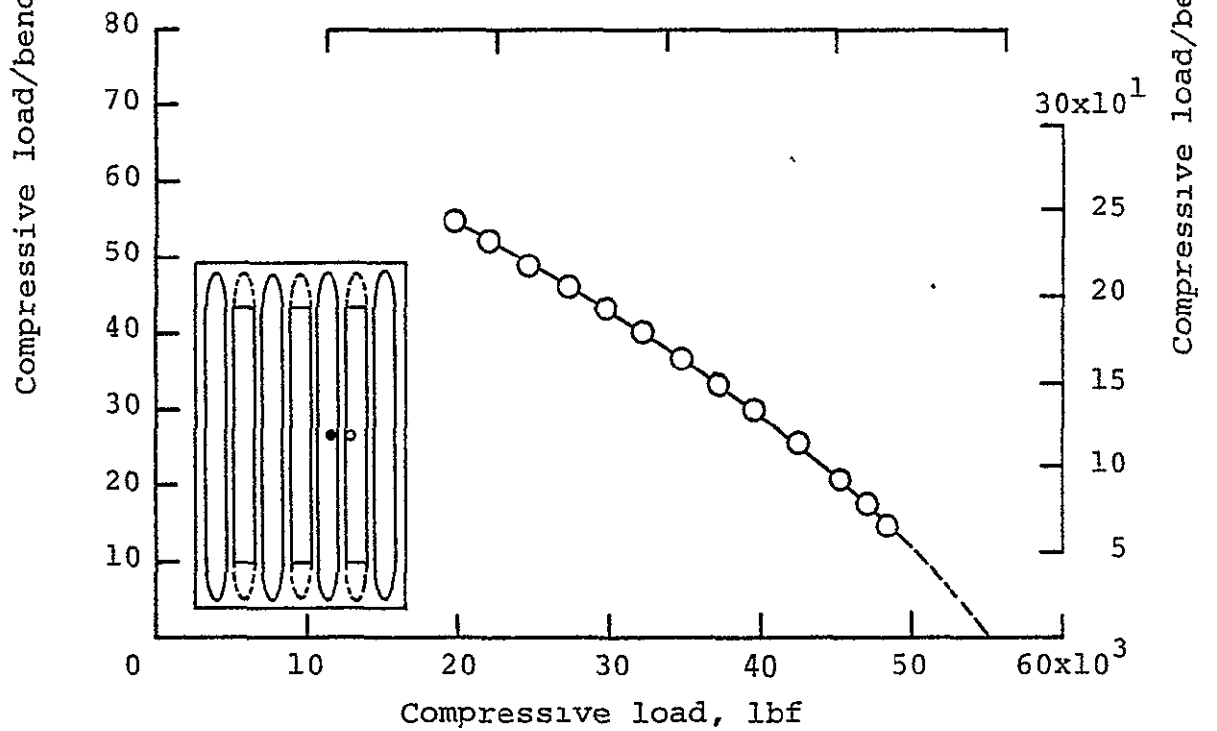
(b)   Strain gages 403 and 404.

Figure A4.   Force/stiffness plots.
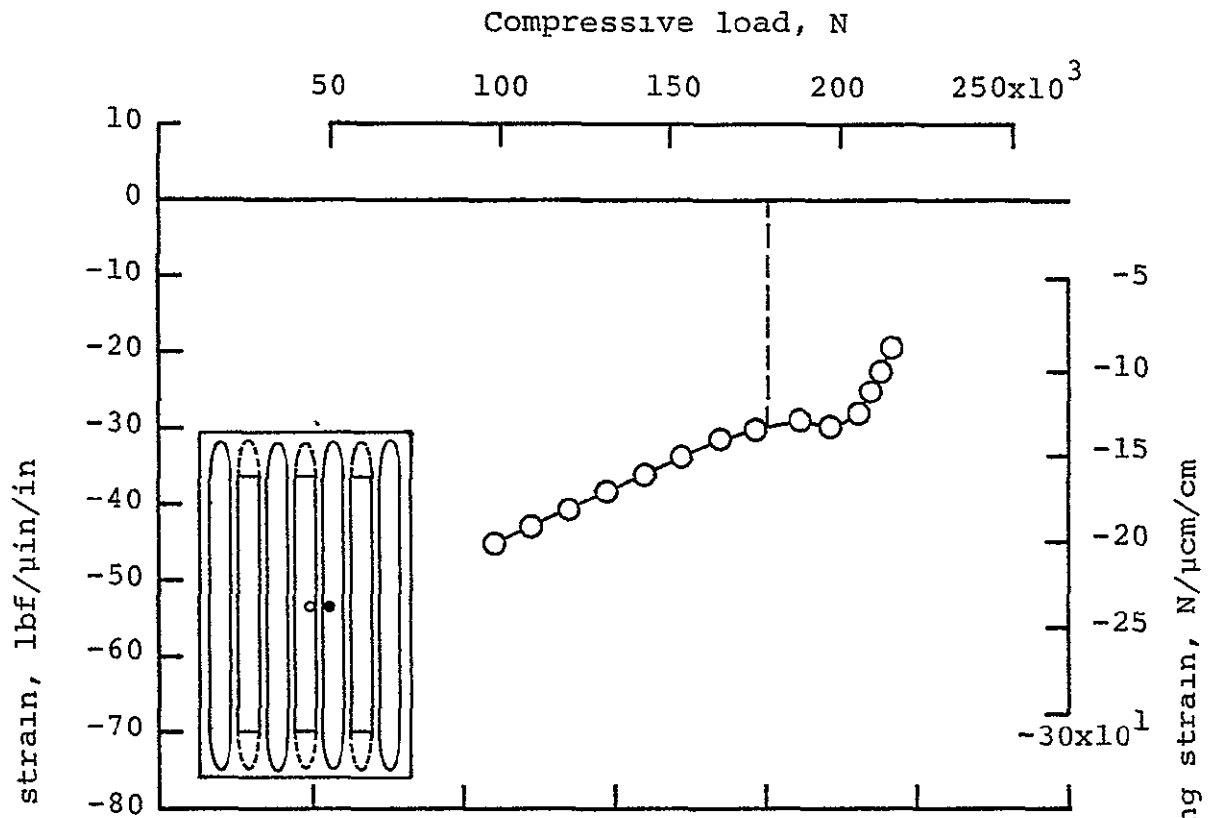
(c)   Strain gages 405 and 406.
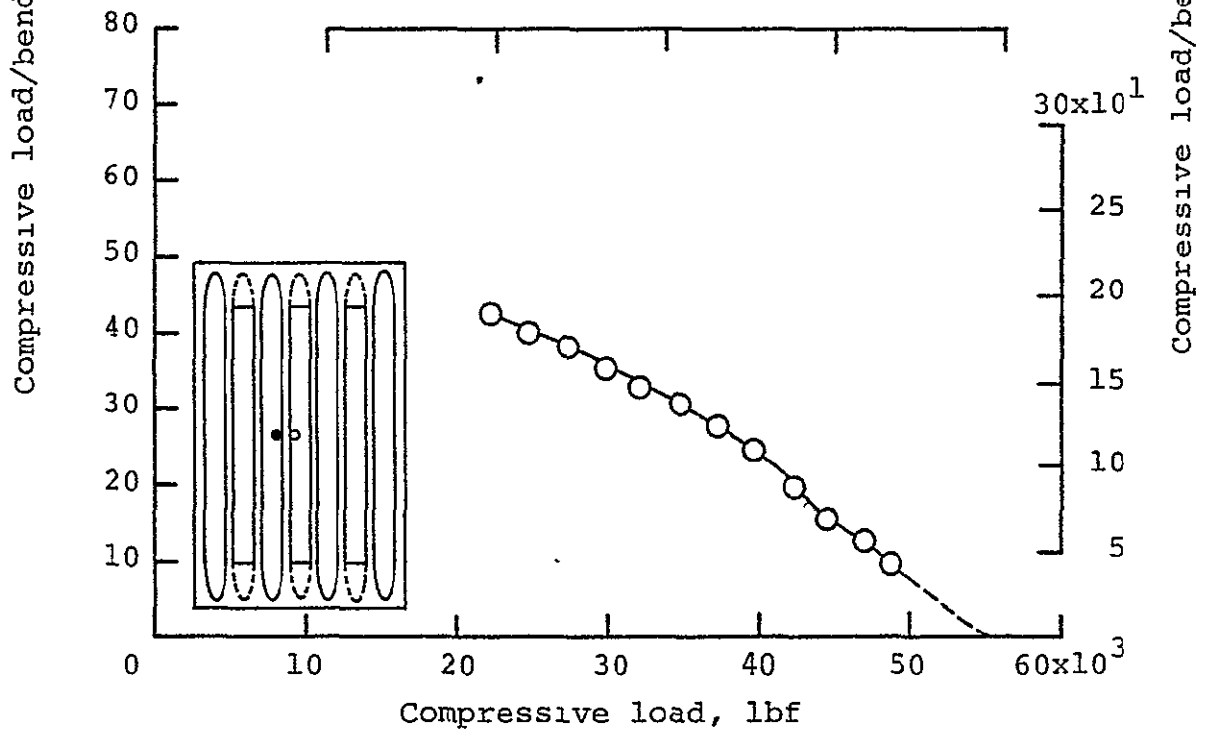
(d)   Strain gages 407 and 408.

Figure A4.   Continued

(e)   Strain gages 409 and 410.

(f)   Strain gages 411 and 412.

Figure A4.   Continued
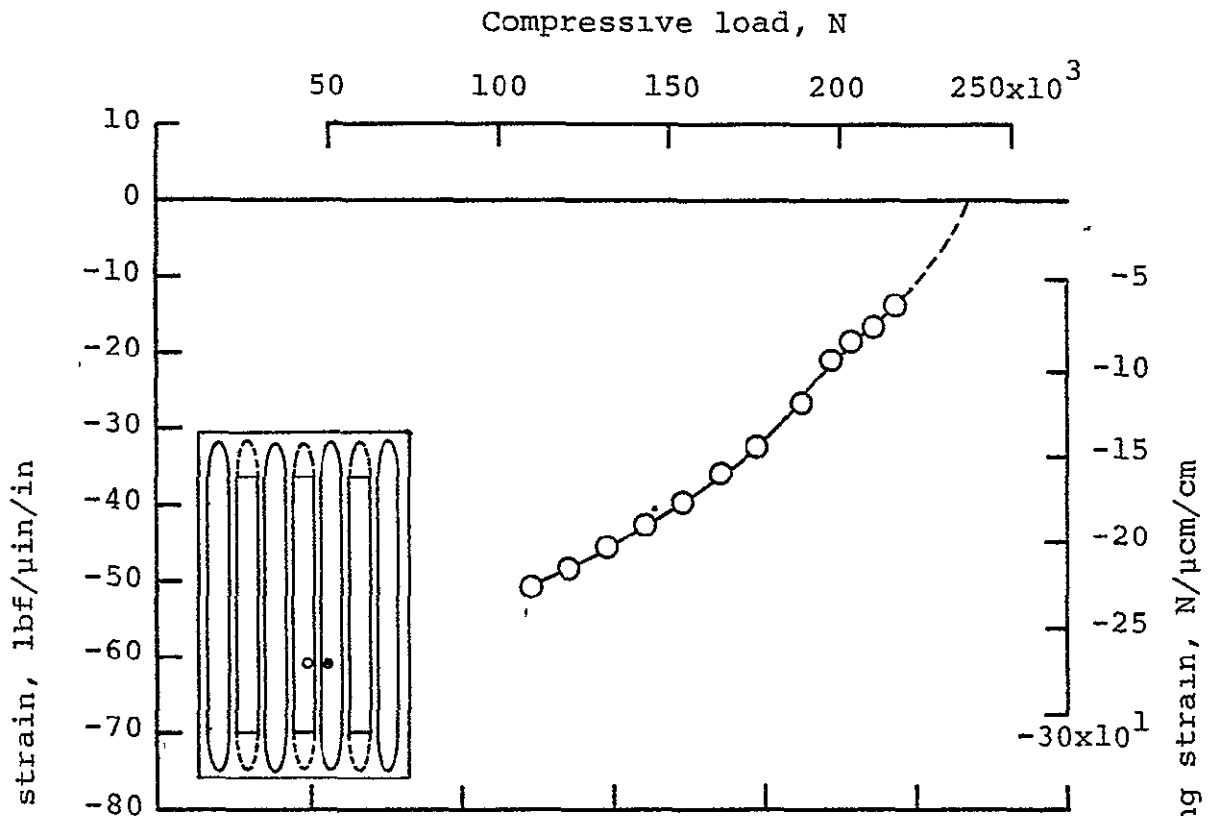
(g)   Strain gages 413 and 414.
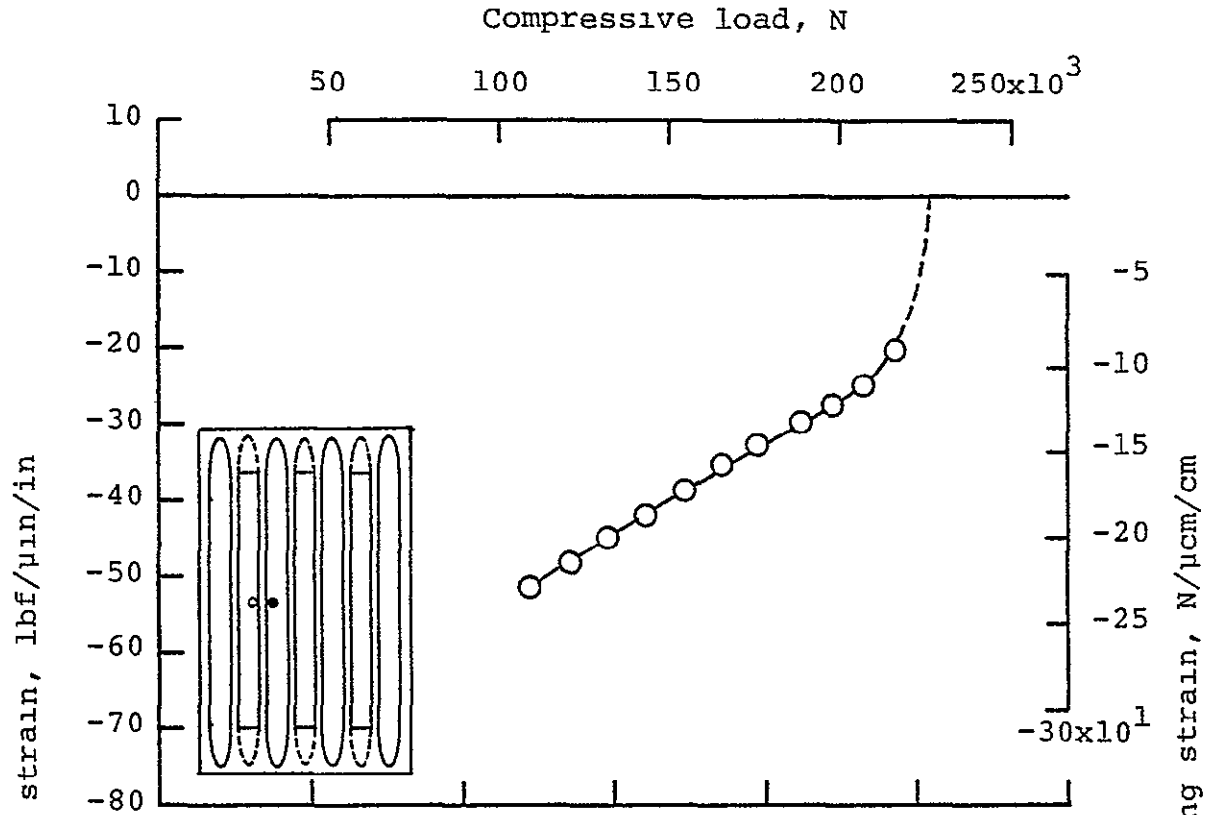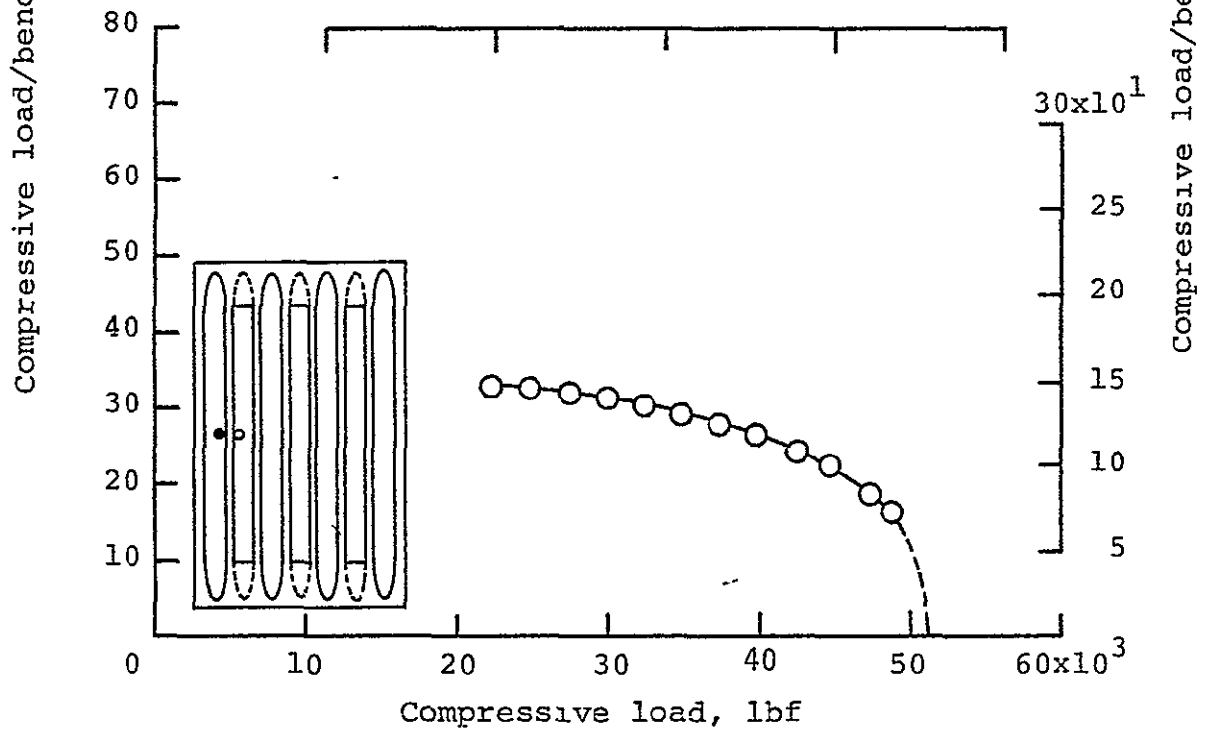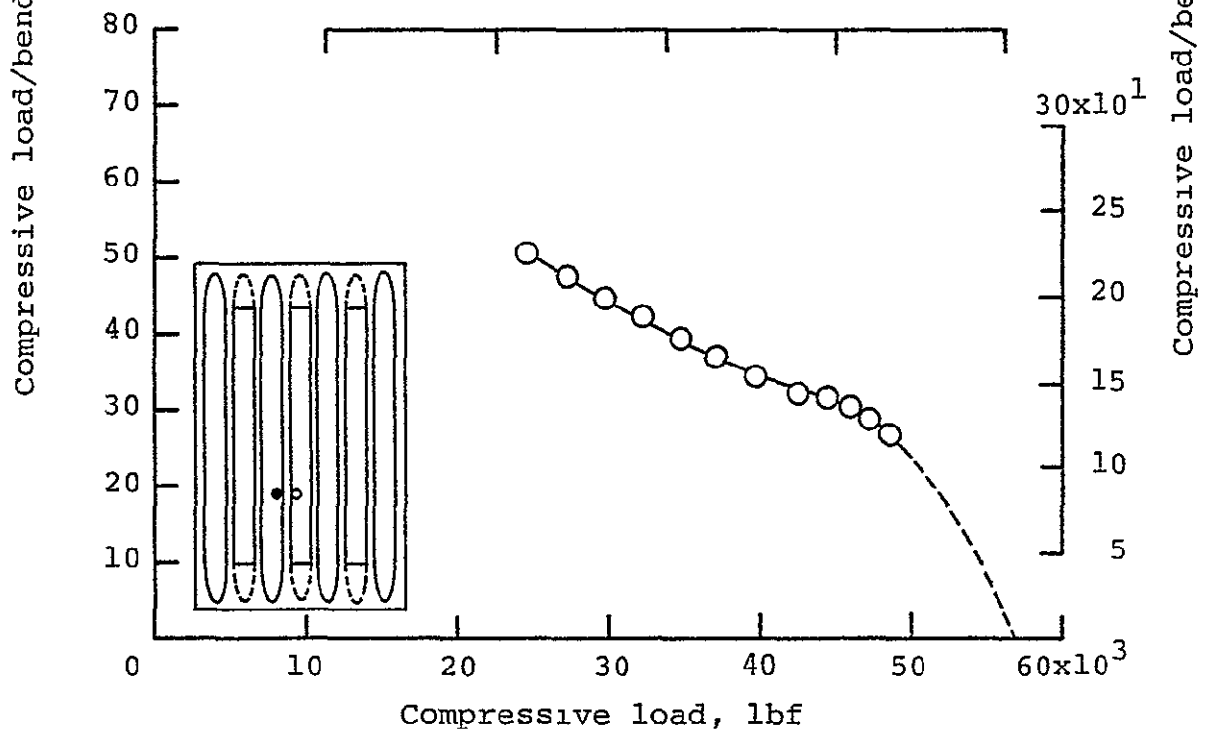

(h)   Strain gages 415 and 416.

Figure A4.   Continued
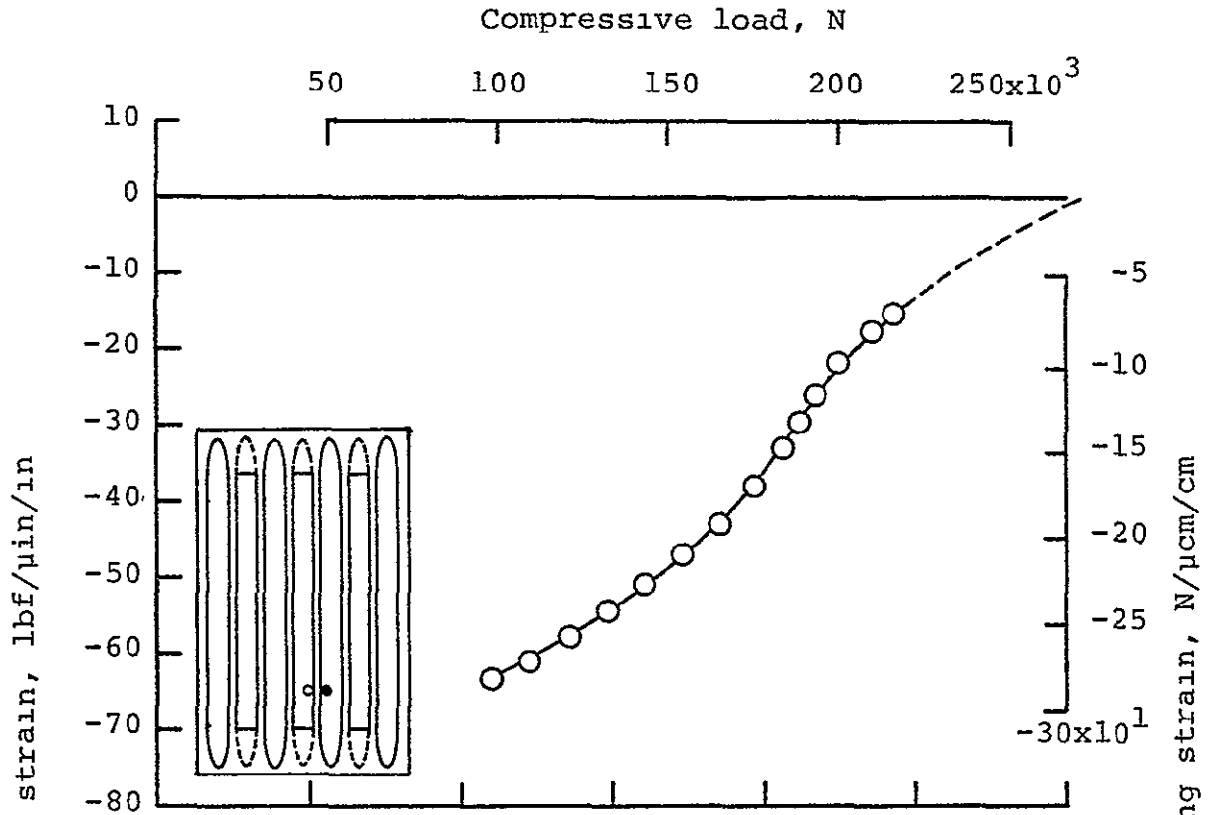
(i)   Strain gages 417 and 418.
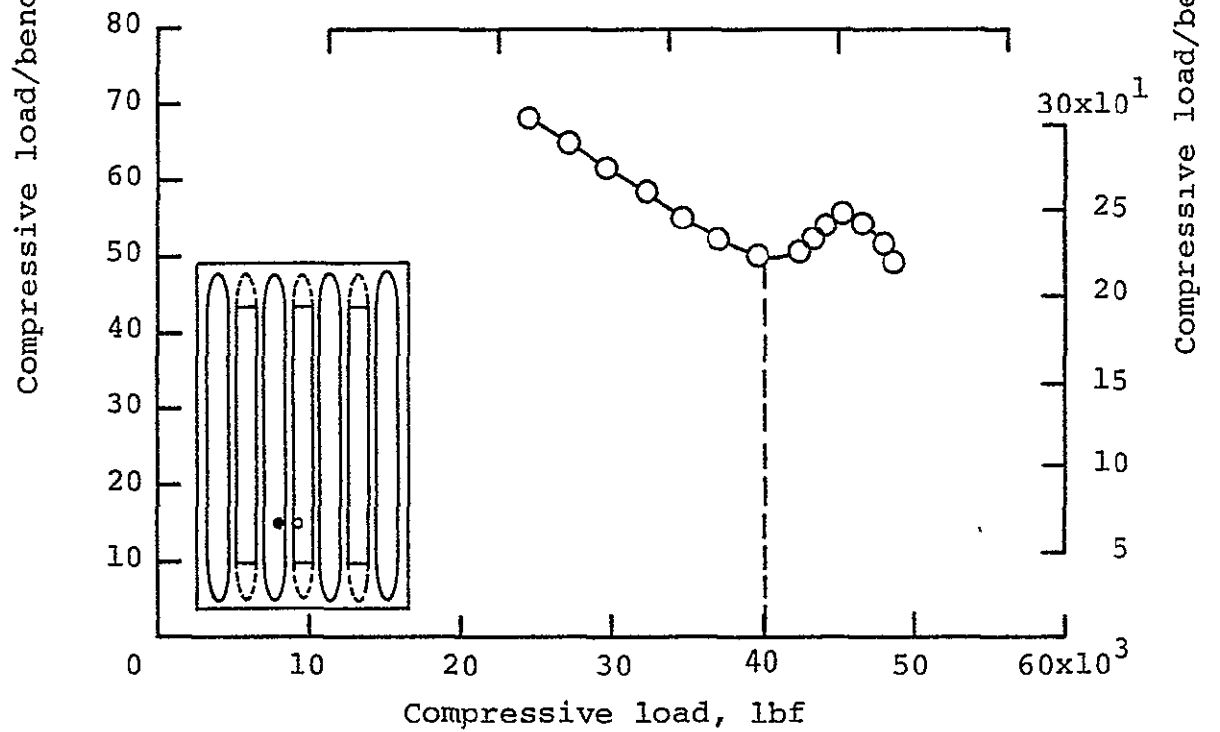
(j)   Strain gages 419 and 420.

Figure A4.   Continued

APPENDIX B

The Force/Stiffness Technique

The Force/Stiffness Technique

The force/stiffness technique is a nondestructive test technique used to experimentally determine the buckling strength of a structure (ref. 13). This method of nondestructive testing is based upon the out-of-plane deflection characteristics of a structure under compressive load.

In figure B1, two strain gages are shown mounted to opposite sides of a panel which is under a compressive load. Initially, as the load is increased, both gages measure a compressive strain. As the column deflects to produce the stresses indicated, gage A measures an additional compressive component due to bending and gage B measures an additional tension component due to bending. When the output of gage B is subtracted from gage A, the resulting strain is that due to panel bending, only. When the compressive load is divided by the difference of the gages and plotted against load, the result is a plot similar to that shown in figure B1. Theoretically, buckling occurs when the curve intersects the load axis. Usually the loading is stopped before the curve intersects the load axis and the curve is extrapolated to an indicated (predicted) buckling load.
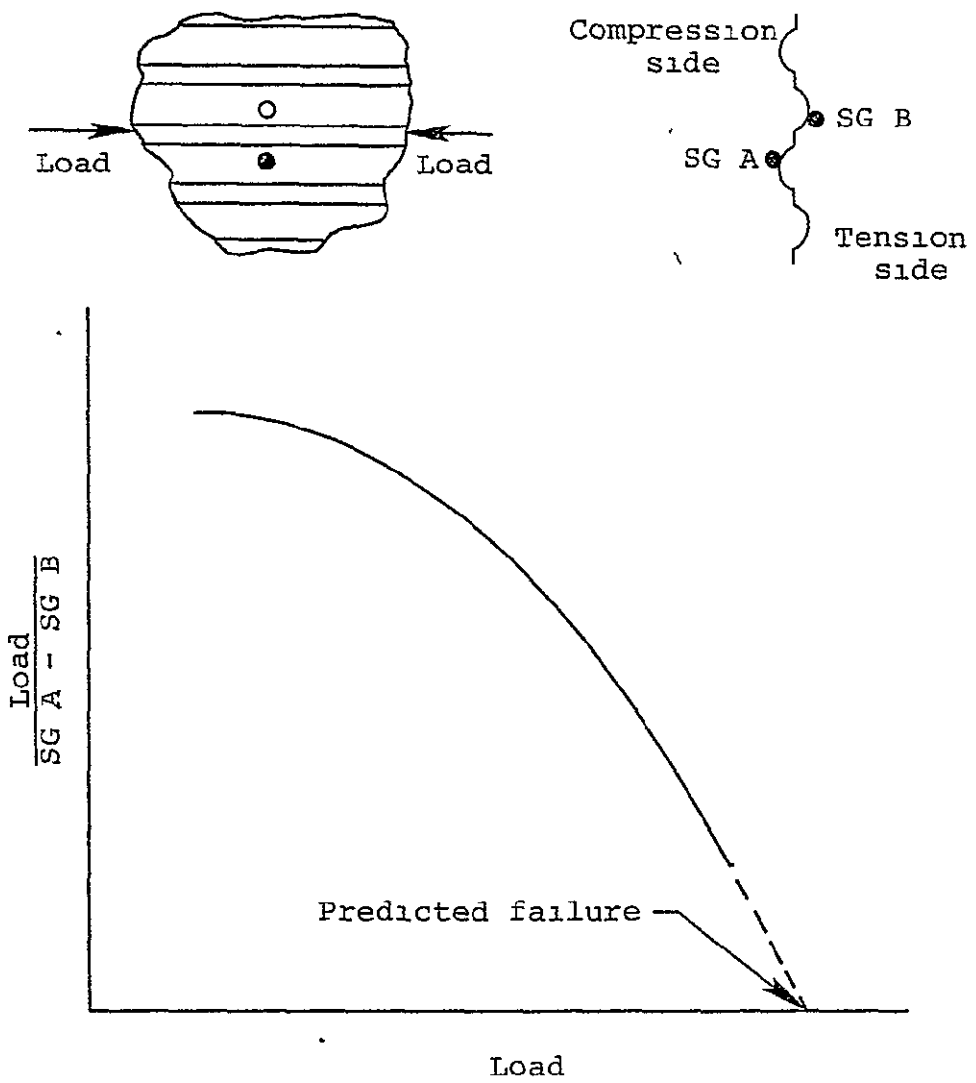
Figure B1. Mechanics of the force/stiffness technique.

APPENDIX C

The Moiré Fringe Technique

The Moiré Fringe Technique .

The second method of measuring out-of-plane displacements of the panel utilized the Moiré fringe technique (ref. 14). This technique is best described with the aid of figures C1 and C2. The Moiré fringe technique requires the use of a camera, a point source of light, and a grid plane, arranged in a manner similar to that shown in figure C1.

The grid plane referred to above is typically made on a sheet of clear distortion free plastic photographic film. A system of equally spaced parallel black lines is then applied to the film in densities ranging up to 500 lines/in (200 lines/cm). The greater the line density, the greater the sensitivity to out-of-plane displacement.

When light is passed through the grid plane, shadows of the lines are cast upon the test specimen as shown in figure C2. As the test specimen deflects out-of-plane (i.e., moves either toward or away from the grid plane) the shadows appear to move creating fringes of dark and light areas. A dark fringe is formed when the shadows from the grid plane fill the spaces between lines on grid plane. Light areas occur when the shadow falls directly beneath a grid plane line. A calibration photo of the beaded panel with no load is shown in figure C3. Proceeding from a dark fringe through a light fringe to another dark fringe in this figure is equivalent to an out-of-plane distance of 0.048 inches (0.122 cm). Therefore, by selecting a stationary reference point (for all load conditions) the out-of-plane dimensions (displacements) can be determined. The stationary point selected in this case was the bottom of the Moiré fringe glass assembly where the assembly

was rigidly attached to the panel.

The fringe in the down beads shown in figure C3 became indecernable as the beads approached the flats. Therefore, paper strips, pointed out in figure C3 were glued to the panel as shown, in such a manner that the fringes could be counted down to the peak of the bead. Out-of-plane displacements of the down beads could then be determined.
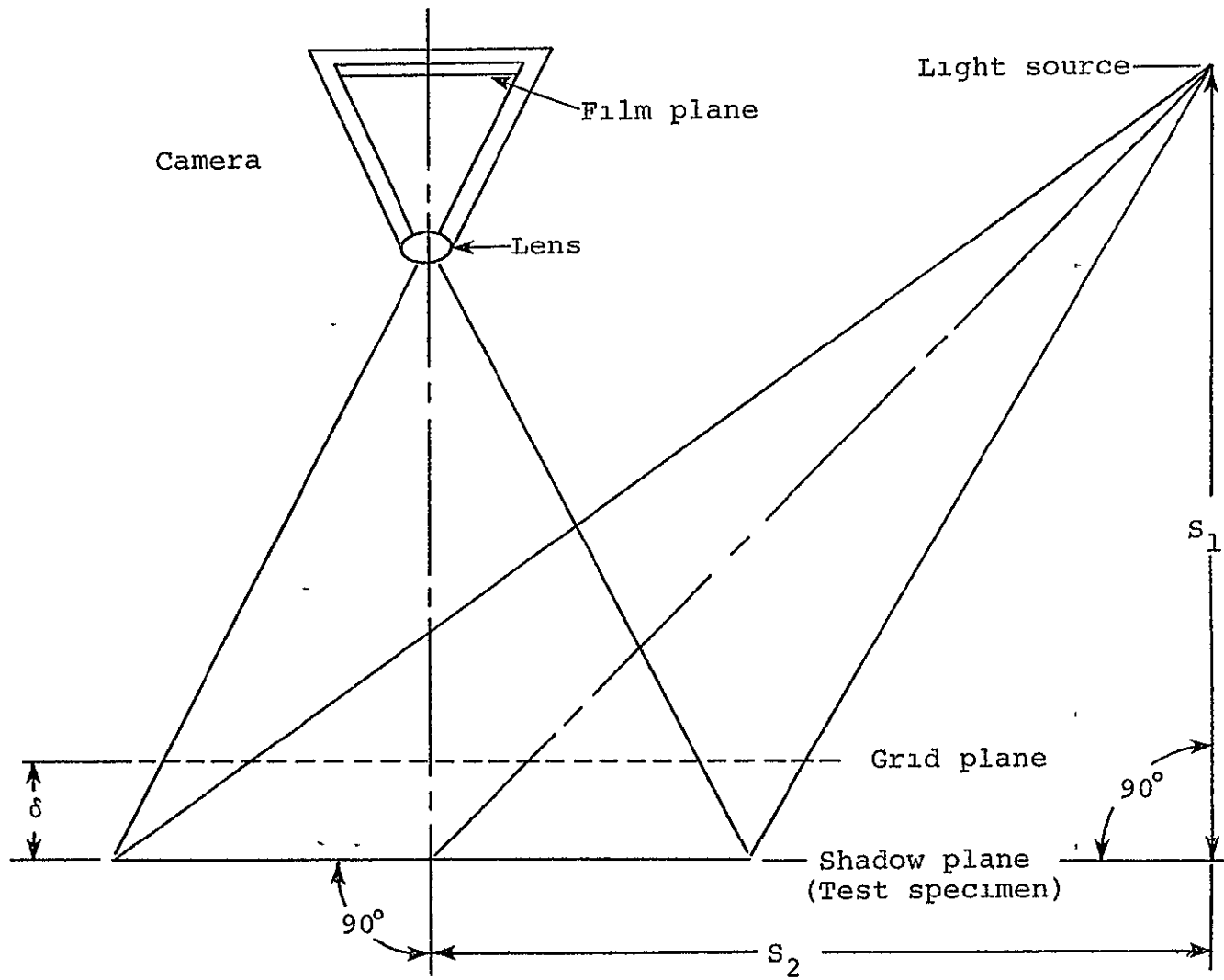
Figure C1.   Moiré fringe equipment setup.

Figure C2. Mechanics of the Moiré fringe technique.

To camera

Light from
source

Θ

Grid plane

1/P

δ

Deflected shadow planes

Initial shadow plane
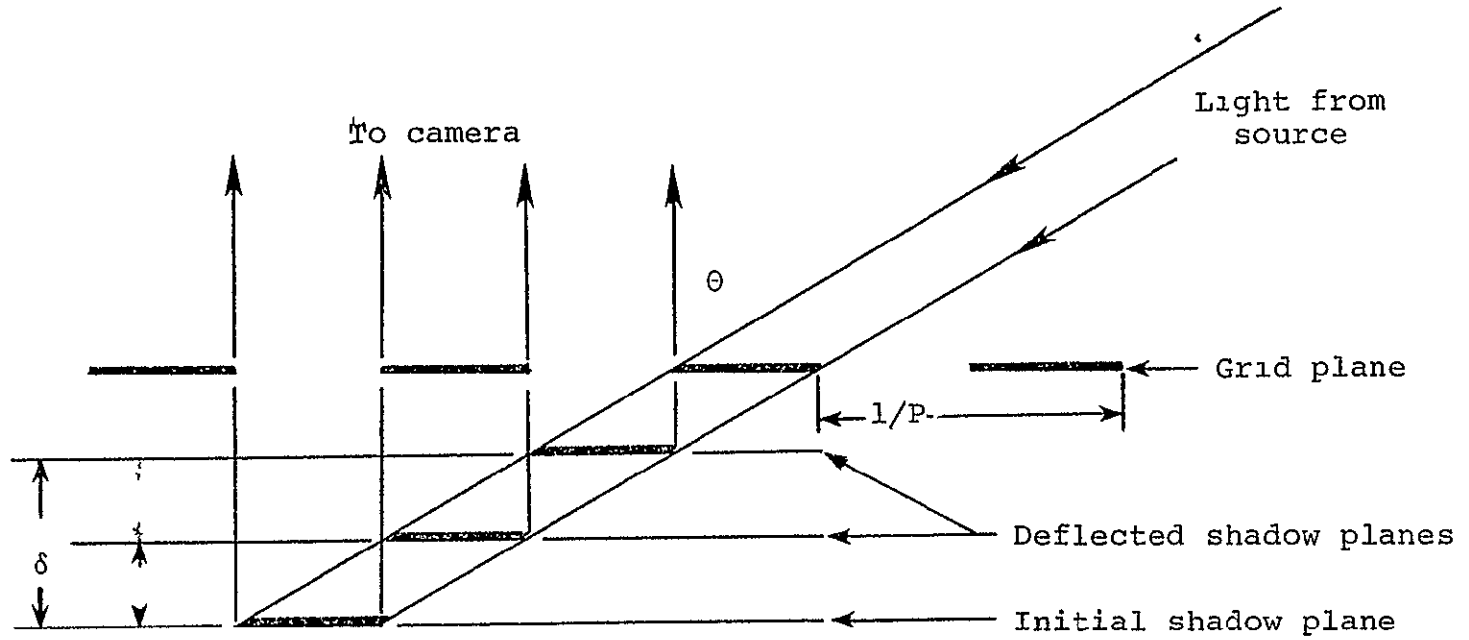
Sensitivity (δ) = 1/(P Tan Θ)   inches/fringe

Where P is the grid pitch in lines/in
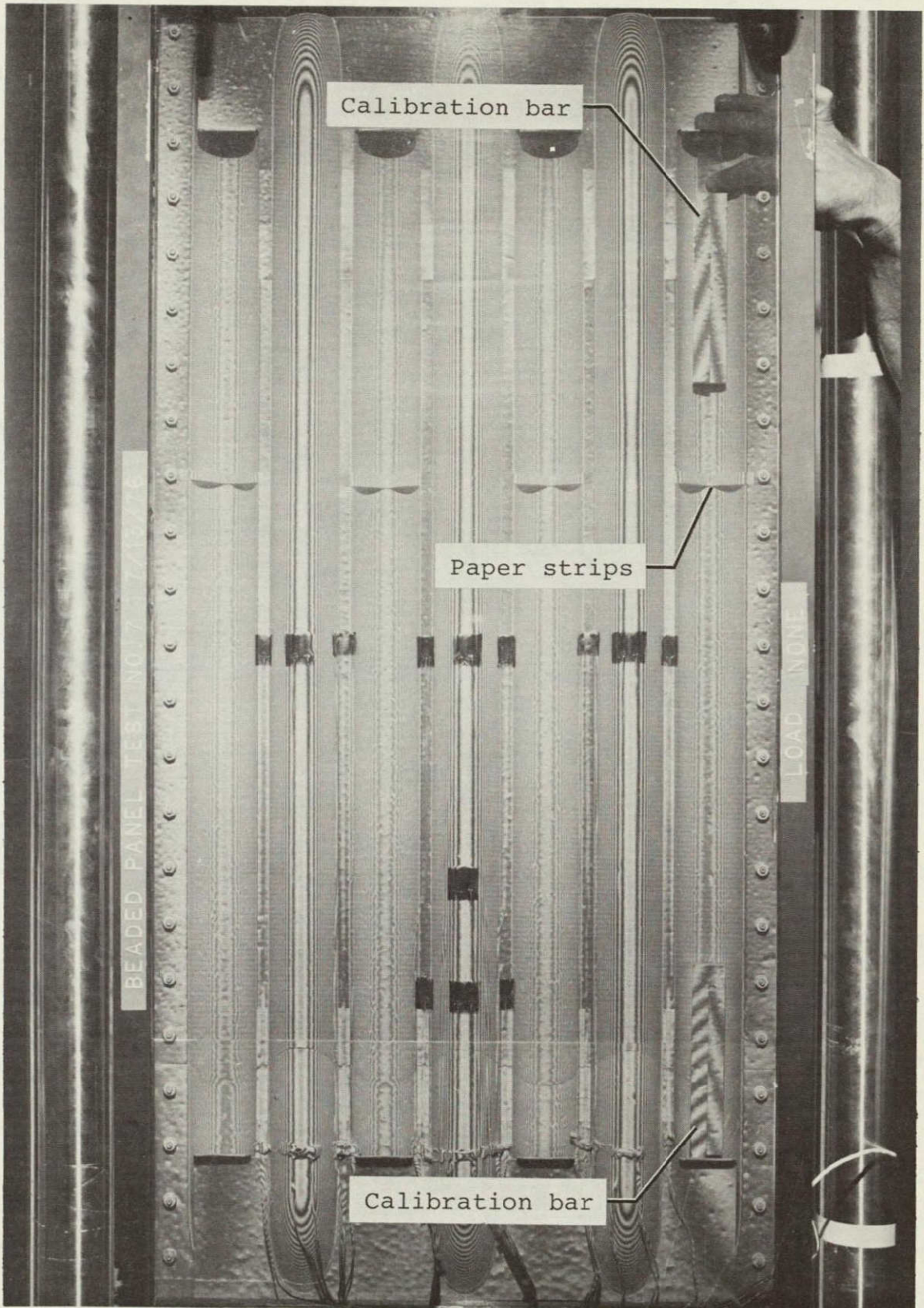
Figure C3. Sample Moiré fringe calibration photograph of the beaded panel.

126

THE DOCTOR OF ENGINEERING PROGRAM

The Doctor of Engineering (D.E.) program at the University of Kansas is a mission oriented program designed to develop creative leadership abilities in its participants. The D.E. program is characterized by a less specialized, broader curriculum than the typical Doctor of Philosophy program. Part of the D.E. curriculum consists of core courses including engineering management, finance, design, systems engineering, and sociotechnological interaction.

The core courses are utilized by the D.E. candidate to develop, plan, and manage an engineering project. The D.E. projects are of sufficient complexity to require several team workers, activity scheduling, and resource management. The technical and managerial results of the project are then reported in the form of a doctoral dissertation.

PROJECT SCHEDULING

Although this project could not be considered extremely large, it was of sufficient complexity to require activity scheduling and coordination to run smoothly. Test preparation as well as the actual testing of the panel required the greatest degree of coordination since a larger number of people were involved.

Table D1 itemizes the major activities of this project and their respective durations. One item not included in Table D1 is the activity related to the development and utilization of the finite element. Nastran model, EDGE3. EDGE3 was not developed until late in the project (after experimental testing) and was therefore, not included in the original scheduling. Figure D1 is an arrow diagram indicating the required sequence of activities as well as the critical path. Figure D2 is the corresponding timetable of activities. As indicated by figure D2, total project duration was about 300 working days or about 14 months. Note that neither the arrow diagram or the timetable in- ' cludes time spent at the University of Kansas attending classes full time.

Table D1: Major Project Activities

| Activity	Remarks	Duration Days
A	Define grid point geometry, elements, etc. for Nastran models EDGE1 and EDGE2.	21
B	Prepare case input for models EDGE1 and EDGE2 to design edge supports.	28
C	Prepare case input to model EDGE2 to analyze general instability mode.	28
D	Define grid point geometry, elements, etc. for Nastran models BEAD, FLAT, and DIAG.	14
E	Analyze other instabilities with BEAD, FLAT, and DIAG with appropriate input.	28
F	Design and fabricate panel end supports and side stiffeners.	42
G	Design and fabricate Moiré grid glass supports	7
H	Draw up data aquisition system plans and set up data aquisition system.	21
I	Assemble edge supports to panel.	2
J	Machine assembled panel ends parallel.	3
K	Draw up instrumentation plans and instrument panel	14
L	Set up testing machine, photographic fixtures and other equipment.	7
M	Adhere Moiré grid to glass and assemble glass supports and glass.	7
N	Establish loading rates and make preliminary check of system.	1
O	Test panel.	21
P	Analyze data.	28
Q	Prepare report.	150
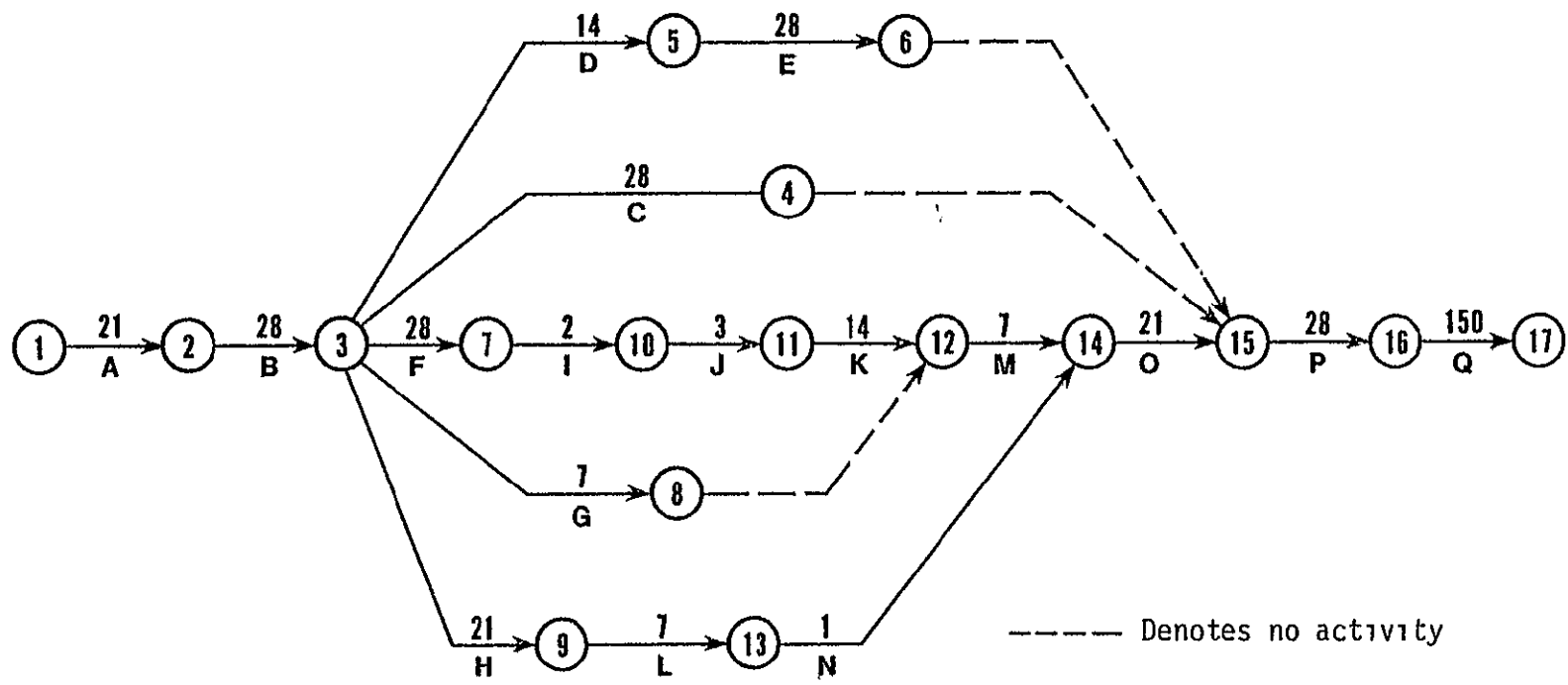
Figure D1. Arrow diagram of the major beaded panel project activities.
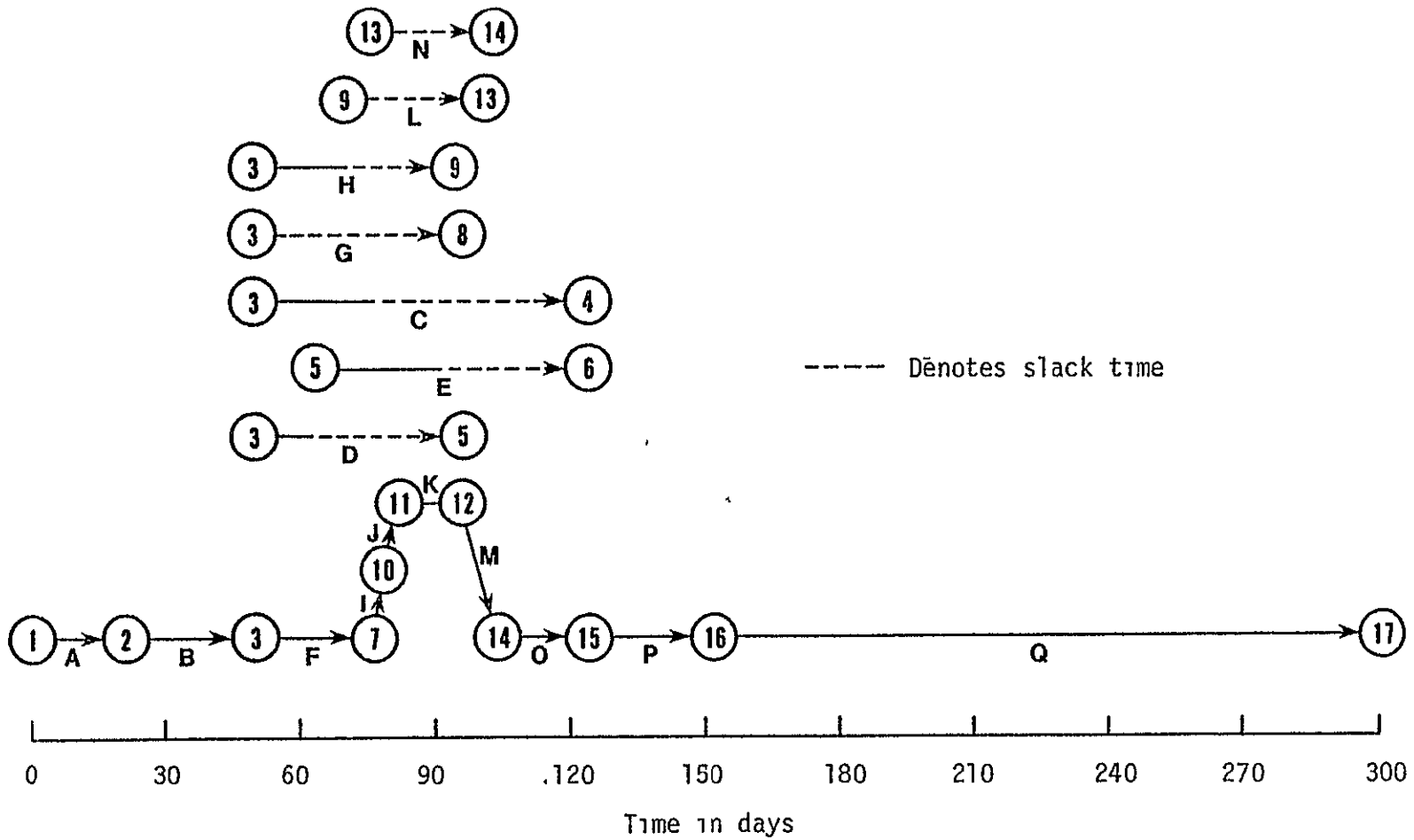
Figure D2. Timetable of major beaded panel project activities.

RESOURCE MANAGEMENT

The majority of this project was completed at NASA's Dryden Flight Research Center. As a result, a number of NASA personnel were involved with this project to some degree. The NASA personnel were directed in their activities (for this project), by the principal investigator (naturally through the appropriate channels). Table D2 is a list of the personnel involved with this project and the time required of each.

The greatest contribution, both in terms of time and consultation, came from Roger Fields, an aerospace engineer in the aerostructures division of the research directorate at DFRC. Mr. Fields was the principal investigator's immediate supervisor at DFRC and an ad hoc

Table D2: Manpower Requirements

Person	Total Hours
Principal Investigator	2000
Ad Hoc Committee Member	750
Committee Chairman	200
Operations Engineer	20
Electronics Technicians-(2)	120
Instrumentation Technician	50
Photo Lab Personnel	20
Technicians-(2)	30
Student Aids	40
Machinists-(3)	30
Total Man Hours	3260

member of the committee supervising this project. Mr. Fields spent countless hours reviewing design procedures, experimental data, and ultimately this report. His advise was particularly useful from a practical (applications) standpoint.

Other NASA personnel involved with this project include Gary Craton and Bill Hensley, electronics technicians responsible for the setup and operation of the data acquisition computer and related electronics. Walter Sefic and Larry Reardon, operations engineers, were responsible for the operation of the MTS testing machine during each test. Clarence Cook, an instrumentation technician, instrumented the panel with strain gages. Two operations technicians, Ralph Sparks and Leon Hatcher, prepared the MTS machine for use and installed brackets on to which displacement transducer and photo equipment were mounted. Other personnel included machinists, photo lab technicians and student aids who reduced and analyzed data.

Technical and theoretical direction was provided by Dr. John Easley, professor of civil engineering at the University of Kansas. Dr. Easley, spent long hours reviewing the paper for correctness of its assertions and conclusions, as well as making two trips to DFRC to observe testing procedures and make suggestions. Dr. Easley was also the chairman of the committee supervising this project.

Another asset to this project was the availability of NASA's physical facilities, test equipment, and computer facilities. Many hours of finite element computer programs were run on the CDC computer at DFRC. Had the CDC computer not been available, it is doubtful that the computer analysis done for this project could have been accomplished.

The Nastran model EDGE3 was so large, however, that it was necessary
to have the buckling analysis done with EDGE3 run on the University
of California at Los Angeles' IBM computer. Other computer facilities
included a SEL 810 data acquisition and control computer complete
with peripheral devices such as TV moniters, a line printer, and strip
charts. The testing machine used to test the panel was an MTS machine
capable of programable loading rates. Other facilities previously
mentioned include an instrumentation lab, a machine shop, and a pho-
tography lab.

REFERENCES

1. Plank, P. P.; Sakata, I. F.; Davis, G. W.; Richie, C. C.: Hypersonic Cruise Vehicle Wing Structure Evaluation, NASA CR-1568, 1970.

2. Hotchkiss, H. H.: Hypersonic Wing Test Structure, Preliminary Draft of a Portion of the Final Report, Part I-Design, Task 4 Wing Optimization, NASA CR-1845, 1973.

3. Greene, Bruce E.: Advanced Beaded and Tublar Structural Panels, Volume 1, Design and Analysis, NASA CR-132460.

4. Plank, P. P.; I. F.; Davis, G. W.; Richie, C. C.: Hypersonic Cruise Vehicle Wing Structure Evaluation, NASA CR-66897-3, 1970.

5. Musgrove, Max D.; Northrop, Russell F.: Advanced Beaded and Tubular Structural Panels, Volume 2, Fabrication, NASA CR- 123482

6. Kirkham, F. S.; Jackson, Robert L.; Weidner, John P.: Study of a High-Speed Research Airplane, AIAA Paper 74-988, August 1974.

7. Shideler, John L.; Bohon, Herman L.; Greene, Bruce E.: Evaluation of Bead-Stiffened Metal Panels. Presented at the ASME/AIAA/SAE 16th Structures, Structural Dynamics, and Materials Conference, May 1975.

8. Musgrove, Max D., Greene, Bruce E.; Shideler, John L.; Bohon, Herman L.: Advanced Beaded and Tubular Structural Panels. Presented at the AIAA/ASME/SAE 14th Structures, Structural Dynamics, and Materials Conference, March 1973.

9. Hearth, Donald P.; Preyes, Albert E.: Hypersonic Technology Approach to an Expanded Program. J. Astronautics and Aeronautics, Dec. 1976.

10. Plank, P. P.; Penning, F. A.; Hypersonic Wing Test Structure Design Analysis, and Fabrication, NASA CR-127490, 1973.

11. Jones, Robert E.; and Greene, Bruce E.: The Force/Stiffness Technique for Nondestructive Buckling Testing, AIAA Paper 74-351, April 1974.

12. Dykes, B.C.: Analysis of Displacements in Large Plates by the Grid-Shadow Moiré Technique; Proceedings of the Fourth International Conference on Experimental Stress Analysis, Cambridge, England 1970.

13. McComas, R. L.: Nastran, NASA's General Purpose Structural Analysis Program, NASA TM X-64528, 1970.

14. Metallic Materials and Elements·for Aerospace Vehicle Structures, MIL-HDBK-5B.

15. Rupert, E. J.: Uhland, G. E., et. al.,· Hypersonic Wing Test Structure, Preliminary Draft of a Portion of the Final Report, Part II-Manufacture Hardware, Task T-Test Specimen, NASA CR-1845.

16. Sefic, Walter J.; Anderson, Karl F.: NASA High Temperature Loads Calibration Laboratory, NASA TM X-1868.

17. Peery, David. J.: Aircraft Structures, McGraw-Hill Book Company, 1950, pp. 347-348.

18. Hewlett Packard HP-65 Math Pac I Linear and Lagrangian Interpolations, Program I-32A

CRINC LABORATORIES

Chemical Engineering Low Temperature Laboratory

Remote Sensing Laboratory

Flight Research Laboratory

Chemical Engineering Heat Transfer Laboratory

Nuclear Engineering Laboratory

Environmental Health Engineering Laboratory

Information Processing Laboratory

Water Resources Institute

Technical Transfer Laboratory

Air Pollution Laboratory

Satellite Applications Laboratory

CRINC